The PHILOSOPHICAL MAGAZINE

FIRST PUBLISHED IN 1798

L. 43 SEVENTH SERIES No. 344 September, 1952

A Journal of Theoretical Experimental and Applied Physics

PRICE 15s. 0d.
Annual Subscription £8 0s. 0d. payable in advance

AND PUBLISHED BY TAYLOR & FRANCIS LTD., RED LION COURT, FLEET ST., LONDON, E.C.4.

ADVANCES IN PHYSICS

A QUARTERLY SUPPLEMENT OF THE PHILOSOPHICAL MAGAZINE

On 1st January, 1952, the first number of this new Quarterly Supplement to the Philosophical Magazine was published. The aim of this Supplement will be to give those interested in physics comprehensive and authoritative accounts of recent important developments. It is felt by the Editor that in view of the rapid advances in many branches of physics, scientists will welcome a journal devoted to articles of this type.

VOLUME 1 OCTOBER 1952 NUMBER 4

PRICE *per part* 15/- *plus postage* **PRICE** *per annum* £2 15s. 0d. *post free*

Printed and Published by
TAYLOR & FRANCIS, LTD., RED LION COURT, FLEET ST., LONDON, E.C.4

LXXXIX. *On the Theory of Beta-Radioactivity*

By A. M. Smith
Department of Natural Philosophy, University of Aberdeen*

[Received April 15, 1952]

Abstract

A comparison of some experimental beta spectra with theoretical predictions when the interaction is taken as a linear combination of the five usual forms has been made, and on this basis the conclusion is that the interaction can only be a mixture of the vector and tensor forms. For two disintegrations involving light nuclei the arbitrariness in the theoretical predictions has been reduced by assuming a shell structure of nuclei and evaluating the nuclear matrix elements involved. From this analysis it is concluded that the interaction responsible for beta decay is a mixture of approximately two parts of vector form to one of tensor.

§ 1. Introduction

In the Fermi theory of beta radioactivity the interaction between light and heavy particle fields is expressed in terms of Dirac's four-component relativistic wave functions for the particles involved in the decay process, in such a way that the interaction is invariant under the Lorentz group of transformations. There are five such expressions, called the scalar, vector, tensor, axial vector and pseudoscalar forms of interaction (S, V, T, A and P in the usual notation). The theory of allowed and forbidden transitions has been developed, for each of these five different forms, by Konopinski and Uhlenbeck (1941). For allowed transitions all forms of interaction predict the same distribution of energy of the emitted beta radiation; for forbidden transitions the results are expressed in terms of correction factors by which the allowed distribution must be multiplied. Each correction factor contains a few nuclear matrix elements, each multiplied by a coefficient which is dependent on the energy of the emitted beta particle, and comparison of theory with experiment is rendered difficult by lack of knowledge concerning the matrix elements. However, the selection rules which the matrix elements impose on the spin and parity changes in the disintegration do limit the correction factors in a few cases to only one matrix element along with its energy dependent coefficient. For example, in the first forbidden correction factor for the tensor or axial vector interactions, the matrix element B_{ij} allows a spin change of 2 units and a parity change, whilst the other matrix elements in

* Communicated by C. Strachan.

this correction factor are zero under these circumstances. Now, several spectra have been measured experimentally such that when the correction factor (B_{ij} shape) (the energy dependent coefficient of $\sum_{i,j}|B_{ij}|^2$) is applied to the conventional Fermi plot, a straight line is obtained. For example there are the spectra of ^{89}Sr, ^{90}Sr, ^{90}Y and ^{91}Y (Langer and Price 1949). Moreover, the Fermi plot of the spectrum of ^{10}Be gives a straight line when corrected for by (S_{ijk} shape)—the second forbidden correction factor for tensor or axial vector interactions when a spin change of 3 units and no parity change are involved (Fulbright and Milton 1949); and so also with ^{40}K when corrected for by the so-called C factor, the coefficient of the matrix element allowing a spin change of 4 units and a parity change in the third forbidden tensor or axial vector correction factors, thereby giving a unique energy dependence (Alburger 1950). Thus the interaction must be, partly at least, of the tensor or axial vector form.

§ 2. A Linear Combination of Invariants

There is no theoretical reason why one form of interaction should be preferred to any other, and so the additions to the correction factors, which arise when a linear combination of the five invariants is considered, have been worked out by the author and are quoted elsewhere (Smith 1951). A linear combination of interactions has been suggested by Fierz (1936) who investigated the effect such a combination would have on the allowed distribution. He showed that if the scalar interaction is combined with the vector, or the tensor with the axial vector, the allowed distribution must be multiplied by $(1+c/w)$ where c is a constant. Since many beta spectra conform to the allowed distribution as predicted by Fermi, such combinations must be impossible.

We take then as the invariant

$$I=\lambda_S S+\lambda_V V+\lambda_T T+\lambda_A A+\lambda_P P$$

with the understanding that

$$\lambda_S\lambda_V=\lambda_T\lambda_A=0.$$

The constants λ are taken to be real.

It is worth noting that those explanations of spectral shapes which have already been established would not be affected by such a combination of interactions. (There has been a recent exception to this—it is possible to explain the shape of the spectrum of ^{36}Cl using a mixture of coefficients of those matrix elements in the second forbidden tensor correction factor which allow the known spin change of 2 units. This will be dealt with more fully in § 5.) Allowed spectra are not affected. Spectra which are explained by (B_{ij} shape) would not be affected, since there is no matrix element in the first forbidden correction factors of either the scalar or vector interactions which allows a spin change of 2 units. The same is true of spectra explained by (S_{ijk} shape) and by the C factor. It is therefore

reasonable to try a combination of interactions with a view to explaining the spectra of nuclei which do not conform to the distributions for single interactions.

§ 3. Comparison with Experiment I

Comparison of theory with experiment is made difficult by the lack of reliable spectra whose shapes have not hitherto been explained. It has been realized in recent years that a considerable amount of distortion can occur at the low energy end of a beta spectrum unless the emitting layer of radioactive material is extremely thin (Albert and Wu 1948). However, the literature has been searched for unexplained spectra which seem to be reliable, and six disintegrations have been selected in which (*a*) the source used was reasonably thin, (*b*) the *ft* value suggests a second forbidden transition. Since a spin change of 3 units would give a spectrum conforming to (S_{ijk} shape), and a spin change of 1 unit would give an allowed transition, we assume that a spin change of 2 units and no change in parity are involved. These assumptions are justified in some cases by predictions of the shell model of nuclei, but should it be impossible to explain any spectrum under these assumed conditions, it need not be taken as a breakdown of the theory. Furthermore, this procedure will not indicate whether the interaction contains the pseudoscalar form, since it gives no contribution to second forbidden transitions with a spin change of two units.

The shape which the correction factor should have is determined by finding the factor by which the conventional Fermi plot must be corrected in order to give a straight line. In this section we examine whether it is possible to combine the coefficients of the matrix elements occurring in the complete correction factors so as to give the experimentally determined correction factors, without making any assumptions concerning the magnitudes of the matrix elements or the proportions in which the interactions are mixed.

The fitting of a combination of so many theoretical curves on to one experimentally determined curve is done by the method of least squares. We have to fit a combination of f_1, f_2, f_3, etc., on to an experimentally determined curve f and this is done by choosing a_1, a_2, a_3 etc., so that

$$\sum_i (a_1 f_{1_i} + a_2 f_{2_i} + a_3 f_{3_i} \cdots - f_i)^2$$

is a minimum, the summation being over points on the curves. This gives rise to a system of linear equations which can be solved for the constants a_1, a_2, a_3, etc. However, some of the functions f_1, f_2, f_3 etc. usually have similar shapes, and consequently there will be approximate linear relationships between them. This will make the matrix of the set of linear equations nearly singular, and the number of functions $f_1, f_2, f_3 \cdots$ must be reduced so that only independent ones are used in the fitting; otherwise it might be possible to get a good fit which would not be allowable, since it might be using the small errors in the linear relationships as

independent functions. Moreover, because of this singularity, we will not be able to deduce anything about ratios of matrix elements or the proportions in which interactions are mixed; we may be able, however, to eliminate certain combinations of interactions as being quite incapable of explaining the spectra considered.

Evaluation of the matrix element coefficients in the correction factors, and the subsequent curve-fitting processes require a very large amount of computational work. For this purpose we require to express the ratios F_1/F and F_2/F^* which appear in the correction factors in forms suitable for computation.

These are

$$\frac{F_1}{F}=\frac{(4!)^2\,\Gamma^2\,(2S+1)}{4\,\Gamma^2\,(2S_1+1)}\,(2p\rho)^{2(S_1-S-1)}\,[(S_1-1)^2+y^2]\times\left[1-\frac{\alpha^2Z^2}{2}\,C+\frac{\alpha^2Z^2y^2}{2}\sum_{n=1}^{\infty}\frac{1}{n(n^2+y^2)}\right]$$

$$\frac{F_2}{F}=\frac{(6!)^2\,\Gamma^2\,(2S+1)}{4\,\Gamma^2\,(2S_2+1)}\,(2p\rho)^{2(S_2-S-2)}[(S_2-1)^2+y^2][(S_2-2)^2+y^2]\times\left[1-\frac{2\alpha^2Z^2}{3}\,C+\frac{2\alpha^2Z^2y^2}{3}\sum_{n=1}^{\infty}\frac{1}{n(n^2+y^2)}\right].$$

Here the symbols have their usual meaning, C is Gauss's number$=0{\cdot}577$ and $y=\alpha ZW/p$. The nuclear radius ρ is given, in relativistic units, by

$$\rho=3{\cdot}67\times10^{-3}\times A^{1/3}$$

where A is the mass number.

For each disintegration the best fits for the four possible combinations, S or V with T or A have been worked out. In addition, the best fit for a pure tensor interaction has been found, this being the only interaction which by itself gives promise of explaining all spectra.

Phosphorus

The $^{32}P\rightarrow{}^{32}S$ disintegration has been reported as giving a straight line Fermi plot by Siegbahn (1946) and by Langer and Price (1949), but a more recent determination by Agnew (1950) gives a Fermi plot which is slightly concave towards the energy axis and has a sudden rise at low energies. A later measurement by Warshaw, Chen, and Appleton (1950) also gives this sudden rise at low energies but gives a straight line Fermi plot above this. The *ft* value, based on Agnew's determination of the end-point energy, is $8{\cdot}6\times10^7$, which classifies the transition as second forbidden, and the conditions $\Delta J=2$, no change of parity, are quite reasonable on the shell model of nuclei. Since Agnew used a very thin source ($<0{\cdot}04$ mg/cm^2) and since the departure from a straight line Fermi plot, apart from the sudden rise in low energies, is in the opposite direction to what one would expect from source thickness distortion, his results have been selected for comparison with second forbidden correction factors. On

* Konopinski and Uhlenbeck, *loc. cit.*, Smith, *loc. cit.*

the assumption that the sudden rise at low energies does not imply complexity of the spectrum, it has been found impossible to fit the experimental data with any of the second forbidden correction factors, and we must conclude that ^{32}P does not fall in this class of transitions. It is probable that this transition is really allowed, in accordance with all the other experimenters, with a spin change of 1 unit. The *ft* value would then be high because of some inner selection rule which is making the allowed matrix element $\int\sigma$ small (See Pursey 1951 a).*

Technetium

The $^{99}Tc \rightarrow {}^{99}Ru$ spectrum has been measured recently by Taimuty (1951) using a fairly thin source (0·17—1·3 mg/cm^2). He found that the Fermi plot was reasonably good when corrected for by (B_{ij} shape), which would make the transition first forbidden with a spin change of 2 and a

Fig. 1

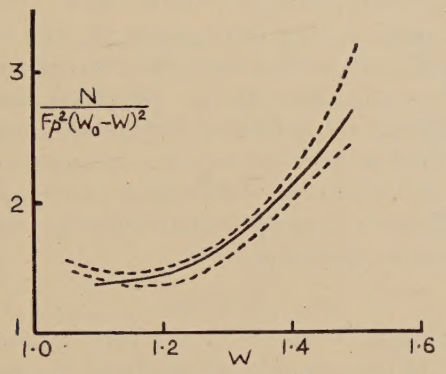

^{99}Tc. Best fit for combination *ST*.

change of parity. The *ft* value, however, is $2{\cdot}3 \times 10^{12}$ which indicates a higher order of forbiddenness, and the shell model suggests a spin change of 2 units with no parity change. Attempts to fit the spectrum with second forbidden correction factors show that it is possible to do so with the tensor interaction alone or with any of the four possible combinations of interactions. A typical fit is shown in fig. 1 where the two dotted curves represent the experimentally determined correction factor for the experimental limits put on the end-point energy, and the solid curve is the best fit obtained from the theoretical curves by the method of least squares.

Tin

The disintegration $^{125}Sn \rightarrow {}^{125}Sb$ has been investigated by Hayward (1950) using a source of thickness estimated at 0·4 mg/cm^2. The *ft* value

* The work of Jensen *et al.* (1952) has just come to the author's notice. They find the spectrum of ^{32}P to be allowed, and suggest that the sudden rise at low energies is due to the presence of the ^{33}P isotope.

is $3{\cdot}7\times10^8$, which puts the transition in the second forbidden class. The decay is obviously complex. Hayward has corrected the usual Fermi plot with (B_{ij} shape) and claims the resulting plot to be a straight line; however, examination of it reveals that it has a definite convexity towards the energy axis. If we assume a spin change of 2 units and no parity change, which is quite reasonable on the shell model, we find that it is possible to explain this spectrum with the tensor interaction alone or with any of the four combinations.

Thulium

^{170}Tm decays by beta emission to ^{170}Yb and this disintegration has also been studied by Agnew who reports it along with ^{32}P, and the Fermi plot he obtains is slightly concave towards the energy axis. The spectrum has been measured by a few other experimenters; Saxon and Richards (1949 a) found that it was of the allowed form; Fraser (1949) considered the decay to be complex, being made up of two transitions of the allowed form; Graham and Tomlin (1949) found it to be allowed. The *ft* value is 7×10^8, and since Agnew used a very thin source ($<0{\cdot}03$ mg/cm^2), his results have been compared with second forbidden correction factors. None of the interactions gives a satisfactory fit. We must conclude that the spin and parity assumptions are not valid for this disintegration, and that it must either be allowed or first forbidden, in accordance with the measurements of Saxon and Richards and of Graham and Tomlin. The deviation from the allowed form in Agnew's measurement is very similar to that in his determination of the spectrum of ^{32}P.

Thallium

The beta spectrum of ^{204}Tl$\rightarrow^{204}$Pb has been measured by Saxon and Richards (1949 b) using a source of thickness $0{\cdot}1$ mg/cm^2. They have corrected the Fermi plot obtained by the (B_{ij} shape), and the resulting plot gives a straight line at the high energy end but becomes convex towards the energy axis at lower energies. This deviation, they consider, cannot be attributed to residual scattering. The *ft* value is 5×10^9, putting the transition in the second forbidden class. Comparison of the theoretical correction factors with the experimental form shows that it is possible to explain this spectrum well by tensor interaction alone, by ST, VT' or VA, but not by SA (see fig. 2).

Radium E

Konopinski and Uhlenbeck (1941) have explained the spectrum of RaE using the second forbidden correction factor for the tensor interaction. The experimental results were by Flammersfeld and also by Langer and Whitaker, but the fit obtained does not agree so well with the experimental work of Neary. Neary's results have since been confirmed by Langer and Price (1949) and the measurements of Langer and Price have been used here for comparison with theory. The *ft* value is $9{\cdot}8\times10^7$, which is consistent with a second forbidden transition. It has been found possible

to explain this spectrum with interactions SA and VT only, the others giving a definite divergence from the experimental curve. Figure 3 (a) shows the best fit for the tensor interaction and for ST; the best fit for VA is similar to that for the tensor interaction. The best fits for VT and SA are almost identical and are shown in fig. 3 (b).

Fig. 2

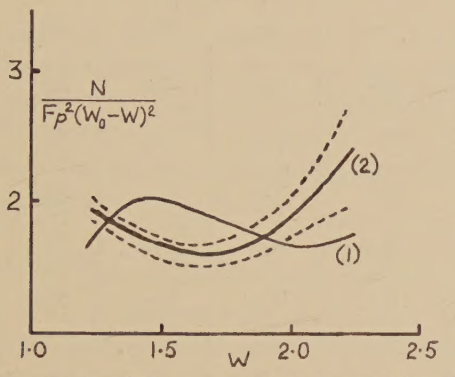

^{204}Tl. Curve (1) is best fit for SA; curve (2) is best fit for ST. Best fits for T, VT, VA are similar to (2).

Fig. 3

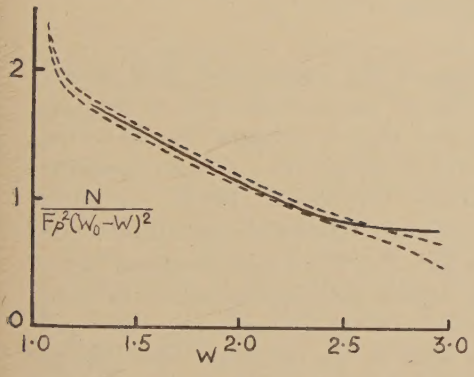

(a)

RaE. Best fit for T or ST.

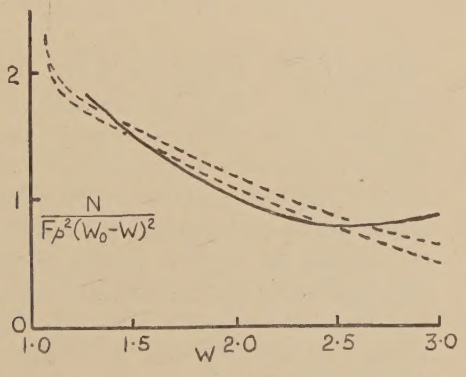

(b)

RaE. Best fit for VT or SA.

The results of this analysis are summarized in table 1, the Yes or No indicating whether a spectrum can or cannot be explained by a particular interaction. Excluding ^{32}P and ^{170}Tm from consideration as second forbidden transitions, we conclude that if our assumptions concerning the spin and parity changes involved in the other disintegrations are correct, then the interaction can only be a mixture of the vector and tensor forms.

One other point emerges from these considerations—the ft value should be looked upon as setting an upper limit to the order of forbiddenness of a transition rather than giving the actual order. The ft values of ^{32}P and

^{170}Tm suggest that they are second forbidden transitions whereas they appear to be allowed or at most first forbidden. In the same way the *ft* value for ^{14}C ($\sim 7 \times 10^8$) classifies its decay as second forbidden although its spectrum has recently been found to be of the allowed form (Feldman and Wu 1949).

Table 1

	^{32}P	^{99}Tc	^{125}Sn	^{170}Tm	^{204}Tl	RaE
T	No	Yes	Yes	No	Yes	No
S and T	No	Yes	Yes	No	Yes	No
S and A	No	Yes	Yes	No	No	Yes
V and T	No	Yes	Yes	No	Yes	Yes
V and A	No	Yes	Yes	No	Yes	No

§ 4. The Nuclear Matrix Elements

The nuclear matrix elements are of the form

$$\sum_k \int V^* O_k Q_k U d\tau$$

where U and V are the wave functions of the initial and final nuclei respectively. Q_k is an operator operating on the isotopic spin of the kth nucleon in the initial nucleus in such a way that it changes the character state of a nucleon from a neutron state to a proton state. O is an operator having the forms given by Konopinski and Uhlenbeck (1941). In their paper they have dropped the operator β, but its retention is essential since it changes the sign of matrix elements like R_{ij}, T_{ij} which combine large components of the initial wave function with large components of the final one, and the sign is of great importance in cross correction factors; moreover, since β does not commute with α, its presence can change completely the values of matrix elements such as A_{ij}. We denote by $A_i^{\beta}{}_j$, $T_i^{\beta}{}_j$ etc., those matrix elements which are the same as A_{ij}, T_{ij} etc., but have the operator β included in the integrand.

In recent years, a considerable amount of evidence has been advanced in favour of the shell structure of nuclei, and this model is used here to work out the matrix elements more exactly. The nucleons are considered as individual particles moving in an average field due to all the others, and so the nuclear wave function will be a sum of products of the nucleon individual particle wave functions, so arranged as to be an eigenfunction of the angular momentum J and of the magnetic quantum number M. We are interested in the matrix elements for a transition from an initial nucleus with angular momentum J_i and magnetic quantum number M_i to a final

nucleus with angular momentum J_f and any magnetic quantum number M_f, and so we must sum the transition probabilities over all permissible values of M_f. Thus, if $P(J_i, M_i; J_f, M_f)$ be the transition probability from an initial state J_i, M_i to a final state J_f, M_f, and Q be the total transition probability to all values of M_f, then

$$Q(J_i, M_i; J_f) = \sum_{M_f=-J_f}^{J_f} P(J_i, M_i; J_f, M_f) \quad . \quad . \quad . \quad . \quad (1)$$

there being $(2J_f+1)$ terms in this summation. Now these transition probabilities have been expressed in terms of the matrix elements of irreducible tensors, along with their energy dependent coefficients, and Wigner (1931) has shown that if $T^{\varrho}_{J_i, M_i; J_f, M_f}$ be the matrix element of the ρ-component of an irreducible tensor for the transition from an initial state J_i, M_i to a final state J_f, M_f, then

$$\sum_{\varrho, M_f} |T^{\varrho}_{J_i, M_i; J_f, M_f}|^2 = \frac{1}{2J_i+1} \sum_{\sigma, M_i', M_f'} |T^{\sigma}_{J_i, M_i'; J_f, M_f'}|^2. \quad . \quad . \quad (2)$$

The right-hand side of (2) is independent of M_i, and so Q in (1) can be written as $Q(J_i; J_f)$. In other words, the transition probability is independent of our choice of axes, as we would expect. Furthermore, since the operators in the matrix elements in beta theory are Hermitian, we obtain from (2)

$$(2J_f+1) \sum_{\varrho, M_i} |T^{\varrho}_{J_f, M_f; J_i, M_i}|^2 = (2J_i+1) \sum_{\varrho, M_f} |T^{\varrho}_{J_i, M_i; J_f, M_f}|^2.$$

From the derivation of Wigner's result, it is obvious that this applies also to scalar products of matrix elements such as $\sum_{ij} A_{ij}^* T_{ij}$. We have, therefore,

$$(2J_f+1)\, Q\,(J_f; J_i) = (2J_i+1)\, Q\,(J_i; J_f). \quad . \quad . \quad . \quad . \quad (3)$$

Thus in working out matrix elements we are at liberty to choose the direction of spin change, since that can be allowed for by (3); we are also at liberty to choose M_i, and we make our choice so as to give a minimum of calculation in the summation (1). We do this by setting J_i equal to the larger of the initial and final spins and putting $M_i = J_i$. Then, beginning with $M_f = J_f$, the summation extends over increasing values of $M_i - M_f$, and selection rules operating on $M_i - M_f$ reduce the summation to a few terms. When one of the spins involved is zero, the summation reduces to one term.

For matrix elements such as T_{ij}, S_{ijk}, in which the operator combines large components of the initial nucleon four-component wave function with large components of the final one, relativistic wave functions are unnecessary, and we use two-component wave functions in the Pauli representation. If $|+1\rangle$ and $|-1\rangle$ are the eigenvectors of the operator corresponding to the z-component of intrinsic spin and belonging to the eigenvalues $\frac{1}{2}\hbar$ and $-\frac{1}{2}\hbar$ respectively, then the individual particle wave functions are of the form

$$\psi(n, l, m)\ |+1\rangle,\ \psi(n, l, m)\ |-1\rangle$$

where n, l and m are the usual quantum numbers. However, in some matrix elements, for example A_{ij}, the operator combines large components with small components, and so the wave functions used should be four-component solutions of Dirac's equation. If χ_3 and χ_4 are the large components of the solution, approximate values for the small components, χ_1 and χ_2, are given by :—

$$\chi_1 = \frac{i}{2M}\left\{\left(\frac{\partial}{\partial x} - i\frac{\partial}{\partial y}\right)\chi_4 + \frac{\partial}{\partial z}\chi_3\right\},$$

$$\chi_2 = \frac{i}{2M}\left\{\left(\frac{\partial}{\partial x} + i\frac{\partial}{\partial y}\right)\chi_3 - \frac{\partial}{\partial z}\chi_4\right\},$$

where M is the ratio of the nucleon mass to the electron mass.

If the nucleon energy is not much greater than its rest energy, χ_3 and χ_4 are solutions of Schrödinger's equation corresponding to the two eigenvalues of one component of the nucleon spin, and so we can extend the non-relativistic nucleon wave functions to four-component approximate relativistic ones if we replace

$\psi(n, l, m)\ |+1\rangle$ by :—

$$\chi_1 = \frac{i}{2M}\frac{\partial\psi}{\partial z}$$

$$\chi_2 = \frac{i}{2M}\left(\frac{\partial}{\partial x} + i\frac{\partial}{\partial y}\right)\psi$$

$$\chi_3 = \psi$$

$$\chi_4 = 0$$

and $\psi(n, l, m)\ |-1\rangle$ by :—

$$\chi_1 = \frac{i}{2M}\left(\frac{\partial}{\partial x} - i\frac{\partial}{\partial y}\right)\psi$$

$$\chi_2 = -\frac{i}{2M}\frac{\partial\psi}{\partial z}$$

$$\chi_3 = 0$$

$$\chi_4 = \psi.$$

There are a few points to be considered in connection with the determination of nuclear wave functions in terms of the individual particle wave functions. Firstly, we must decide which system of angular momentum coupling is likely to be the better approximation, the Russell–Saunders or RS form, or the j–j form. This will depend on the particular nuclei in which we are interested, the requirement being a plausible nuclear configuration whose wave function is an eigenfunction of angular momentum corresponding to a given eigenvalue. In dealing with shells of high l number which are about half-filled, the number of ways in which the particles can be accommodated is very large and there may be a few possible wave functions corresponding to a given pair of values J, M. These wave functions are much too unwieldy for calculations. In such cases it is simpler to use j–j coupling since this requires smaller shells, and we can make the simplifying assumption that particles can pair off to give zero contribution to the spin.

Secondly, we are not interested in shells which are complete in the initial and final nuclei. The operator Q_k, operating on a nucleon in a closed shell in the initial nucleus, gives zero if the nucleon is in a proton character state, and if it is in a neutron state it changes to a proton state, thereby becoming orthogonal to its opposite number in the final nucleus.

Finally, since the operator in the nuclear matrix elements operates on only one nucleon wave function at a time, we get contributions to the matrix elements only from those parts of the initial and final nuclear wave functions which are exactly the same except for, at most, one of the individual particle wave functions. In all other cases we get zero contribution because of the orthogonality properties of these wave functions.

We consider now the matrix elements for the transition $^{36}_{17}\mathrm{Cl} \xrightarrow{\beta^-} {}^{36}_{18}\mathrm{A}$. The spin of this chlorine isotope has been measured by Townes and Aamodt (1949), who obtained the value 2, and ^{36}A, being an even-even nucleus, is assumed to have zero spin. From the table given by Mayer (1949) a plausible configuration for ^{36}Cl, assuming j–j coupling, would be :—

Protons	$(1s)^2(1p)^6(1d_{5/2})^6(1d_{3/2})^2(2s)^1$
Neutrons	$(1s)^2(1p)^6(1d_{5/2})^6(2s)^2(1d_{3/2})^3$

For ^{36}A the protons and neutrons both have the same arrangement, namely

$$(1s)^2(1p)^6(1d_{5/2})^6(2s)^2(1d_{3/2})^2.$$

Transitions from the chlorine arrangement to the argon arrangement conform to the parity requirements of second forbidden transitions. In accordance with the discussion above, we set $J_i=2$, $M_i=2$, $J_f=0$, $M_f=0$, and so we must make up a wave function from the chlorine arrangement with $J=2$, $M=2$, and a wave function from the argon arrangement with $J=0$, $M=0$. For chlorine, we assume that the two protons in $1d_{3/2}$ states are paired together to give zero contribution to the nuclear spin, and we make the same assumption about the two protons in $1d_{3/2}$ states in argon ; thus the sub-wave-function of these two protons is the same in both nuclei and we need not consider them. For the remaining nucleons in unfilled shells in chlorine, the only wave function corresponding to $M=2$, taking into account the exclusion principle, is

$$\{(\tfrac{3}{2}, 2, \tfrac{3}{2})N\}\{(\tfrac{3}{2}, 2, \tfrac{1}{2})N\}\{(\tfrac{3}{2}, 2, -\tfrac{1}{2})N\}\{(\tfrac{1}{2}, 0, \tfrac{1}{2})P\}. \quad . \quad . \quad (3)$$

The N and P indicate the character states of the nucleons and the numbers in brackets are the j, l, and m quantum numbers. This expression represents the Slater determinant giving a completely antisymmetrical wave function for the four nucleons :—

$$(4!)^{-1/2} \begin{vmatrix} (\frac{3}{2}, 2, \frac{3}{2})N(1) & (\frac{3}{2}, 2, \frac{1}{2})N(1) & (\frac{3}{2}, 2, -\frac{1}{2})N(1) & (\frac{1}{2}, 0, \frac{1}{2})P(1) \\ (\frac{3}{2}, 2, \frac{3}{2})N(2) & (\frac{3}{2}, 2, \frac{1}{2})N(2) & (\frac{3}{2}, 2, -\frac{1}{2})N(2) & (\frac{1}{2}, 0, \frac{1}{2})P(2) \\ — & — & — & — \\ — & — & — & — \end{vmatrix}$$

For ^{36}A, the two neutrons in $1d_{3/2}$ states and the two protons in 2s states can combine in two ways to give $M=0$; these are

$$A=\{(\tfrac{3}{2}, 2, \tfrac{3}{2})N\}\{(\tfrac{3}{2}, 2, -\tfrac{3}{2})N\}\{(\tfrac{1}{2}, 0, \tfrac{1}{2})P\}\{(\tfrac{1}{2}, 0, -\tfrac{1}{2})P\} \quad . \quad (4a)$$

$$B=\{(\tfrac{3}{2}, 2, \tfrac{1}{2})N\}\{(\tfrac{3}{2}, 2, -\tfrac{1}{2})N\}\{(\tfrac{1}{2}, 0, \tfrac{1}{2})P\}\{(\tfrac{1}{2}, 0, -\tfrac{1}{2})P\} \quad . \quad (4b)$$

and the eigenfunction for $J=0$, $M=0$ is some combination of A and B. Examination of (3) and (4), however, shows that A gives no contribution to the matrix elements since two of the individual particle wave functions are different in the initial and final nuclei. The whole contribution to the matrix elements comes from B, and since we are interested only in the ratios of matrix elements for the purposes of curve fitting, a multiplying constant for B is unimportant. Thus with (3) as the initial wave function and (4 b) as the final one, the matrix element of an operator O reduces to

$$\int\{(\tfrac{1}{2},\ 0,\ -\tfrac{1}{2})P\}^{*}OQ\{(\tfrac{3}{2},\ 2,\ \tfrac{3}{2})\ N\}\ d\tau. \quad . \quad . \quad . \quad . \quad . \quad . \quad (5)$$

The angular and spin part of the wave function $(\frac{1}{2},\ 0,\ -\frac{1}{2})$ is $Y_{00}\,|-1\rangle$ and for $(\frac{3}{2},\ 2,\ \frac{3}{2})$ it is $5^{-1/2}(Y_{21}\,|+1\rangle+2Y_{22}\,|-1\rangle)$. (Here the $Y_{l,m}$ follow Rose's definition (1937).)

For the radial part of the wave functions we assume that the nucleons move in an oscillator potential well, so that the particle wave function is a product of three functions, corresponding to the three co-ordinates, such as

$$f_{n_x}(x)=\exp\,(-\tfrac{1}{2}kx^2)\quad H_{n_x}(\sqrt{k}x) \quad . \quad . \quad . \quad . \quad . \quad (6)$$

where k is a parameter such that $k^{-1/2}$ is of the order of magnitude of the nuclear radius, and $H_n(\xi)$ are the Hermite polynomials. In the table giving her proposed scheme for nuclear shell structure, Mayer (1949) gives the spectroscopic term and the oscillator quantum number N corresponding to each nucleon state, and we combine products of the functions (6) to give

$$\Sigma\ C_{n_x n_y n_z}\ f_{n_x}(x)\ f_{n_y}(y)\ f_{n_z}(z) \quad . \quad . \quad . \quad . \quad . \quad . \quad (7)$$

where $n_x+n_y+n_z=N$; the function (7) is the product of a radial function and a spherical harmonic corresponding to the given spectroscopic term. The radial function for the 2s states, with a corresponding spectroscopic term 2s and oscillator number 2, is

$$\left(\frac{4k^3}{9\pi}\right)^{1/4}\exp\,(-\tfrac{1}{2}kr^2)\ \ (2kr^2-3).$$

For the 1d states the oscillator quantum number is 2 and the spectroscopic term 3d, so that the radial part of the wave function is

$$\left(\frac{16}{15}\right)^{1/2}\left(\frac{k^7}{\pi}\right)^{1/4} r^2\exp\,(-\tfrac{1}{2}kr^2).$$

Thus the wave functions in (5) become

$$\left(\frac{1}{2},\ 0,\ -\frac{1}{2}\right)=\left(\frac{4k^3}{9\pi}\right)^{1/4}\exp\,(-\tfrac{1}{2}kr^2)\ \ (2kr^2-3)\ \ Y_{00}\,|-1\rangle \quad . \quad . \quad . \quad . \quad (8)$$

$$\left(\frac{3}{2},\ 2,\ \frac{3}{2}\right)=\left(\frac{16}{15}\right)^{1/2}\left(\frac{k^7}{\pi}\right)^{1/4} r^2\exp\,(-\tfrac{1}{2}kr^2)\ 5^{-1/2}(Y_{21}\,|+1\rangle+2Y_{22}\,|-1\rangle)$$

$$. \quad . \quad . \quad . \quad . \quad . \quad (9)$$

and we are now in a position to work out for this particular disintegration those matrix elements which do not require extension of the wave functions to the four-component representation, namely R_{ij} and T_{ij}.
We get

x^2	y^2	z^2	yz	zx	xy	
(1	−1	0	0	0	i)	$\times \frac{2}{\sqrt{15}k}$

so that the matrix elements R_{ij} are

$$R_{ij}= \begin{array}{c} \\ i\downarrow \end{array} \overset{\overset{j}{\longrightarrow}}{\begin{bmatrix} 1 & i & 0 \\ i & -1 & 0 \\ 0 & 0 & 0 \end{bmatrix}} \times \frac{2}{\sqrt{15}k}$$

and

	x^2	y^2	z^2	yz	zx	xy	
σ_x	0	0	0	i	1	0	$\times \frac{1}{\sqrt{15}k}$.
σ_y	0	0	0	−1	i	0	
σ_z	−2	2	0	0	0	$-2i$	

A check on these values is that the matrix elements S_{ijk} should be zero, since they forbid the spin change $0 \leftrightarrow 2$. From these values we get

$$T_{ij}= \begin{array}{c} \\ i\downarrow \end{array} \overset{\overset{j}{\longrightarrow}}{\begin{bmatrix} i & -1 & 0 \\ -1 & -i & 0 \\ 0 & 0 & 0 \end{bmatrix}} \times \frac{6}{\sqrt{15}k}.$$

In order to evaluate the matrix elements A_{ij} and $A_{ij}{}^{\beta}$, we must extend the wave functions in (8) and (9) to the four-component representation. Doing this we find that A_{ij} and $A_{ij}{}^{\beta}$ are all zero for this transition.

We evaluate now the nuclear matrix elements for the transition ${}^{99}_{43}\mathrm{Tc} \overset{\beta^-}{\rightarrow} {}^{99}_{44}\mathrm{Ru}$. From Mayer's table a plausible configuration for ^{99}Tc is:—

3 Protons in $1g_{9/2}$,

6 Neutrons in $2d_{5/2}$ (complete subshell),

giving a spin of 9/2, in agreement with the experimental value (Kessler and Meggers 1950), and for ^{99}Ru

4 Protons in $1g_{9/2}$,

5 Neutrons in $2d_{5/2}$,

giving a spin of 5/2. Thus we get a spin change of 2 units and no change in parity, conforming to second forbidden requirements. We set $J_i=9/2$, $M_i=9/2$, and sum the transitions to $J_f=5/2$, $M_f=5/2$, 3/2. (We need go no further since $\Delta M=4$ is not allowed by any second forbidden matrix

elements.) The six neutrons in $2d_{5/2}$ states in ^{99}Tc form a complete subshell and so give no contribution to the nuclear spin, and, of the three protons in $1g_{9/2}$ states, two can be paired off to give zero spin. The remaining proton is therefore in a $(\frac{9}{2}, 4, \frac{9}{2})$ state. For ^{99}Ru the 4 protons are paired off to give zero spin; for $M_f=5/2$ all the $2d_{5/2}$ neutron states are filled except $(\frac{5}{2}, 2, -\frac{5}{2})$, and for $M_f=3/2$ they are all filled except $(\frac{5}{2}, 2, -\frac{3}{2})$. We therefore evaluate the matrix elements of operator O for the two transitions, by considering

$$\int\{(\tfrac{9}{2}, 4, -\tfrac{9}{2})P\}^* OQ\{(\tfrac{5}{2}, 2, -\tfrac{5}{2})N\}\, d\tau$$

and

$$\int\{(\tfrac{9}{2}, 4, -\tfrac{9}{2})P\}^* OQ\{(\tfrac{5}{2}, 2, -\tfrac{3}{2})N\}\, d\tau.$$

For the 1g states, the oscillator quantum number is 4 and the spectroscopic term 5g, and so the wave function for the $(\frac{9}{2}, 4, -\frac{9}{2})$ state is

$$\left(\frac{128}{4725}\right)^{1/2}\left(\frac{k^{11}}{\pi}\right)^{1/4} r^4 \exp(-\tfrac{1}{2}kr^2)\, Y_{4-4}|-1\rangle.$$

For the 2d states, the oscillator quantum number is also 4 and the spectroscopic term is 4d, and so the wave function for the $(\frac{5}{2}, 2, -\frac{5}{2})$ state is

$$\left(\frac{8}{105}\right)^{1/2}\left(\frac{k^7}{\pi}\right)^{1/4}(2kr^4-7r^2)\exp(-\tfrac{1}{2}kr^2)\, Y_{2-2}|-1\rangle$$

and for the $(\frac{5}{2}, 2, -\frac{3}{2})$ state is

$$\left(\frac{8}{105}\right)^{1/2}\left(\frac{k^7}{\pi}\right)^{1/4}(2kr^4-7r^2)\exp(-\tfrac{1}{2}kr^2)5^{-1/2}(Y_{2-2}|+1\rangle-2Y_{2-1}|-1\rangle).$$

We are now in a position to evaluate the matrix elements R_{ij}, T_{ij}, S_{ijk}. For the transition to the $M_f=5/2$ state, these are :—

$$R_{ij}= \begin{bmatrix} 1 & i & 0 \\ i & -1 & 0 \\ 0 & 0 & 0 \end{bmatrix} \times \frac{C}{k},$$

C being a constant arising from the normalization factors,

$$T_{ij}= \begin{bmatrix} i & -1 & 0 \\ -1 & i & 0 \\ 0 & 0 & 0 \end{bmatrix} \times \frac{2C}{k},$$

$$\left.\begin{aligned} S_{113} &= 1 \\ S_{123} &= i \\ S_{223} &= -1 \end{aligned}\right\} \times \frac{2C}{k}, \text{ all other } S_{ijk}=0.$$

For the transition to the $M_f=3/2$ state, we get :—

$$R_{ij}=0, \quad T_{ij}=0,$$

$$\left.\begin{aligned} S_{111}&= 1 \\ S_{112}&= i \\ S_{122}&= 1 \\ S_{222}&= -i \end{aligned}\right\} \times \frac{6C}{5k}, \text{ all other } S_{ijk}=0.$$

When we extend the wave functions to the four-component representation, we find that A_{ij} and $A_{ij}{}^{\beta}$ are all zero for both transitions.

The ratios of the matrix elements which we have found are summarized in table 2. Products containing $R_{ij}{}^{\beta}$, $T_{ij}{}^{\beta}$ are found from

$$R_{ij}{}^{\beta}=-R_{ij}, \quad T_{ij}{}^{\beta}=-T_{ij},$$

and all other matrix elements and products which are not quoted are zero.

Table 2. Ratios of Matrix Elements

	$\sum_{ij} \lvert R_{ij}\rvert^2$	$\sum_{ij} \lvert T_{ij}\rvert^2$	$\sum_{ijk} \lvert S_{ijk}\rvert^2$	$\sum_{ij} R_{ij}{}^{*} T_{ij}$
$^{36}\mathrm{Cl} \xrightarrow{\beta^-} {}^{36}\mathrm{A}$	1	9	0	$3i$
$^{99}\mathrm{Tc} \xrightarrow{\beta^-} {}^{99}\mathrm{Ru}$	1	4	$\frac{96}{5}$	$2i$

It is worth adding here that, although these matrix elements have been evaluated with an explicit form of the radial wave function for the individual particles, the ratios obtained (i.e. the ratios of successive columns in table 2) are substantially independent of this form. Certainly this is true for those matrix elements which combine large components of the wave function with large components, since the same integral

$$\int_0^{\infty} R_1 R_2 r^4 \, dr$$

is involved in each case. It seems probable that the matrix elements A_{ij} would not be much affected by use of a different radial function, and indeed in cases where the final state of the disintegrating nucleon has the same radial function as the initial state, A_{ij} is completely independent of the form of the function. The integrals involved are of the form

$$\int_0^{\infty} R^2 r^2 dr, \text{ which is 1 by normalization,}$$

and

$$\int_0^{\infty} RR' r^3 \, dr = -\tfrac{3}{2} \int_0^{\infty} R^2 r^2 \, dr = -\tfrac{3}{2}.$$

The detailed forms of the tensors T_{ij}, R_{ij}, etc., would be the same no matter what radial function were used, since all elements of a given tensor would be multiplied by the same factor. This is of particular importance in scalar products such as $\sum_{ij} T_{ij}{}^{*} R_{ij}$, etc.

§ 5. Comparison with Experiment II

Much of the arbitrariness involved in fitting the theoretical correction factors on to the experimental curve is eliminated now that we have estimates for the ratios of matrix elements. The problem is now to fit

$$\lambda_1^2 f+\lambda_1\lambda_2 g+\lambda_2^2 h$$

on to an experimental curve e, where λ_1, λ_2 are constants determining the proportions in which two given interactions are mixed, f and h are the correction factors for the two interactions singly, and g is the cross correction factor; f, g and h are evaluated using the ratios of matrix elements. We have therefore to choose λ_1, λ_2 so that

$$\sum_i (\lambda_1^2 f_i+\lambda_1\lambda_2 g_i+\lambda_2^2 h_i-e_i)^2$$

is a minimum, the summation being over points on the curves. Minimization of this expression leads to two simultaneous third degree equations for λ_1 and λ_2 which would be rather difficult to solve. However, it was pointed out in § 3 that approximate linear relationships frequently exist among the coefficients of the matrix elements, and we make use of this property here by looking for a linear relationship between f, g and h, i.e. we express h in terms of f and g,

$$h=\alpha f+\beta g.$$

The problem of curve fitting then reduces to the fitting of two curves, i.e. we now make

$$\sum_i (af_i+bg_i-e_i)^2$$

a minimum, and the values of a and b, along with α and β, give us λ_1 and λ_2. In all the cases considered here, such linear relationships have been found, almost all of them accurate to within 1%.

The beta spectrum of ^{36}Cl has been measured by Wu and Feldman (1949), using a source of thickness 0·3 mg/cm^2, and they found that when the Fermi plot is corrected by (S_{ijk} shape) the result is a straight line. However, the measured spin of ^{36}Cl is 2 and so this cannot be the explanation of its spectrum. Longmire, Wu and Townes (1949) tried to fit the spectrum with a second forbidden correction factor using arbitrary values for those matrix elements which allow a spin change of 2→0. They found this impossible to do, and went on to try the effect of a combination of interactions. According to them it is possible to fit the spectrum with the combinations ST, VT or VA, but not with SA. Since then, Wu and Feldman (1951) have revised the attempt to fit the spectrum with a pure tensor interaction, and found that it is possible to do so. Similar results have recently been obtained by Fulbright and Milton (1951), whose measurement of the spectrum agrees with that of Wu and Feldman, except that they found fewer electrons at low energies.

The measurements of Wu and Feldman have been used here for comparison of theory with experiment. The process of curve fitting has been carried out for the four combinations of interactions as before and also for the tensor interaction by itself. (In this case there is only one curve for the tensor interaction.) None of the interactions gives a really close fit. Certainly the tensor interaction, ST and VA can be ruled out. The curves obtained from SA and VT are very similar and are fairly close to the experimental curve. They are shown in fig. 4 (a). However, the coefficients obtained in fitting the correction factor for S and A give imaginary values for the ratio $\lambda_S : \lambda_A$, and since we assumed these constants to be real, we cannot accept this fit. For V and T we obtain

$$\frac{\lambda_V}{\lambda_T} = \frac{2{\cdot}4}{1} \text{ or } \frac{1}{11}.$$

The corrected Fermi plot, obtained by dividing the original by the square root of the theoretical curve in fig. 4 (a), is shown in fig. 4 (b). It deviates from a straight line at low energies, but above this it is almost straight.

Fig. 4

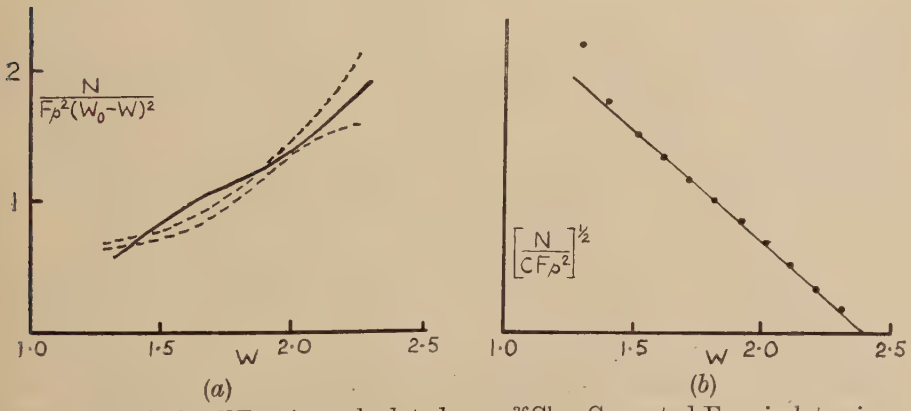

^{36}Cl. Best fit for VT, using calculated ratios for matrix elements.

^{36}Cl. Corrected Fermi plot using correction factor shown in fig. 4(a).

It is interesting to note that this deviation is in the direction which would result from source thickness distortion, and that it would be reduced using Fulbright and Milton's results.

This process has been applied also to the transition $^{99}\text{Tc} \xrightarrow{\beta^-} {}^{99}\text{Ru}$, using the ratios of matrix elements in table 2. Both SA and VT give good fits, as shown in fig. 5 (a), but the others are very poor. The ratios of the constants obtained are

$$\frac{\lambda_S}{\lambda_A} = 1{\cdot}5 \text{ or } 0{\cdot}66,$$

$$\frac{\lambda_V}{\lambda_T} = 1{\cdot}6 \text{ or } 0{\cdot}63,$$

and if we take this in conjunction with the results for ^{36}Cl and the results of § 3 we conclude that the interaction is approximately two parts of vector to one of tensor. When one considers the possibility of experimental errors, the uncertainty in the nuclear radius, and the crudeness of the nuclear model used for the evaluation of the matrix elements, the agreement between these results is very satisfactory. The corrected Fermi plot of ^{99}Tc for the V and T combination is shown in fig. 5 (*b*); it is a straight line for most of the energy range, deviating from it only at low energies, again in the way which would be caused by distortion due to source thickness.

Fig. 5

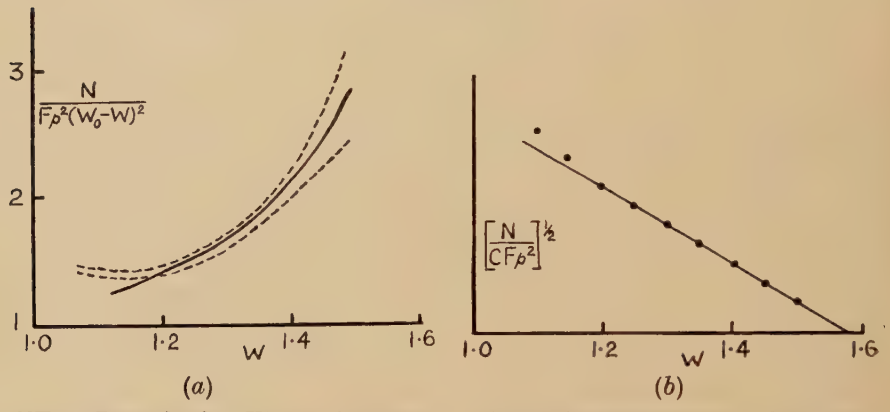

^{99}Tc. Best fit for VT or SA, using calculated ratios for matrix elements.

^{99}Tc. Corrected Fermi plot using correction factor shown in fig. 5(*a*).

§ 6. Conclusion

In recent months there has been a number of papers published in connection with a combination of the five interactions in beta-decay. Moszkowski (1951) has applied matrix elements calculated by Wigner from group-theoretical considerations to the difference in *ft* values of ^{3}H and ^{6}He, and also to the branching ratio in the decay of ^{7}Be, and obtains the result that the interaction is approximately 1 part of Fermi type (S or V) to 2 parts of Gamow-Teller type (T or A). The cross correction factors for an arbitrary degree of forbiddenness have recently been published by Pursey (1951 b). He applies his results for first forbidden transitions to several nuclei whose spectra have the allowed shape but whose *ft* values are high, and concludes that it is possible to explain these as first forbidden transitions if the interaction is mainly T with a small admixture of S or V, or mainly V with an admixture of A.

Biedenharn and Rose (1951) have shown that the assumption of real values for the λ in the invariant is no restriction on the theory.

From a detailed consideration of *ft* values for allowed transitions, Horie and Umezawa (1951) deduce that the interaction is mainly Fermi type (S or V) and that the Gamow-Teller type (T or A) is subsidiary. Finally,

Tolhoek and de Groot (1951) have proposed two principles of symmetry in consequence of which the coefficients λ in the invariant must be real and the interaction can be combinations of S, A and P only, or a combination of V and T only.

In conclusion, then, our result that the interaction is two parts vector to one of tensor disagrees with the considerations of Moszkowski and of Pursey, but agrees with those of Horie and Umezawa, and it conforms to the requirements of the symmetry principles of Tolhoek and de Groot.

Acknowledgments

The author wishes to express his thanks to Dr. C. Strachan for suggesting this problem and for many interesting and stimulating discussions. He is also indebted to Dr. F. H. C. Marriott for his advice on curve-fitting, to the University of Aberdeen for a grant to cover the cost of computational assistance, and to the Mathematics Department for computational facilities.

References

Agnew, H. M., 1950, *Phys. Rev.* [2], **77,** 655.
Albert, R. D., and Wu, C. S., 1948, *Phys. Rev.* [2], **74,** 847.
Alburger, D. E., 1950, *Phys. Rev.* [2], **78,** 629.
Biedenharn, L. C., and Rose, M. E., 1951, *Phys. Rev.* [2], **83,** 459.
Feldman, L., and Wu, C. S., 1949, *Phys. Rev.* [2], **75,** 1286.
Fierz, M., 1936, *Zeits. f. Physik,* **104,** 553.
Fraser, J. S., 1949, *Phys. Rev.* [2], **76,** 1540.
Fulbright, H. W., and Milton, J. C. D., 1949, *Phys. Rev.* [2], **76,** 1271 ; 1951, *Ibid.*, **82,** 274.
Graham, R. L., and Tomlin, D. H., 1949, *Nature, Lond.*, **164,** 278.
Hayward, R. W., 1950, *Phys. Rev.* [2], **79,** 409.
Horie, H., and Umezawa, M., 1951, *Phys. Rev.* [2], **83,** 1253.
Jensen, E. N., Nichols, R. T., Clement, J., and Pohm, A., 1952, *Phys. Rev.* [2], **85,** 112.
Kessler, K. G., and Meggers, W. F., 1950, *Phys. Rev.* [2], **80,** 905.
Konopinski, E. J., and Uhlenbeck, G. E., 1941, *Phys. Rev.* [2], **60,** 308.
Langer, L. M., and Price, H. C., 1949, *Phys. Rev.* [2], **76,** 641.
Longmire, C., Wu, C. S., and Townes, C. H., 1949, *Phys. Rev.* [2], **76,** 695.
Mayer, M. G., 1949, *Phys. Rev.* [2], **75,** 1969.
Moszkowski, S. A., 1951, *Phys. Rev.* [2], **82,** 118.
Pursey, D. L., 1951 a, *Proc. Phys. Soc.* A, **64,** 1138 ; 1951 b, *Phil. Mag.*, **42,** 1193.
Rose, M. E., 1937, *Phys. Rev.* [2], **51,** 484.
Saxon, D., and Richards, J., 1949 a, *Phys. Rev.* [2], **76,** 186; 1949 b, *Ibid.*, **76,** 982.
Siegbahn, K., 1946, *Phys. Rev.* [2], **70,** 127.
Smith, A. M., 1951, *Phys. Rev.* [2], **82,** 955.
Taimuty, S. I., 1951, *Phys. Rev.* [2], **81,** 461.
Tolhoek, H. A., and de Groot, S. R., 1951, *Phys. Rev.* [2], **84,** 150.
Townes, C. H., and Aamodt, L. C., 1949, *Phys. Rev.* [2], **76,** 693.
Warshaw, S. D., Chen, J. J. L., and Appleton, G. L., 1950, *Phys. Rev.* [2], **80,** 288.
Wigner, E., 1931, *Gruppentheorie* (Ann Arbor : Edwards Brothers).
Wu, C. S., and Feldman, L., 1949, *Phys. Rev.* [2], **76,** 693 ; 1951, *Ibid.*, **82,** 457.

XC. *The Energy Distribution of Alpha-Particles emitted from Nuclear Disintegrations*

By P. E. Hodgson
Imperial College of Science and Technology, London*

[Received June 6, 1952]

Summary

The energy distributions of the alpha-particles emitted from small nuclear disintegrations caused by the cosmic radiation in photographic emulsion have been found. These are analysed into the parts due to the light and the heavy elements of the emulsion, and the variation of nuclear temperature and effective potential barrier height with star size found for each.

§ 1. Introduction

Several investigators (Harding, Lattimore and Perkins 1949, Perkins 1950, Bernardini, Cortini and Manfredini 1950, Cortini 1950) have measured the energy distribution of the alpha-particles emitted from nuclear disintegrations in photographic emulsions exposed to the cosmic radiation. These results give the mean energy distribution averaged over stars of several numbers of tracks, or sizes. This tends to obscure any variation of the energy distribution with energy.

In this paper, the alpha-particle energy distribution is given for stars of several sizes. The contributions of the disintegrations in the light and heavy elements of the emulsion are evaluated separately, and the variation of the nuclear temperature and potential barrier height with star size evaluated for each.

§ 2. Experimental Procedure

The observations were made on disintegrations in C2 emulsion exposed horizontally to the cosmic radiation on the Jungfraujoch and processed in the usual manner. C2 emulsion was chosen rather than the more sensitive G5 so that the tracks of alpha-particles could be readily distinguished from those of protons.

The stars were classified according to their numbers of tracks and, for those of less than seven tracks, according as they had a recoil or not. A recoil is a short, thick track due to the residual nucleus. Tracks less than four microns in length were counted as recoils.

One thousand stars were examined, and the ranges of all the alpha-particles emitted from them which ended in the emulsion were recorded. The energy of each alpha-particle was found using the

* Communicated by Sir George Thomson, F.R.S.

range–energy relations of Lattes, Fowler and Cuer (1947), extrapolated when necessary to higher energies. The usual geometrical corrections to allow for those particles leaving the emulsion were applied throughout.

§ 3. Experimental Results

The energy distributions of the alpha-particles from three-, four-, and five- and six-track stars, with and without recoil fragments, are shown in figs. 1 to 6.

Fig. 1

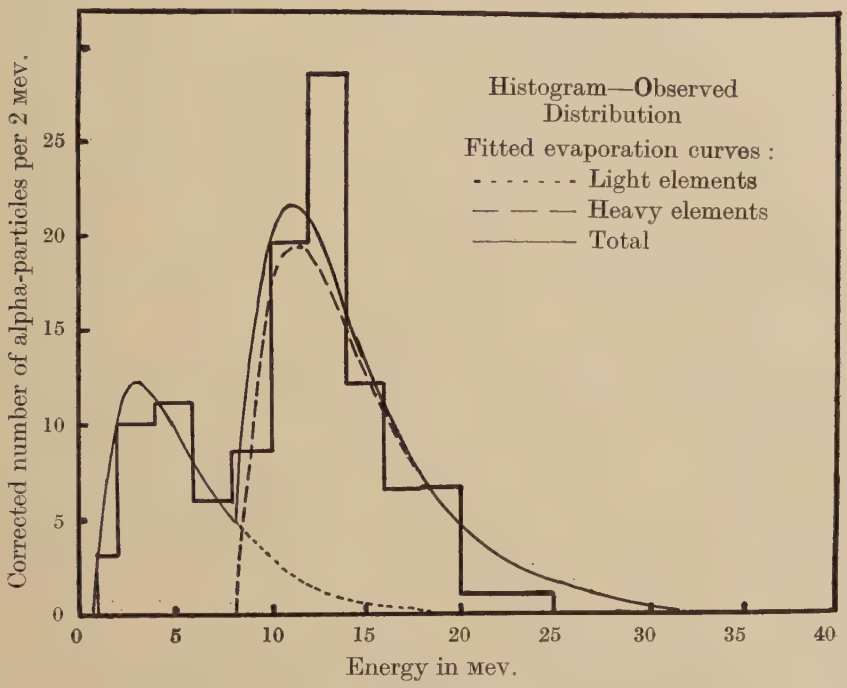

Energy distribution of alpha-particles from three-track stars with recoil fragments, together with fitted evaporation curves.

Comparison of the energy distributions for stars of the same size but with and without recoil fragments enables the contributions of the stars in light and heavy elements to be evaluated separately.

Harding (1949 b) has shown that most of the stars with recoil fragments are due to the disintegration of the heavy elements silver and bromine, while most of the stars without recoil fragments are formed in the light elements carbon, nitrogen and oxygen. There are therefore more alpha-particles from heavy elements among those from stars with recoils, and less from those without recoils, than from all stars taken together. The following procedure was used to separate the total energy distribution into its component parts due to disintegrations in the light and heavy elements. It is based on the assumptions that there are no low energy

(<8 MeV for three-track stars ; <6 MeV for four) alpha-particles emitted from heavy elements and no high-energy (>15 MeV) alpha-particles emitted from the light elements.

Fig. 2

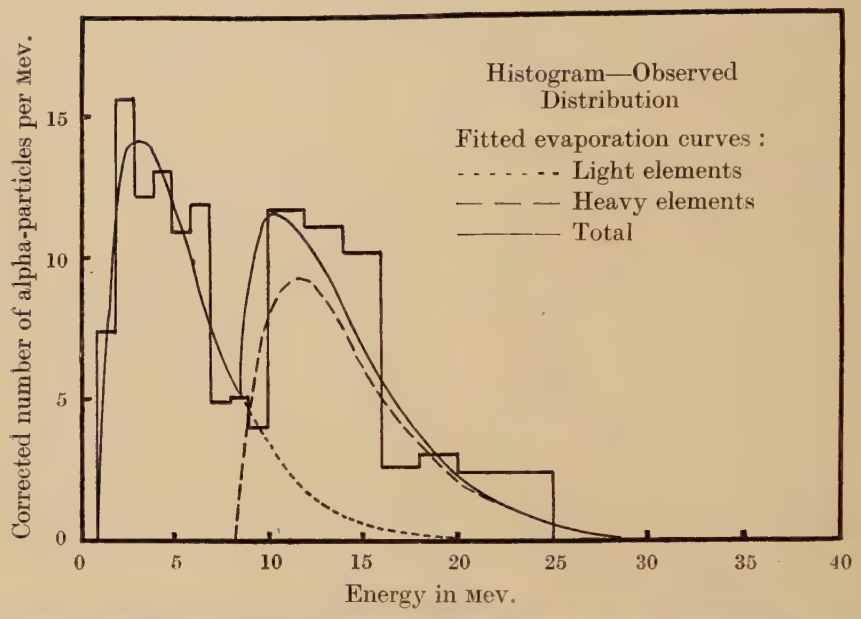

Energy distribution of alpha-particles from three-track stars without recoil fragments, together with fitted evaporation curves.

Fig. 3

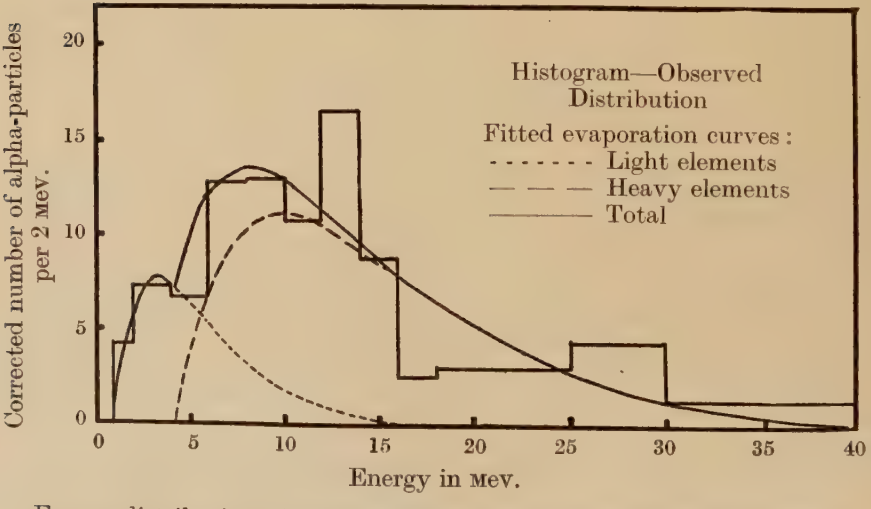

Energy distribution of alpha-particles from four-track stars with recoil fragments, together with fitted evaporation curves.

Fig. 4

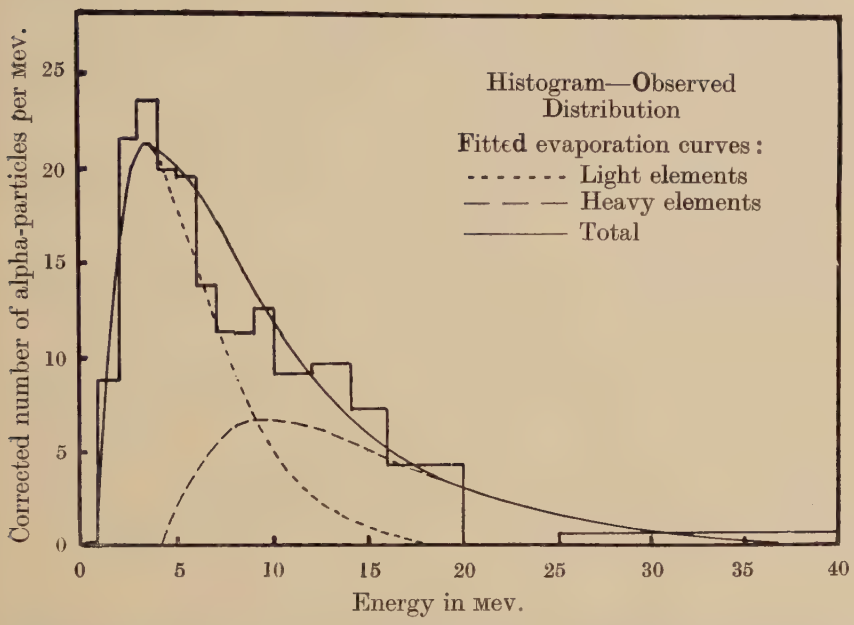

Energy distribution of alpha-particles from four-track stars without recoil fragments, together with fitted evaporation curves.

Fig. 5

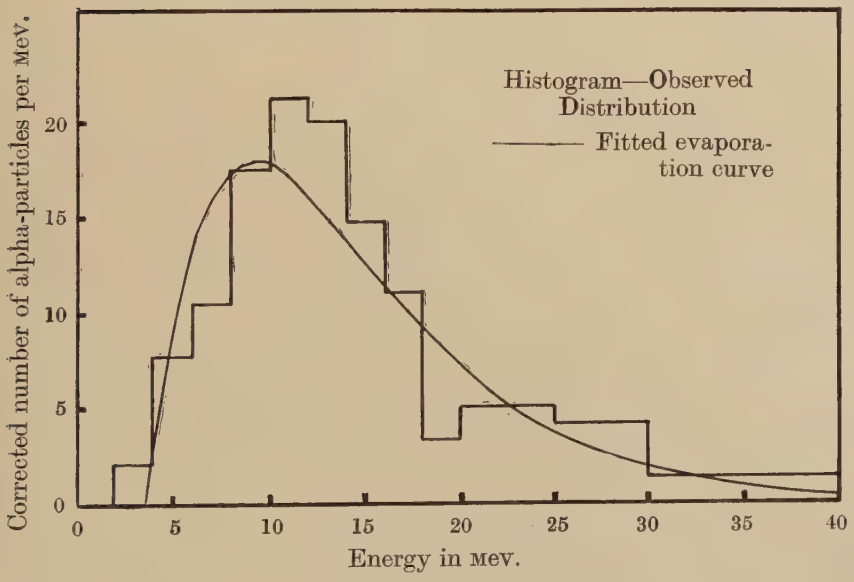

Energy distribution of alpha-particles from five- and six-track stars with recoil fragments, together with fitted evaporation curve.

The observed energy distribution for stars without recoils was in each case multiplied by the factor which made the number of particles of low energy (as defined above) equal to the number of particles in the same energy region of the corresponding distribution of particles from stars with recoils. The energy distribution of the alpha-particles from the heavy elements alone was then obtained by subtracting these two distributions. This was fitted by the best evaporation curve of the form

$$P(E)\,dE = \frac{E-V}{T^2}\exp\left(-\frac{E-V}{T}\right)dE$$

where T, the mean nuclear temperature, and V, the mean potential barrier height for the de-excitation process, are adjustable constants.

Fig. 6

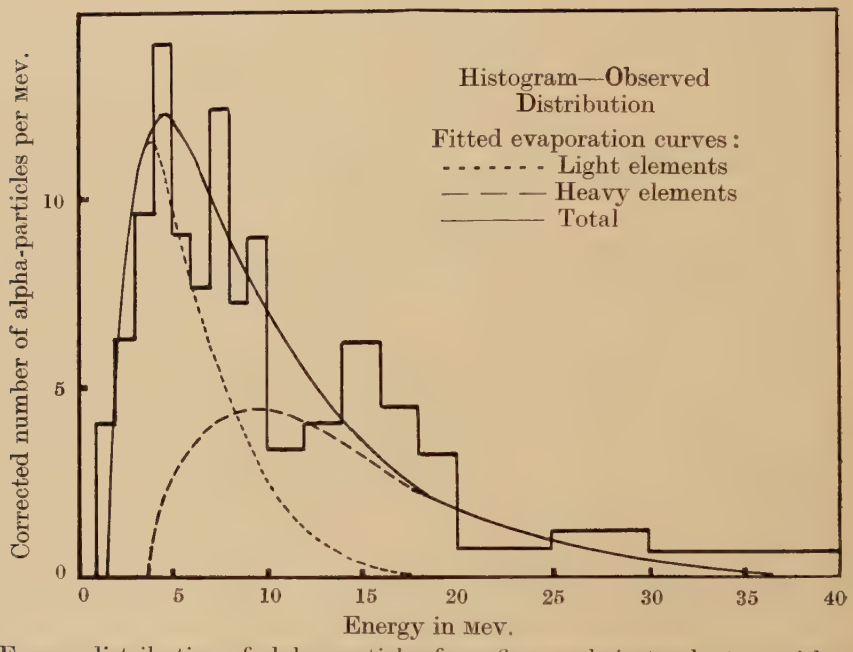

Energy distribution of alpha-particles from five- and six-track stars without recoil fragments, together with fitted evaporation curves.

The energy distribution for five- and six-track stars in heavy elements was obtained by fitting an evaporation curve directly to the distribution for stars with recoils, as it is most unlikely that any of these could have been formed in the light elements.

Owing to the small probability of an energetic alpha-particle ending in the emulsion, the correction factors of those that do are rather high. This makes the final values of T and V rather sensitive to the number of such particles in the distribution concerned. In order to minimize this effect, the distribution for energies above 20 Mev was added for all stars of three to six tracks, both with and without recoil fragments, and

divided among the individual distributions in proportion to the number of particles from heavy elements as determined from a preliminary calculation without high-energy averaging. This procedure does not invalidate the results, since Bernardini, Cortini and Manfredini showed that the distribution of the *high-energy* alpha-particles varies little, if at all, with energy. The distributions shown in the figures are as observed, but the final values of T and V were calculated using this high-energy averaging.

These energy distributions of alpha-particles from stars in heavy elements were then subtracted from the corresponding energy distributions for stars without recoils, so that the number of particles of more than

Fig. 7

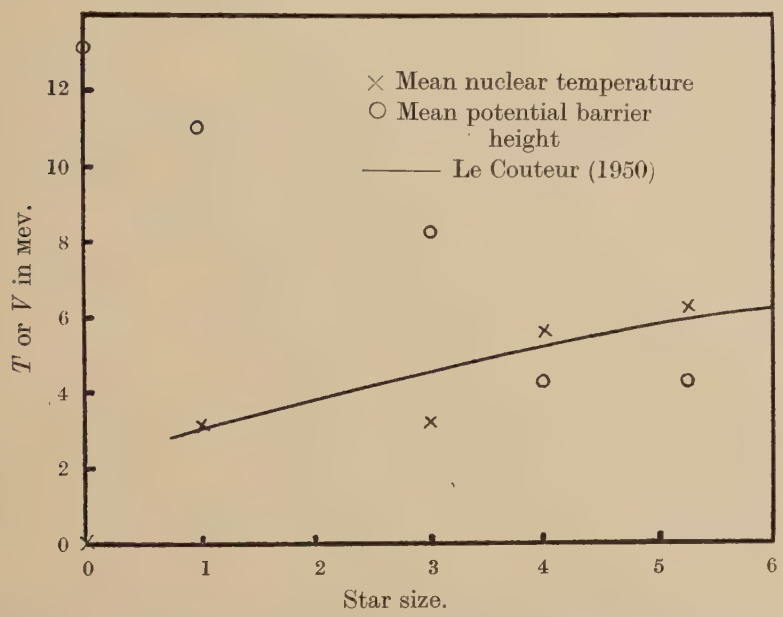

Variation of mean nuclear temperature and mean potential barrier height with star size for disintegrations of heavy elements.

15 Mev was reduced to zero. The energy distributions of the alpha-particles from the light elements obtained in this way were also fitted by evaporation curves, and the best values of T and V determined.

The evaporation curves found in this way are included in figs. 1 to 6 in each case, and the corresponding values of T and V are plotted in figs. 7 and 8 as a function of star size for the heavy and light elements respectively.

The energy distribution of alpha-particles from one-track stars formed by π^--mesons given by Menon, Muirhead and Rochat (1950) has been analysed in a similar way, and the resulting values of T and V are also plotted in figs. 7 and 8.

The alpha-particles from the disintegrations of light elements may also be found using the sandwich emulsion technique developed by Harding (1949 a). A composite emulsion consisting of alternate layers of pure gelatin and emulsion was exposed and processed. It was examined for disintegrations in the gelatin layer, which must occur in carbon, nitrogen or oxygen. Twenty-six such disintegrations, of mean size 3·65, were measured, and the energy distribution of the alpha-particles found. The values of T and V appropriate to this distribution are also plotted in fig. 8.

The values of the potential barrier height for the unexcited nuclei are interpolated from results given by Bethe (1937).

As these energy distributions were fitted by a formula having two adjustable constants, the values of T and V are subject to some uncertainty, which is estimated to be of the order of 30%.

Fig. 8

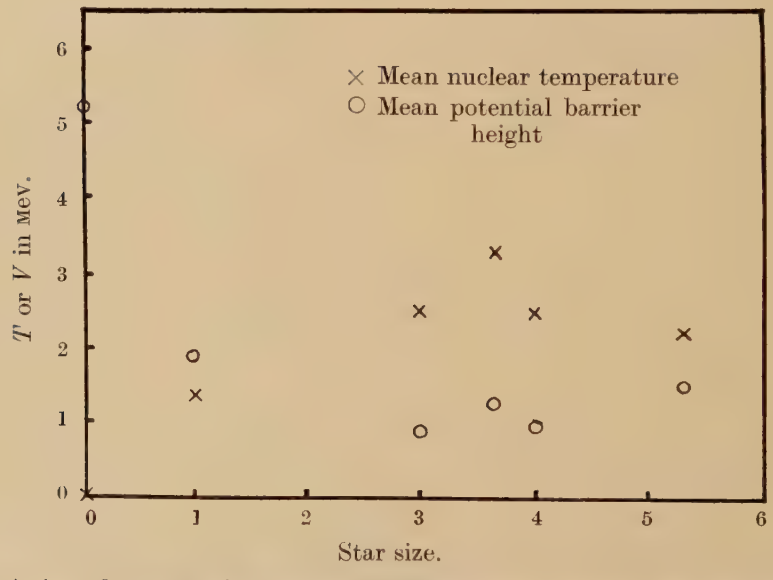

Variation of mean nuclear temperature and mean potential barrier height with star size for disintegrations of light elements.

This method of analysing the total energy distribution into its components due to disintegrations in the light and heavy elements rests on the assumption that there are no alpha-particles of less than 8 and 6 MeV emitted from three- and four-track disintegrations in heavy elements. This is, however, rather less stringent than that of Perkins (1949), who assumed that all alpha-particles of less than 10 MeV are emitted from light nuclei.

It was also assumed that there are no high-energy alpha-particles emitted from light elements. The results from the sandwich plates showed that such particles are sometimes, though rarely, emitted.

As stars of the same size are produced by particles of a range of energies, the results for each star size correspond to the mean of a wide distribution of excitation energies. This mean excitation energy, however, increases regularly with star size.

The energy distributions of the alpha-particles emitted from disintegrations of more than six tracks were also measured, and found to be in good agreement with the results of Harding, Lattimore and Perkins (1949) and of Bernardini, Cortini and Manfredini (1950).

§ 4. Discussion

The results given in figs. 7 and 8 show that, for the disintegrations of heavy nuclei, the nuclear temperature rises and the mean effective potential barrier falls with increasing star size which corresponds, on the average, to increasing excitation energy. These results are in accord with expectation, since the more highly excited a nucleus is, the higher its temperature and the more its effective potential barrier is reduced by its violent oscillations. The variation of nuclear temperature with star size is in good agreement with the calculations of Le Couteur (1950), which, however, refer to the initial temperature. But since the alpha-particles are probably emitted at the start of the disintegration, this is not much different from the mean temperature over the period of alpha-particle emission determined here.

The results for disintegrations in light nuclei show similar trends for small star sizes, but both the temperature and the barrier height appear to level off to constant values for the more energetic disintegrations. This is what would be expected if there is a limit to the excitation energy of a nucleus, and hence also to its temperature. The de-excitation of a nucleus excited to this maximum temperature results in its complete disintegration. The potential barrier is very low during the latter part of this process and so its mean value over the whole de-excitation is but a small fraction of its value for the nucleus in its ground state. This maximum excitation is only attained for the heavy nuclei at much higher energies than those investigated here.

Acknowledgments

I should like to express my thanks to Professor Sir George Thomson and Dr. K. J. Le Couteur for valuable discussions of this work.

References

Bethe, H. A., 1937, *Rev. Mod. Phys.*, **9**, 172.
Bernardini, G., Cortini, G., and Manfredini, A., 1950, *Phys. Rev.*, **79**, 952.
Cortini, G., 1949, *Nuovo Cimento*, **6**, 470.
Harding, J. B., 1949 a, *Nature, Lond.*, **163**, 440 ; 1949 b, *Phil. Mag.*, **40**, 530.
Harding, J. B., Lattimore, S., and Perkins, D. H., 1949, *Proc. Roy. Soc.* A, **196**, 325.
Lattes, C. M. G., Fowler, P. H., and Cuer, P., 1947, *Proc. Phys. Soc.*, **59**, 883.
Le Couteur, K. J., 1950, *Proc. Phys. Soc.* A, **63**, 259.
Menon, M. G. K., Muirhead, H., and Rochat, O., 1950, *Phil. Mag.*, **41**, 583.
Perkins, D. H., 1949, *Phil. Mag.*, **40**, 601 ; 1950, *Ibid.*, **41**, 138.

XCI. *Some Viscous Fluid Flow Problems I: Jet Emerging from a Hole in a Plane Wall*

By H. B. Squire
Imperial College, London, S.W.7*

[Received May 30, 1952]

Summary

An exact solution of the equations of viscous fluid flow for axially-symmetric motion is studied for a special case : this is shown to give the flow for a jet emerging from a hole in an infinite plane wall. Some examples of the calculated streamlines are given.

§1. Introduction

It was shown in a previous paper (Squire 1951) that some exact solutions of the equations of viscous fluid flow for axially-symmetric flow could be obtained by assuming that the stream function ψ is of the form

$$\psi = \nu r f(\mu) \quad . \quad . \quad . \quad . \quad . \quad . \quad . \quad . \quad . \quad (1)$$

where r, θ, ϕ are spherical polar coordinates with θ measured from the axis of symmetry (fig. 1), $\mu = \cos\theta$, and ν is the kinematic viscosity. The component velocities are $(u, v, 0)$ measured in the directions (r, θ, ϕ) respectively, and

$$\left.\begin{aligned} u &= \frac{1}{r^2 \sin\theta}\frac{\partial\psi}{\partial\theta} = -\frac{\nu}{r}f'(\mu) \\ v &= -\frac{1}{r\sin\theta}\frac{\partial\psi}{\partial r} = -\frac{\nu}{r}\frac{f(\mu)}{\sqrt{(1-\mu^2)}} \end{aligned}\right\} \quad . \quad . \quad . \quad . \quad . \quad . \quad (2)$$

These velocities are inversely proportional to the distance from the origin. It was also shown by Squire (1951) that the function f satisfies the equation

$$f^2 = 4\mu f + 2(1-\mu^2)f' + \Sigma(\mu) \quad . \quad . \quad . \quad . \quad . \quad . \quad . \quad (3)$$

where $\Sigma(\mu)$ is a quadratic function of μ whose three coefficients are arbitrary, being constants of integration of the fourth order differential equation satisfied by f. The solution for the special case $\Sigma(\mu) \equiv 0$ was studied and shown to give the flow for a jet in an infinite expanse of fluid.

A further example of the solutions of (3) is derived in the present note.

---

* Communicated by the Author.

§2. Transformation of the Equation for the Stream Function

Equation (3) can be transformed into a linear equation by a standard method such as that given by Forsyth (1929). Putting

$$f=-2(1-\mu^2)\frac{g'}{g} \quad . \quad . \quad . \quad . \quad . \quad . \quad . \quad . \quad . \quad (4)$$

and substituting in (3) gives

$$g''-\frac{\Sigma(\mu)}{(1-\mu^2)^2}g=0. \quad . \quad . \quad . \quad . \quad . \quad . \quad . \quad . \quad . \quad (5)$$

This equation is a form of the hypergeometric equation and known methods of analysis can therefore be applied. When two independent solutions g_1 and g_2 of (5) have been obtained the function f is given by Forsyth (1929)

$$f=-2(1-\mu^2)\left[\frac{g_1'+cg_2'}{g_1+cg_2}\right] \quad . \quad . \quad . \quad . \quad . \quad . \quad . \quad (6)$$

where c is a constant of integration.

§3. Solution of Equation (5) in a Special Case

If we take $\Sigma(\mu)$ to be of the form

$$\Sigma(\mu)=-(4b^2+1)(1-\mu)^2$$

where b is an undetermined constant, (5) becomes

$$g''+\frac{(4b^2+1)}{4(1+\mu)^2}g=0. \quad . \quad . \quad . \quad . \quad . \quad . \quad . \quad . \quad (7)$$

The solutions of this equation are

$$g=(1+\mu)^n$$

where

$$n=\tfrac{1}{2}\pm(-1)^{1\cdot 2}b.$$

It will appear later that b is real for the jet problem under consideration and then two (real) independent solutions of (7) are

$$g_1=(1+\mu)^{1/2}\cos M,$$

and

$$g_2=(1+\mu)^{1/2}\sin M,$$

where

$$M=b\log(1+\mu).$$

From (6) we then obtain

$$f=(1-\mu)\left[-1+2b\left(\frac{\sin M-c\cos M}{\cos M+c\sin M}\right)\right]. \quad . \quad . \quad . \quad (8)$$

§4. Jet Emerging from a Hole in a Plane Wall

We shall now show that the above solution can be applied to calculate the flow due to a jet emerging normally to a plane wall from a small hole. The wall is taken to be the plane $\mu=0$ ($\theta=\pi/2$). The boundary condition of zero velocity normal to the wall is satisfied but not the

condition of zero tangential velocity. The wall is a streamline and hence $f=0$ on $\mu=0$; also on the wall $M=0$ and hence from (8)

$$1+2cb=0.$$

Thus

$$f=\frac{(1+4b^2)(1-\mu)}{2b\cot[b\log(1+\mu)]-1}. \quad \ldots\ldots \quad (9)$$

A numerical study of (9) shows that jet flow is obtained for positive values of b up to a value for which the denominator is zero on the axis of the jet $\mu=1$ ($\theta=0$). This occurs when

$$2b\cot(b\log 2)=1$$

for which the significant root is

$$b=1{\cdot}8937.$$

Fig. 1

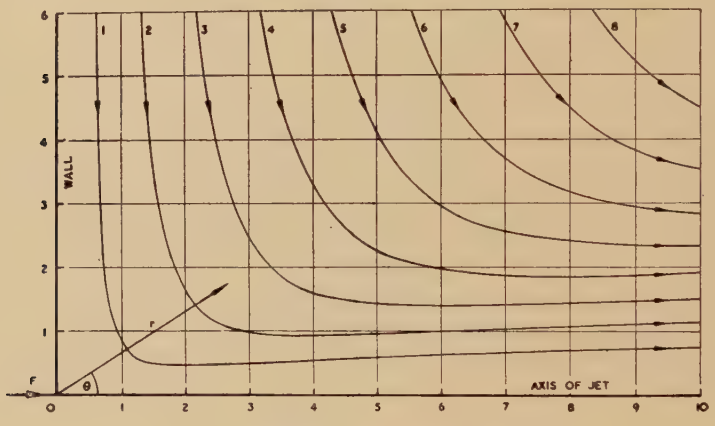

Jet emerging from hole in wall.
$b=1{\cdot}85$. $F/\rho\nu^2\approx 1{\cdot}2\times 10^3$.

The interesting cases of narrow (high speed) jets are obtained by taking values of the constant b just below this limit.

Some examples are given in figs. 1–3 which show the streamlines for the cases

$$b=1{\cdot}85, \qquad 1{\cdot}88, \qquad 1{\cdot}8937.$$

Figure 3 shows the inflow in the limiting case of a very high speed jet.

§ 5. Discussion

The flows calculated above and depicted in figs. 1–3 can be described in a general way as the fields of flow due to a jet emerging from an orifice in a wall, for a range of values of the viscosity or of the jet momentum. There is, however, zero mass flow across the wall $\mu=0$ and the flows are more accurately described as the consequence of the application of a force F at the origin acting in the direction of the resulting jet (see Squire 1951). In general the determination of the magnitude of this force is rather complicated, but in the case of the narrow jets the force

is approximately equal to the rate of change of momentum of the fluid crossing a plane parallel to the wall. The values of $F/\rho\nu^2$ determined in this way are given in figs. 1–3.

It is interesting to note that the inflow into this jet is a viscous flow and is not exactly the inflow towards a uniform line sink situated on the jet axis, which would at first sight be expected: this is clearly shown in fig. 3.

Fig. 2

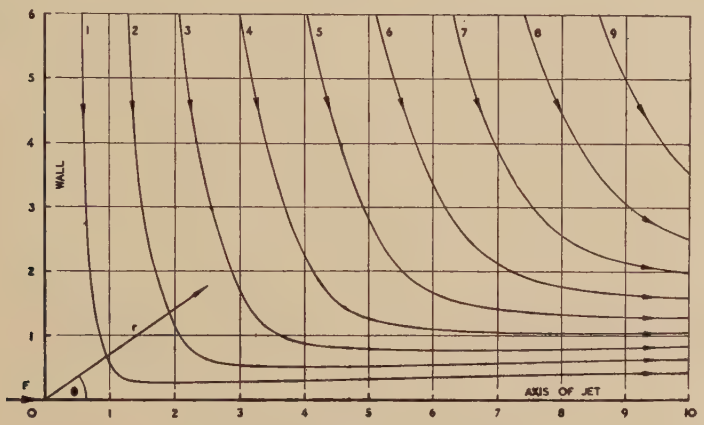

Jet emerging from hole in wall.
$b=1{\cdot}88$. $F/\rho\nu^2 \approx 3{\cdot}8\times10^3$.

Fig. 3

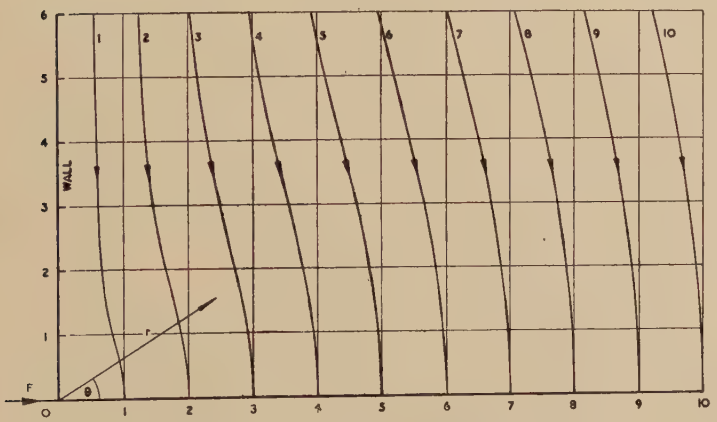

Limiting case of inflow into high speed jet.
$b=1{\cdot}8937$. $F\longrightarrow\infty$.

§ 6. Further Work

The flow due to a line sink normal to a wall with zero velocity at the wall is included among the solutions of (3) and (5); this problem is now being investigated.

References

Forsyth, 1929, *Differential Equations* (London: Macmillan), pp. 191–192.
Squire, 1951, *Quart. J. Mech. and Appl. Maths.*, **4**, 321.

XCII. *Heat Conductivity of Superconductive Lead below* 1° K

By J. L. Olsen* and C. A. Renton
Clarendon Laboratory, Oxford†

[Received June 21, 1952]

In view of the particular interest which the heat conductivity of superconductors has at very low temperatures the measurements by Mendelssohn and Rosenberg (1952) on a lead single crystal have now been extended into the range below 1° K. Measurements on tin and tantalum at very low temperatures have been reported by Daunt and Heer (1949) and Goodman (1951) but no directly observed data have so far been given. In both these cases the temperature was measured at the *ends* of the specimen by pills of compressed paramagnetic salt of high heat capacity. In order to avoid the uncertainties in interpretation involved in this method we have employed the standard procedure of measuring the temperature at two intermediate places along the specimen by means of carbon thermometers. Heat was supplied electrically at one end of the specimen while the other was thermally connected to a pill of paramagnetic salt which merely served as a heat sink.

The heating wattage was of the order of $10\,\mu$ watts. This may be compared with the heat dissipated in the thermometers which lay between $0{\cdot}1\,\mu$ watt at 1° and approximately $0{\cdot}02\,\mu$ watt at the lowest temperatures. The heat influx through the leads amounted to somewhat less than $0{\cdot}1\,\mu$ watt. The small mass of the carbon thermometers and the low specific heat of the specimen made the attainment of temperature equilibrium very rapid, and permitted reliable calibration of the thermometers. This also meant that the thermal conductivity of the specimen during a magnetic cycle could be measured without the temperature of the pill changing by more than a few hundredths of a degree between the beginning and the end of the cycle. (There is of course always some magnetic heating when a field is applied, and cooling when it is removed.)

Results

The thermal conductivity in the superconducting state is shown plotted against the temperature in fig. 1. The normal conductivity was too large to allow measurements on the same specimen, but the results of Mendelssohn and Rosenberg (1952) on this sample indicate that it would be of the order of 6 watt/degree cm at 1° K.

Figure 2 shows a logarithmic plot of the results yielding a rough proportionality of the heat conduction to T^3 between 0·4° K and 0·9° K. Above this temperature the rise becomes more rapid. If, as might be expected in the present case (Olsen 1952), the electronic scattering of the lattice vibrations is very small and if the heat conductivity is purely

* Now at the Eidgenössische Technische Hochschule, Zürich.
† Communicated by Dr. K. Mendelssohn, F.R.S.

Fig. 1

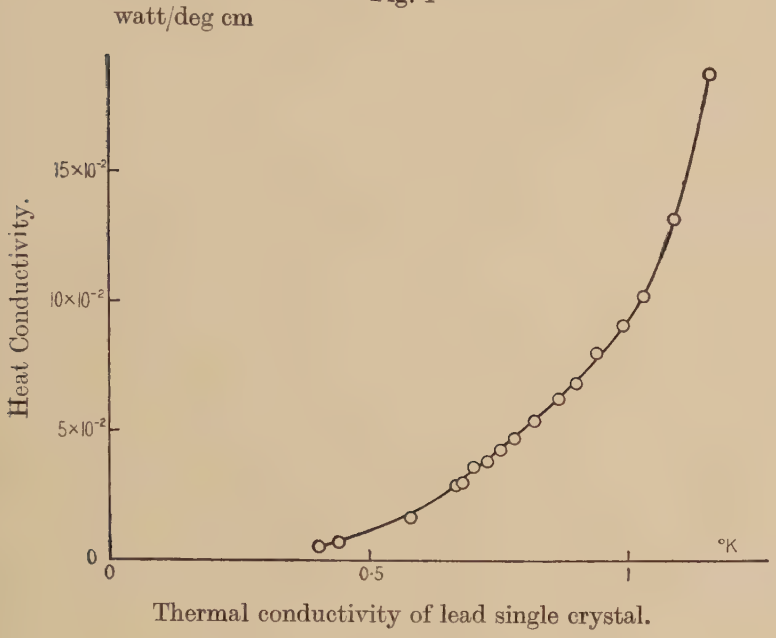

Thermal conductivity of lead single crystal.

Fig. 2

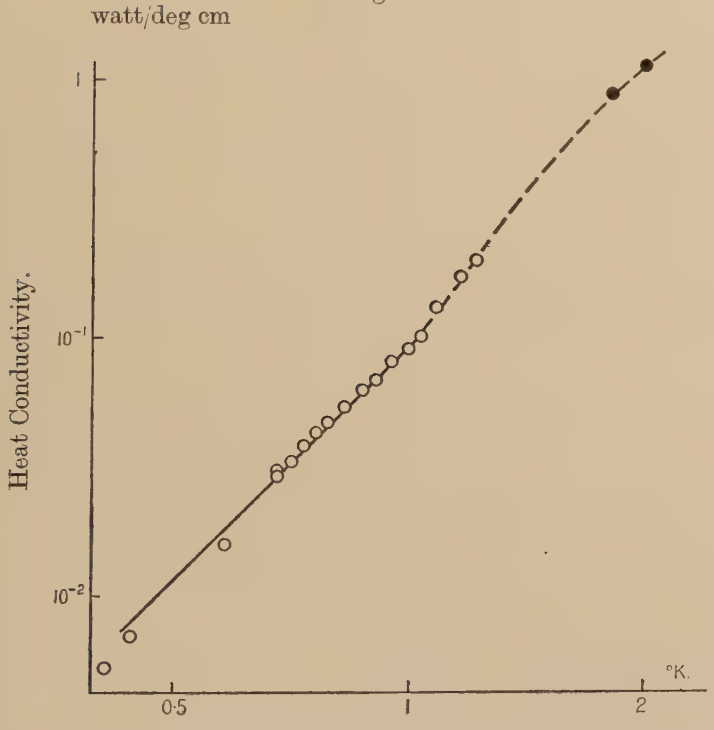

Thermal conductivity plotted against temperature on a logarithmic scale. ○ Present results. ● Results of Mendelssohn and Rosenberg (1952). Full line gives T^3 law.

due to the lattice then according to Casimir's (1938) calculation it should be equal to AT^3. However, it should be noted that the theoretical value of the constant A is five times higher than the observed one in this case.

In fig. 3 the heat resistance of the specimen in 3 magnetic cycles at temperatures of 0·43° K, 0·59° K and 1·5° K is shown. In all three cases there occurs the rise of heat resistance in the intermediate state observed earlier by Mendelssohn and Olsen (1950) and also by Webber and Spohr (1951). In the two cycles below 1° K a correction has been made for the slight temperature change caused by the application of a magnetic field to the pill.

Fig. 3

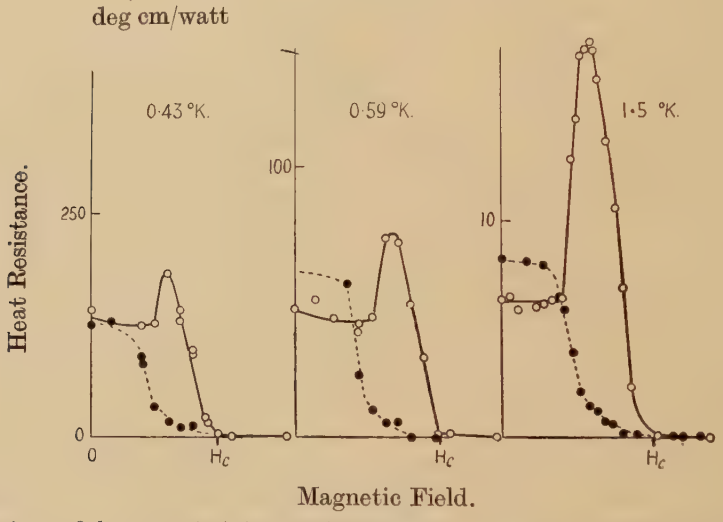

Variation of heat resistivity with magnetic field at 0·43° K, 0·59° K and 1·5° K. ○——○ Field increasing, ●– – –● Field decreasing. In all cases the heat resistance in the normal state ($H > H_c$) was too small to be measured.

Acknowledgments

We would like to thank Dr. K. Mendelssohn, F.R.S. who initiated this research for his interest and advice. We are also grateful to the Nuffield Foundation for a research fellowship allowing one of us (J. L. O.) to carry out the present work.

References

Casimir, H. B. G., 1938, *Physica*, **5**, 495.
Daunt, J. G., and Heer, C. V., 1949, *Phys. Rev.*, **76**, 854.
Goodman, B., 1951, *Int. Low Temp. Conf. (Oxford) Report.*
Mendelssohn, K., and Rosenberg, H. M., 1952, *Proc. Phys. Soc.* A, **65**, 388.
Olsen, J. L., 1952, *Proc. Phys. Soc.* A, **65**, 518.
Webber, R. T., and Spohr, D. A., 1951, *Phys. Rev.*, **84**, 863.

XCIII. *The Growth of Crystals of the Hexagonal Metals from their Vapours*

By A. J. Forty
H. H. Wills Physical Laboratory, University of Bristol*

[Received June 5, 1952]

Abstract

The techniques for preparation of well-developed growth surfaces of crystals of the hexagonal metals are described. A subsequent examination of the surfaces under the phase contrast microscope reveals growth steps which are probably monomolecular. Spiral growth hills on basal surfaces of magnesium and cadmium crystals indicate that these grow by the screw dislocation mechanism. The growth patterns on basal surfaces of zinc can only be explained by a spreading of (0001) monolayers, which are catalyzed by a foreign nucleus, probably zinc oxide. Similar nuclei incorporated in zinc crystals during growth are revealed by evaporation from the habit faces. The possibilities of performing plastic deformation experiments with these crystals are discussed.

§1. General Introduction

The concepts of the Edge Dislocation (Taylor 1934) and the Screw Dislocation (Burgers 1939) were originally proposed, on purely theoretical grounds, to account for the mechanical properties of real metal crystals. There is already considerable experimental evidence in support of the application of the concept of the screw dislocation to account for the growth of real crystals from low degrees of supersaturation (Frank 1949, 1952). The studies of growth surfaces, to be described in a later section, verify that with the possible exception of zinc, the hexagonal metals grow by the screw dislocation mechanism. This provides the first direct observation of the existence of screw dislocations in metal crystals.

Of the possible methods for preparing single crystals of these metals, growth from their vapours *in vacuo* or in an inert atmosphere is the most satisfactory for this investigation. This provides crystallographic surfaces, suitable for a sensitive microscopic examination, which are relatively free from chemical overgrowths.

A high ratio of ambient vapour pressure to equilibrium vapour pressure is necessary to nucleate stable crystals. The vapour pressures at the melting points, that is the triple point pressures, are listed for the common metals in table 1.† To nucleate crystals on the walls of a containing vessel it is generally necessary, initially, to heat a stock of metal above its melting point. The crystals are then developed at a

* Communicated by the Author.

† Note : These values are obtained from data given in the *International Critical Tables*, Vol. III.

lower supersaturation by decreasing the temperature of the stock to below its melting point. For the hexagonal metals, whose triple point pressures lie between 10^{-1} and 10^{-2} millimetres of mercury, crystal platelets can be established on cooler parts of the stock without the initial overheating. The subsequent rate of growth of the habit faces, and therefore the lateral separation of growth steps on these, depends on the degree of supersaturation close to them. This is governed by the shape of the vapour pressure curve in the region of the melting point and

Table 1. Vapour Pressures of the Common Metals at their Melting Points (p in mm Hg)

Metal	Melting Point T_M °K	$\log_{10} p$
Mn	1515	0·090
Zn	692	−0·812
Cd	594	−1·370
Mo	2895	−1·436
Fe	1800	−1·488
Ba	1123	−1·495
Ca	1083	−1·590
Mg	932	−1·597
Ag	1233	−1·838
Sb	904	−1·879
Ni	1728	−2·250
W	3660	−2·880
Au	1336	−5·197
Hg	234	−5·378
Cu	1357	−5·656
Na	370	−7·047
K	335	−7·067
Pb	600	−8·573
Sn	505	−24·307

the difference between the temperatures of the stock of subliming metal and the growing crystal. A supersaturation of about 0·001 is required for the growth steps to be easily resolved under the optical microscope ; that is, p_s/p_c must be 1·001, where p_s, p_c are the equilibrium vapour pressures of stock and growing crystal respectively. With magnesium, for example, if the stock is at a temperature of 620° c the growing crystal must be only 1/30 degree lower. It might be considered that this necessitates careful control of temperatures, but platelets several millimetres wide with surfaces true to the crystallographic plane to within about 10 seconds of arc have been grown with comparatively crude methods of heating. A very careful measurement and control of actual temperatures of the stock and growing crystals would be extremely difficult.

The essential feature of the techniques described below is the use of a single source of heat for both stock and crystals ; good crystals grow where there is a suitably small difference of temperatures between them and the stock. The constancy of temperature to be maintained by the heater depends largely on the shape of the vapour pressure curve close to the working temperature. For magnesium, a tolerance of ± 10 degrees, giving only 5% deviation in the degree of supersaturation, is permissible.

§ 2. Preparation of the Crystals

Flat hexagonal platelets of magnesium have been grown by subliming pure magnesium turnings (99·99% Mg) at 620° c in a slow stream of argon. The turnings are heated in a nickel foil liner in an electrically-heated nickel tube. Crystals, several millimetres wide, grow on the stock after about 15 hours. Those crystals growing on the outside of the stock usually have higher quality surfaces than those inside.

Zinc has a triple point pressure higher than that of magnesium. Large flat hexagonal platelets can be grown by heating small pieces of zinc rod at about 400° c for five hours in a sealed quartz tube, initially evacuated to about 10^{-3} mm·mercury. The larger crystals grow on a substrate of zinc deposited on the wall of the quartz tube when heating was commenced. If the metal is heated in a slow stream of argon at the same temperature, similar crystals can be grown in about 10 hours.

It has been found that large basal faces of zinc can be prepared by heating the metal (99·9% zinc) in argon or *in vacuo* in a quartz tube to well above its melting point. The zinc evaporates rapidly and condenses in large spherical droplets on the upper, cooler parts of the tube. When the heater is removed, the droplets cool slowly and large facets are developed on the free surfaces. These facets have a crystallographic quality comparable with that of the platelets grown directly from the vapour. It is thought that the perfection of the facets can be attributed to the freezing of a melt with a large free surface, and subsequent evaporation during the slow cooling of the solid.

Cadmium has a lower triple point pressure than zinc and consequently it is rather more difficult to grow large crystals. Flat hexagonal platelets, suitable for microscopic examination, can be grown by heating cadmium rod or turnings in a sealed, evacuated quartz tube at 300° c for 24 hours. As in the case of zinc, it is convenient, for easy nucleation of crystals, to deposit a substrate of cadmium on the walls of the tube by overheating initially. Basal surfaces of cadmium can also be developed by the droplet technique described for zinc. These are usually covered with cadmium dendrites and are unsuitable for the present investigation.

§ 3. Examination of Growth Surfaces

The flat platelets, with the basal (0001) surfaces well developed, are very suitable for examination under the optical microscope. Usually, the surfaces depart from the true crystallographic (0001) plane by only

a few seconds of arc, so that a sensitive examination under reflection, phase constrast illumination is possible. The surfaces have a high reflectivity and the silvering technique normally adopted for the observation of monolayers on other crystals is unnecessary. The crystals are seldom bigger than 2 or 3 millimetres wide and are mounted on plasticine on a stage whose tilt can be adjusted so that their surfaces are normal to the axis of the microscope. Very small steps, less than 20 Å high, can be detected only when this condition is fulfilled. Under favourable conditions of illumination, depending on the absence of light scattered from nearby coarse growth structures or other crystals, growth layers which are almost certainly monolayers have been detected.

§ 4. Growth Patterns on Magnesium Crystals

The growth steps, illustrated in the following micrographs are barely visible through the visual eyepiece of the microscope. By employing suitable photographic techniques, the forms of growth hills can usually be seen on a micrograph. The low visibility of the growth steps suggests that their height is less than 20 Å. (The phase contrast microscope used has been calibrated by measurement of visibilities of steps on silvered cleavage surfaces of mica, whose heights were measured by multiple-beam interferometry—Forty 1952.) Other considerations, such as the absence of a hollow core for the screw dislocations observed and the similar visibilities of steps in different growth hills on different crystals, indicate that the growth layers are monomolecular.

Often, after the magnesium crystals have been mounted on the plasticine for some time, the surfaces become coarsely speckled. The speckle is frequently concentrated along the edges of the monolayers giving them a visibility of practically unity under phase contrast illumination. Figure 1 (Plate LXI) is a phase contrast micrograph of a small crystal with the growth steps ' decorated ' in this striking manner ; the steps appear bright on a darker speckled background. This particular crystal had been in contact with air and plasticine for 24 hours. It is thought that the decoration is due to the creep of a film of reactive material, possibly fatty acid, from the plasticine. This might combine with magnesium oxide, which is expected to be concentrated along the edges of growth layers, to form a ridge of material at the steps. The phase contrast microscope is particularly sensitive to this form of surface singularity. The observations made on this phenomenon suggest that the exposures of the surface to both air and plasticine are critical. So far, all experiments to produce the ' decoration ' under controlled conditions by spreading films of stearic acid, oleic acid and liquid paraffin have been unsuccessful. This is not the first time that a ' decoration ' of growth steps has aided their observation. Micro-etch pits concentrated along the edges of monolayers on natural beryl (Griffin 1951) and ridges of crystalline overgrowth, probably quartz, concentrated along growth

steps on silicon carbide crystals (Vand 1951) have greatly improved their visibility.

Monolayers have been detected on about 50% of the crystals examined. It is a characteristic feature of most of the magnesium crystals that there is only one growth hill on a basal surface. In almost every case where the centre of a growth hill can be resolved, the step-line is a spiral or several spirals, centred on screw dislocations with Burgers vectors having a component normal to the basal plane. This is the first direct observation of screw dislocations in metal crystals ; with the exception of a rather abnormal example in gold (Amelinckx 1952).

Crystals growing on single screw dislocations are illustrated in figs. 1, 2, 3 (Plate LXI). The step-lines are usually curvilinear but they tend sometimes towards a trigonal shape in accordance with the symmetry of the (0001) surface.

Some growth hills consist of several parallel spiral ramps ; the step-lines terminate on a row or cluster of similar screw dislocations. Figure 4 (Plate LXII) shows a crystal growing from a cluster of co-operating screw dislocations. Figure 5 (Plate LXII) illustrates a growth hill with eleven parallel spiral step-lines centred on a row of eleven equal co-operating screw dislocations. These rows or clusters of equal screw dislocations could result from the disintegration of a large screw dislocation in the platelet. There is, however, very little conclusive evidence for the formation of large screw dislocation groups in the hexagonal metals.

Crystals growing from two or more screw dislocations of opposite hand have not been observed. There are a few examples of growth hills with step-lines in closed loops but there is no terrace at the centre ; the growth layers are probably nucleated by a speck of magnesium oxide or other foreign material in these cases. Figure 6 (Plate LXII), which illustrates such a growth hill, is also of interest because it illustrates the domination of several screw dislocations by the growth layers from the foreign nucleus.

Sometimes growth layers are nucleated from the edges or corners of the crystals. If the degree of supersaturation is high enough and the crystal contains no screw dislocations or foreign surface nuclei, then the corners of the surface are favoured sites for nucleation of layers. In some of the examples of growth from the corners, and probably in all cases of growth from the edges of the surface, contact with an adjacent crystal may be responsible for the nucleation of layers. Figure 7 (Plate LXIII) shows (0001) monolayers spreading from a corner of a platelet, while fig. 8 (Plate LXIII) illustrates nucleation from a contact with another crystal.

Usually, the pyramidal and prism faces of all the hexagonal metals are coarsely striated, but some have high crystallographic quality. Even with phase contrast illumination, growth steps cannot be detected on these. This may mean either that they are absent or that they are too small to be seen with the present equipment.

§ 5. Growth Patterns on Cadmium Crystals

These surfaces are very similar to those of magnesium crystals. Growth layers, probably about 5 Å in thickness, whose visibility is slightly less than that of monolayers on magnesium, can be detected under careful phase contrast examination. Growth hills, centred on screw dislocations or nucleated from corners and edges of the platelets have been observed. Figure 9 (Plate LXIII) shows a spiral growth hill on a cadmium (0001) surface.

§ 6. Growth Patterns on Zinc Crystals

Zinc Platelets Grown Directly from Vapour

The basal surfaces of the crystals grown *in vacuo* or in argon have similar quality except that the dark speckle which is characteristic of all zinc growth surfaces is slightly denser when the crystals are grown *in vacuo*. The speckle, probably a coarse overgrowth of zinc oxide, can be intensified by steaming the surface of a freshly grown crystal. It is often concentrated along the edges of growth layers which appear as dark irregular lines on a brighter background under phase contrast illumination. This ' decoration ' of growth steps on zinc is well illustrated by fig. 10 (Plate LXIV). This shows monolayers which are probably only 5 A thick ; no measurements have been made.

Although a large number of crystals have been examined and growth hills have been observed on many of these, there is no evidence for spiral growth of zinc. Usually, as illustrated in figs. 10, 11 (Plate LXIV), the step-lines form closed loops with a speck of material at the centre. Unlike magnesium and cadmium, there are several growth hills on each basal surface of zinc. This is a form of crystal growth from a low degree of supersaturation in which dislocations do not play a necessary role. The termination of growth steps in the surface indicates the presence of screw dislocations in the crystals but they are completely dominated by the layers from the two-dimensional growth centres.

It is well-known that thin films of crystalline zinc oxide grow on zinc metal with the basal planes of the two similar hexagonal structures in contact and with the $[10\bar{1}0]$ directions coincident. There is, however, some doubt about the exact nature of the structure of the layers of zinc oxide immediately adjacent to the zinc substrate. Early electron diffraction experiments (Finch and Quarrell 1933, 1934) indicated that these layers are deformed to account for the 20% misfit between the two lattices. This is the so-called pseudomorphic growth of zinc oxide on zinc which has been discussed in connection with some theories of crystalline overgrowth (Frank and van der Merwe 1949, Mott and Cabrera 1950). However, recent attempts (Raether 1950, Lucas 1951) with more refined electron diffraction techniques have failed to detect the pseudomorphic layers. The structure of thin films of zinc oxide, only a few monolayers thick, growing on a basal plane of zinc, appears to be undistorted ; a hexagonal network of zinc atoms in the oxide lattice with $a=3{\cdot}22$ A grows on a hexagonal network of zinc atoms in the metal lattice with $a=2{\cdot}67$ Å.

It seems likely that the growth layers observed on the basal surfaces are monolayers of zinc nucleated from small crystalline overgrowths of zinc oxide. The stock of subliming metal is a possible source of this oxide, since it is known that zinc oxide sublimes fairly easily if it is heated with zinc metal (Morse and White 1889). A zinc oxide crystal can serve as a nucleus for monolayers of zinc if it has stable size and shape and ensures coincidence of the hexagonal networks after a ' vernier repeat ' (for example, a repeat of 35 zinc atoms in the metal substrate and 29 zinc atoms in the oxide overgrowth along a common $[10\bar{1}0]$ direction). As soon as the nuclei are exhausted, others begin to operate at other parts of the surface. It follows that a quantity of crystalline zinc oxide must be incorporated randomly throughout the metal crystal. Since the c-spacing of zinc oxide exceeds that of zinc by 6%, one zinc oxide crystal can initiate at most 17 successive layers of zinc without stacking faults : but if, as it appears, several zinc oxide crystals are active as growth catalysts at the same time, it is possible for correct growth to continue, merely producing periodic incoherence between the structures of the oxide crystals and the metal. Any place where an oxide crystal is buried in the lattice will, in general, be a centre of strain.

Zinc Crystals Grown by the Slow Cooling of Free Surfaces of Droplets

The polycrystalline beads have a large number of randomly oriented facets. The appearance of hexagonal evaporation pits on most of these surfaces has identified them as basal (0001) habit faces of zinc. Some coarsely striated surfaces are obviously prism faces.

Generally, the surfaces are similar in appearance to those of the zinc platelets grown directly from the vapour. They have the characteristic speckle which often decorates the edges of monolayers. The phase contrast image of the steps shows that they form stepped valleys in the surface, probably due to evaporation. Figure 12 (Plate LXIV) shows that the step-lines form closed loops around dark hexagonal or triangular features ; these latter are probably polyhedral crystals of zinc oxide. Again, zinc evaporates from the basal surface by a two-dimensional process, catalyzed by small crystals of zinc oxide embodied in the metal. Another striking feature of the surfaces is the high density of small hexagonal or triangular pits with only one or two steps. The depths of these steps vary between about 5 and 100 Å. There are usually one or more large black clumps of material, also hexagonal or triangular in shape, at the centre of the pits (see fig. 13 (Plate LXIV) which is a phase contrast micrograph of a typical surface). It is thought that these are evaporation pits with large polyhedral crystals of zinc oxide at the centre.

§ 7. General Discussion of the Growth Patterns on the Hexagonal Metals

Of the three metals examined, screw dislocations are responsible for the growth of magnesium and cadmium crystals from their vapours, but zinc provides an interesting exception. The two-dimensional nucleation of

monolayers of zinc is probably catalyzed by crystalline overgrowths of zinc oxide. The observations of growth markings on crystals grown directly from the vapour, and evaporation markings on the polycrystalline beads show that zinc oxide crystals must be incorporated during growth. It is interesting to note that the catalysis is frequently observed only on zinc surfaces, and that zinc is the only hexagonal metal having an oxide with hexagonal structure ; magnesium and cadmium oxides are both cubic. It is difficult to understand why the growth of magnesium is not catalyzed by magnesium oxide more often, if the oxide grows with its (111) plane in contact with the (0001) plane of the magnesium substrate. The supply of oxide available during growth is probably very important.

Usually, there are only one or two screw dislocations with Burgers vectors along [0001] directions in each crystal grown from the vapour. This is expected under the conditions of slow growth. Several crystals have crystallographically perfect basal surfaces but cannot be regarded as perfect crystals because they may contain edge dislocations or screw dislocations with no [0001] component.

§ 8. Possibility of Plastic Deformation Experiments with the Hexagonal Metals

Although some deformation markings which could represent slip lines with $[11\bar{2}]$ directions in the basal surfaces of these metals have been observed, it is not easy to demonstrate that movement of screw dislocations could be responsible for these. So far, no movement of screw dislocations has been observed under very crudely applied stresses, but this is probably because other forms of deformation take place more easily. The most common of these is *bending* of the basal planes by a small angle, only a few minutes of arc according to goniometric measurements. The ridge line in the basal surface, a diffuse line under phase contrast illumination, is sometimes approximately normal and sometimes approximately parallel to an edge of the hexagonal crystals ; that is bending is along either $[10\bar{1}]$ or $[1\bar{2}1]$ directions in the basal plane. Figures 1, 4, 5 illustrate these ridges ; a theory of phase contrast imaging (Hopkins, private communication) shows that the image of a sharp ridge should be a bright, diffuse band. Sometimes the bending is produced during growth, perhaps during the final cooling ; the step-lines are then observed to be kinked across the ridges.

Acknowledgments

My best thanks are due to Dr. F. C. Frank for his interest and for many helpful suggestions. I gratefully acknowledge financial assistance from the Department of Scientific and Industrial Research.

References

Amelinckx, S., 1952, *Phil. Mag.*, **43**, 562.
Burgers, J. M., 1939, *Proc. Kon. Ned. Akad. Wet.*, **42**, 293.
Finch, G. I., and Quarrell, A. G., 1933, *Proc. Roy. Soc.* A, **141**, 398 ; 1934, *Proc. Phys. Soc.*, **46**, 148.

FORTY, A. J., 1952, *Ph.D. Thesis* (Bristol).
FRANK, F. C., 1949, *Disc. Far. Soc.*, **5** (*Crystal Growth*), 49 ; 1951, *Acta. Cryst.*, **4,** 497 ; 1952, *Phil. Mag. Supplement*, Vol. 1, No. 1.
FRANK, F. C., and VAN DER MERWE, 1949, *Proc. Roy. Soc.* A, **198,** 216.
GRIFFIN, L. J., 1951, *Phil. Mag.*, **42,** 775.
HOPKINS, H., 1952, private communication.
LUCAS, L. N. D., 1951, *Proc. Phys. Soc.* A, **64,** 943.
MORSE, H. N., and WHITE, N., 1889, *Amer. Chem. Journal*, **11,** 258.
MOTT, N. F., and CABRERA, N., 1950, *Rep. on Progr. in Physics*, **12,** 163 (London : Physical Society).
RAETHER, H., 1950, *J. Phys. Radium*, **11,** 11.
TAYLOR, G. I., 1934, *Proc. Roy. Soc.* A, **145,** 362.
VAND, V., 1951, *Phil. Mag.*, **42,** 1384.

EXPLANATION OF PLATES

All photographs are taken under reflection, phase contrast illumination, ×325.

Fig. 1

Showing a magnesium crystal containing a single screw dislocation. The step-line has been decorated by exposure to air and plasticine for 24 hours.

Figs. 2 and 3

Magnesium crystal with spiral growth hill on (0001) surface.

Fig. 4

Magnesium crystal with a growth hill centred on 13 similar screw dislocations.

Fig. 5

Magnesium crystal with a growth hill centred on 11 similar screw dislocations.

Fig. 6

Showing two-dimensional nucleation on a magnesium (0001) surface. Note the screw dislocations which are dominated by the growth layers on the right of the growth hill.

Fig. 7

Showing nucleation of monolayers from the corner of a magnesium crystal.

Fig. 8

Growth layers on magnesium nucleated from a contact with an adjacent crystal.

Fig. 9

A hexagonal platelet of cadmium with a single spiral growth hill.

Fig. 10

Showing a hexagonal platelet of zinc with several growth hills on the basal surface. The growth layers are thought to be initiated by small zinc oxide crystals at the centres of the hills.

Fig. 11

Showing another zinc crystal with several growth hills with step-lines forming closed loops.

Fig. 12

Showing monolayers on a basal surface of zinc crystal grown by the slow cooling of a droplet. The monolayers are produced by evaporation which is initiated from the crystal of zinc oxide at the centre.

Fig. 13

An evaporation pit on a basal surface of zinc revealing a polyhedral crystal of oxide.

XCIV. *A Determination of the Doppler Effect for Gamma-Rays of 4·5 and 4·8* MeV

By G. A. Jones and D. H. Wilkinson
Cavendish Laboratory, Cambridge*

[Received June 13, 1952]

Abstract

The Doppler Effect has been observed for the gamma-rays of 4·5 and 4·8 MeV emitted in cascade when alpha-particles of 958 kev are captured in ^{7}Li. The gamma-rays are detected in a NaI(Tl) crystal placed successively in forward and backward directions from the lithium target; the observed shift in energy between the two directions is $(1{\cdot}15\pm0{\cdot}12)\%$ and the theoretical first-order Doppler shift is 1·30%. It is remarked that these observations show the possibility of investigating certain gamma-ray life-times in the range 10^{-14} sec upwards.

§ 1. Introduction

It would be very surprising if gamma-rays did not show the Doppler shift. Such a shift has, indeed, been dramatically demonstrated for gamma-rays of 65 MeV from the decay of the π^0 meson in flight (Bjorklund, Crandall, Moyer and York 1950). Doppler broadening of the 478 kev gamma-ray line from ^{7}Li* has been observed by Elliott and Bell (1949) and broadening and shifting of the same line has been observed by Rasmussen, Lauritsen and Lauritsen (1949). The success of the experiments of Moon (1951) on resonant scattering of gamma-rays imply the existence of a Doppler shift for the gamma-rays of 411 kev from ^{198}Hg. Du Mond, Lind and Watson (1949) and Hedgran and Lind (1951) have observed the Doppler broadening of the annihilation line from thermalized positrons. In none of these experiments, however, is the Doppler shift itself measured for an emitter of known velocity relative to the observer. The present note describes such measurements which demonstrate that the usual first-order Doppler formula is correct to within about 10% for gamma-rays of 4·8 and 4·5 MeV emitted from a body of speed 0·008 that of light.

§ 2. Gamma-ray Source

It was desired to put in evidence as large a Doppler shift as possible using a 1 MV accelerator. Experiments such as those of Rasmussen *et al.* (1949) in which the gamma-ray is emitted from a nucleus recoiling from

* Communicated by the Authors.

the emission of a heavy particle suffer from the disadvantage that the velocity of the emitting body relative to the observer is compounded of that due to the capture of the bombarding particle and that due to subsequent emission of the product particle; unless coincidence techniques are used the velocity of the emitting body is not well defined. We therefore chose to use radiative capture in which case the momentum of the emitting body is that of the bombarding particle. The greatest shift may be obtained in the reaction $^{2}H(p\gamma)^{3}He$, but this reaction is not resonant and so the stability of the bombarding proton energy is important. We chose to examine the gamma-rays from $^{7}Li(\alpha\gamma)^{11}B$. In the range of alpha-particle energy accessible to us this reaction shows three resonances at 401, 819 and 958 kev (Bennett, Roys and Toppel 1951). Of these the highest is strongest by a factor of about five. If, then, a thick target containing ^{7}Li is bombarded with alpha-particles of energy greater than 958 kev, the initial speed of the emitting body is well-defined as 0·00825c (if we neglect for the time being the effect of all but the highest resonance) and is in the direction of the bombarding beam of alpha-particles.

§ 3. Measurements

The gamma-rays were examined with a 1-in. cube of NaI(Tl) and an E.M.I. multiplier type 6262. The resolution of this system was fair: the pulse distribution from the 660 kev gamma-ray of ^{137}Cs (strictly ^{137}Ba) had a full width at half maximum of $8\frac{1}{2}\%$ and a peak-to-valley ratio of rather better than 10 : 1 for an uncollimated source.

We found that the most frequent mode of de-excitation of the 9·27 Mev level in ^{11}B formed at the 958 kev resonance is via the level at 4·46 Mev. We have worked with the combination of 4·81 and 4·46 Mev gamma-rays; the 4·81 Mev gamma-ray is emitted first and the measured width of 6 kev of this resonance assures us that it is emitted in about 10^{-19} sec. It is probable that the cascade is of two electric dipoles and this in turn makes it probable that the life-time of the 4·46 Mev gamma-ray is about 10^{-16} (see Weisskopf 1951). Both these life-times are less than the slowing-down time of the ^{11}B—of order 10^{-13} sec.

We found that the relative abundance of the two lines is a function of the angle of observation relative to the alpha-particle beam; this demands that our angles of observation be symmetrically situated about the plane normal to the alpha-particle beam.* Our working angles were about 48° and 132° relative to the alpha-particle beam. The centre of the crystal was 5·6 cm from the target of LiOH and, when we take the average $\overline{\cos\theta}$ over the crystal, the expected shift in energy between the two positions is 1·09%.

* All the states involved in this process appear to be sharp enough to prohibit the mixing of parities necessary to give a fore–aft asymmetry.

Owing to the smallness of the effect sought we could not trust the overall stability of the detecting system during the several counting periods of about $\frac{3}{4}$ hour each needed to compile adequate statistics. Our procedure was to run for about 2 min on the gamma-rays from ^{11}B then change the amplifier gain and run for a similar period and a similar number of counts on the gamma-rays from ^{137}Cs, then back to the ^{11}B gamma-rays and so on. This gave a composite distribution of the two sets of gamma-rays ; each distribution contained about 20 runs of each sort. The change in gain of the amplifier was arranged to bring the ^{137}Cs gamma-ray peak to a level comparable with that of the ^{11}B peak but sufficiently far below it for the interesting portions of the two distributions to have a negligible effect on each other.* In this way the only element of the system on whose stability we had to rely to a high degree was the attenuator of the amplifier. In point of fact the stability of the whole system of crystal, multiplier, amplifier and kicksorter changed by only 0·3% throughout the whole experiment of 6 hours. The kicksorter was of the type described by Hutchinson and Scarrott (1951), and we would like to express our thanks to Dr. G. W. Hutchinson for his kindness in loaning it to us. Six complete runs were performed, three at each angle, forming three pairs that were compared separately.

§ 4. Results

Our procedure in analysing the results was to split each distribution into two parts : part A contained those channels that were predominantly filled with ^{137}Cs counts, and part B consisted of those channels above the ^{137}Cs peak where the effect of the latter could be ignored. No use was made of the distribution between parts A and B. The distributions were plotted logarithmically both in numbers of counts per channel and in pulse height. Part A of a run at a forward angle was then compared with part A of its companion run at a backward angle ; the two distributions were superposed on a light box and adjusted by eye until it was judged that the best fit had been attained. Each experimenter estimated that this fitting was made to about $\pm 0{\cdot}10\%$† in pulse height and the independent judgments of the two experimenters agreed to within a comparable precision. Parts B of the same two distributions were similarly and independently compared. In this way the fitting of parts A could not affect the fitting of parts B, and any possible changes in mean sensitivity throughout the two runs were eliminated. The fitting of parts B was to about $\pm 0{\cdot}15\%$. This means that the overall estimated accuracy in each measurement of the Doppler shift (ratio of energies) is about $\pm 0{\cdot}18\%$. The three shifts obtained were 1·20, 1·22 and 1·01%, giving a mean shift of $(1{\cdot}15 \pm 0{\cdot}12)\%$. We may note that the spread between these independent determinations is of the order

* That part of the ^{11}B distribution that lies beneath the ^{137}Cs peak is rather flat.

† Throughout this paper $\pm$ means probable error.

of our estimated error in making the fit. As a check we compared parts A and B of distributions taken at the same angle and the independent fittings of the two parts agreed to within the expected limits.

Figure 1 shows one of the three pairs of distributions; the scales have been adjusted according to the fitting in ordinate and abscissa of the ^{137}Cs peak, part A. It is seen that the ^{11}B peaks (peak I is due to the 4·46 MEV line, peak II to that at 4·81 MEV), part B, display a clear shift. The statistical errors may be estimated from the number of pulses involved.* Figure 2 shows an enlargement of the interesting region of part B. A further adjustment has been made between figs. 1 and 2 in ordinate only.

Fig. 1

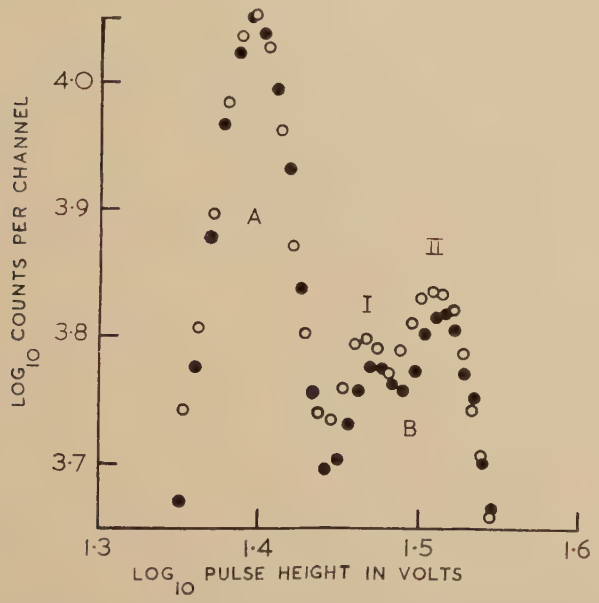

Pulse height distribution at 48° (filled circles) and 132° (open circles). Region A is principally due to ^{137}Cs, region B to ^{11}B—peak I due to 4·46 MEV line, peak II to 4·81 MEV line.

§ 5. DISCUSSION

It is clear that the Doppler shift exists and that its magnitude accords roughly with expectation. A more detailed comparison of theory and experiment is complicated by several factors. One is that the peaks of part B do not represent the whole gamma-ray energy, but are due to pair creation in which both annihilation quanta escape from the crystal.

* There is little difference between the absolute ordinate scales for the two distributions.

In this case the expected shift would not be 1·09% but rather 1·38%. However, as is shown by a study of the 4·45 Mev line from ^{12}C, a strong subsidiary peak at higher energy corresponding to the capture in the crystal of one annihilation quantum exists, whose strength of about 50% relative to the 'two-escape' peak accords with expectation. For this peak alone the expected shift is 1·22%, while for the relatively weak peak due to capture of both annihilation quanta the shift is 1·09%. When these complications are taken into account, as also the relatively small contributions from the lower resonances with smaller shifts, the expected shift for our method of fitting becomes 1·30%. This is rather larger, though not significantly so, than our experimental figure of (1·15±0·12)%, and we may consider that the Doppler effect for gamma-rays has been confirmed to within our experimental uncertainty of about 10%.

Fig. 2

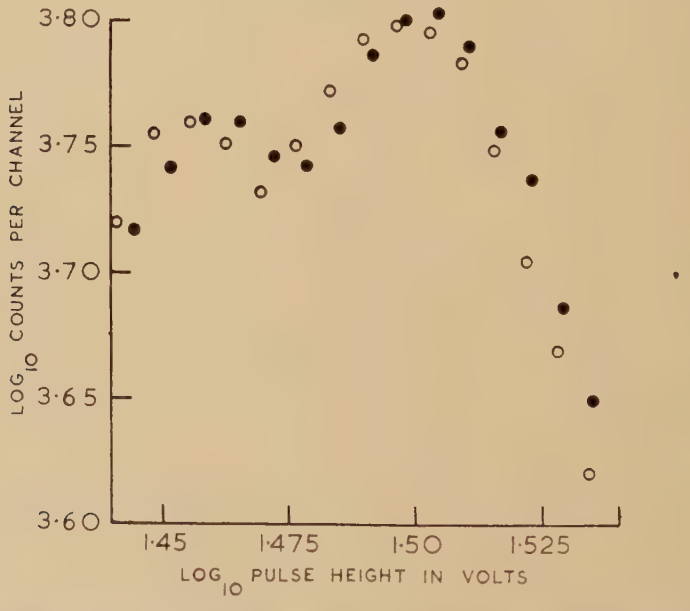

Enlargement of region B of fig. 1 with adjustment in ordinate only.

It may be noted that the sense of the discrepancy is such as would be produced by a partial slowing down of the ^{11}B before emitting the gamma-rays. However, as remarked above, we are certain that the 4·81 Mev line at any rate is emitting in about 10^{-19} sec and that there are good reasons for supposing that the life-time of the 4·46 Mev line is only about 10^{-16} sec, while the slowing down time is of order 10^{-13} sec. Furthermore we see from the figures, particularly fig. 2 that the 4·46 Mev line (peak I) is certainly shifted, and not noticeably less so than the 4·81 Mev line (peak II).

§ 6. APPLICATIONS OF THE METHOD

In addition to verifying the Doppler shift this work shows the possibility of using the technique for the determination of life-times of certain excited nuclear states. In general we must suppose that coincidence techniques must be applied, together with provision for slowing down the recoiling nuclei in a determinate time. If this can be done it will become possible to measure certain gamma-ray life-times in the range 10^{-14} sec upwards. We are at present engaged in applying this technique to the 6·14 MEV level of ^{16}O.

REFERENCES

BENNETT, W. E., ROYS, P. A., and TOPPEL, B. J., 1951, *Phys. Rev.*, **82,** 20.
BJORKLUND, R., CRANDALL, W. E., MOYER, B. J., and YORK, H. F., 1950, *Phys. Rev.*, **77,** 213.
DU MOND, J. W. M., LIND, D. A., and WATSON, B. B., 1949, *Phys. Rev.*, **75,** 1226.
ELLIOTT, L. G., and BELL, R. E., 1949, *Phys. Rev.*, **76,** 168.
HEDGRAN, A., and LIND, D. A., 1951, *Phys. Rev.*, **82,** 126.
HUTCHINSON, G. W., and SCARROTT, G. G., 1951, *Phil. Mag.*, **42,** 792.
MOON, P. B., 1951, *Proc. Phys. Soc.* A, **64,** 76.
RASMUSSEN, V. K., LAURITSEN, C. C., and LAURITSEN, T., 1949, *Phys. Rev.*, **75,** 199.
WEISSKOPF, V. F., 1951, *Phys. Rev.*, **83,** 1073.

XCV. *Energy Expenditure per Ion Pair for Electrons and α-particles*

By J. M. Valentine and S. C. Curran
Department of Natural Philosophy, The University, Glasgow, W.2*

[Received July 7, 1952]

Abstract

Work on the energy expenditure per ion pair, V, by means of end-corrected ion chambers and proportional counters is extended to include ionization by Po α-particles. The gases argon, helium, hydrogen, nitrogen, air, oxygen and methane are studied. Curves of ion current against percentage of argon admixed with the other gases are plotted and the ratio V gas/V argon determined in each case. Previous values of V obtained with electrons are discussed and small differences in the corresponding values of V in the electron and α-particle cases are noted.

Introduction

The average energy expenditure per ion pair, V, for electrons in various gases together with the ratio V gas/V argon have recently been investigated with proportional counters (Curran, Cockroft and Insch 1950, Valentine 1952). In the latter work a close agreement between the ratios V gas/V argon for slow electrons and for very energetic (340 Mev) protons (as obtained by Bakker and Segré 1951) was noted. In view of this agreement, it was decided to investigate the ionization of the same gases by Po α-particles using the same method as for electrons.

Experimental Results

The method of using end-corrected cylinders as proportional counters and ionization chambers is immediately applicable to α-particles. The source was made by dipping a thick silver foil (area $\sim \frac{1}{2}$ cm^2) into a solution of Radium D+E+F in hydrochloric acid. It was mounted on a probe running parallel to the central wire of the chamber and maintained at the voltage corresponding to its position in the field. The back of the foil was covered with 'Glyptol' sealing paint so that all the α-particles were emitted towards the central wire. The energy distribution of the α-particles was examined by using the chamber as a proportional counter. The peak obtained was symmetrical except for a slight preponderance of low energy particles making the average energy of the pulse distribution 97% of the peak energy. There are probably two causes for this energy loss, (i) finite thickness of the source, (ii) excitation of metastable states in argon; this energy would be lost in a proportional counter pulse, but detected in ion chamber operation. We deduce that the energy of

* Communicated by the Authors.

the particles, so far as it affects ionization current, may be between 97 and 100% of its known value and we adopt 98·5% as the most probable value.

An absolute value of V for argon was found by determining the count rate of the source together with the saturation ion current produced by the α-particles in argon. After a careful examination of the various factors affecting the result the value $V_A = 25{\cdot}9$ ev was obtained. Relative values of V were obtained from the ratios $V\text{gas}/V_A$, which were found for the gases, helium, hydrogen, nitrogen, air, oxygen and methane, by measuring the ratio of the saturation ion current produced in the gas to that produced in argon.

A further check on the relative values was obtained by plotting curves of ion current against percentage of argon admixed with the other gases. The numerical results are shown in table 1, columns 4 and 5, and the mixture curves in fig. 1.

Table 1

	Electrons		Po α-particles		340 MeV protons
Gas	V in ev	$V\text{gas}/V_A$	V in ev	$V\text{gas}/V_A$	$V\text{gas}/V_A$
A	27·0	1·00	25·9	1·00	1·00
He	32·5	1·20	31·7	1·22	1·17
H_2	38·0	1·41	37·0	1·43	1·38
N_2	35·8	1·32	36·0	1·39	1·31
Air	35·0	1·29	35·2	1·36	1·30
O_2	32·2	1·19	32·2	1·24	1·23
CH_4	30·2	1·11	29·0	1·12	—

Discussion and Conclusions

The absolute value of $V_A = 25{\cdot}9$ ev, obtained with Po α-particles, is in fair agreement with the value of 25·4 ev extensively used, but it is low compared with the more recent value of 28·3 ev obtained by Cranshaw and Harvey (1948). It should be noted, however, that their results on the variation of V_A with α-particle energy are in marked constrast to those of Jesse, Forstat and Sadauskis (1950). A possible source of discrepancy is discussed by Hanna (1950). Jesse *et al.* measured the total ionization using a slow recorder while Cranshaw and Harvey measured only the immediately available ionization. The latter method might miss delayed secondary electrons from metastable argon atoms and

so tend to give higher values for V. As the present work employed a total ionization method, we would expect the lower value. Indirect evidence in support of the value of $V_A = 25{\cdot}9$ ev is obtained by consideration of the values $V_{N_2} = 36{\cdot}0$ ev and V air $= 35{\cdot}2$ ev obtained using this value of V_A together with the measured ratios. These derived values are in good agreement with the recent values of $V_{N_2} = 36{\cdot}3 \pm 0{\cdot}4$ ev, V air $= 34{\cdot}7 \pm 0{\cdot}5$ ev obtained by Alder, Huber and Metzger (1947) and the value of V air $= 35{\cdot}1$ ev, for Ra C′ α-particles, quoted by Gray (1944). The ratios V gas$/V_A$ are unlikely to be much in error and a value of $V_A = 28{\cdot}3$ ev would give $V_{N_2} = 39{\cdot}5$ ev—a value higher than any obtained by recent workers.

Fig. 1

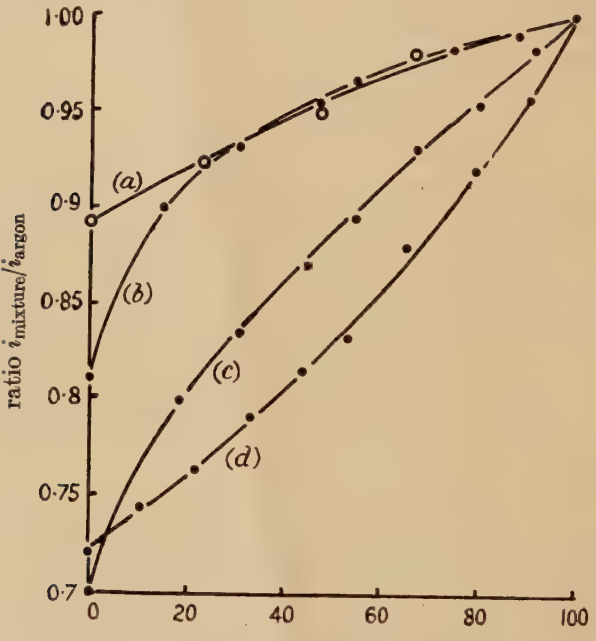

Ratio of ion currents in gas mixtures. Argon with (*a*) methane, (*b*) helium, (*c*) hydrogen, (*d*) nitrogen.

From table 1 it can be seen that the relative values obtained with α-particles are very close to those obtained with electrons except in the case of nitrogen and air. This may be due to an increase in V_{N_2} for low energy electrons. From a consideration of previous results (Valentine 1952), this increase is unlikely to take place for electrons of energy >200 ev, in contradiction with the work of Pigge (1934) but in agreement with the results of Freund (1935) and Breunig (1936).

Values of V for the various gases were first obtained, using the above technique, by Curran *et al.* (1950). Improvements in the method and the elimination of some sources of error (Valentine 1952) led to different values being observed in some cases. Table 1 summarizes the most recent values for electrons and α-particles obtained by the method and these values are considered to be more reliable than any of our earlier results. The sources of error have been carefully investigated and the values in table 1 are considered to be correct to about $\pm 2\%$.

We should like to thank Professor P. I. Dee for his close interest in this work and his valued support.

References

Alder, F., Huber, P., and Metzger, F., 1947, *Helv. phys. Acta*, **20,** 234.
Bakker, C. J., and Segrè, E., 1951, *Phys. Rev.*, **81,** 489.
Breunig, E., 1936, *Ann. Phys., Lpz.*, **25,** 467.
Cranshaw, T. E., and Harvey, J. A., 1948, *Canad. J. Res.* A, **26,** 243.
Curran, S. C., Cockroft, A. L., and Insch, G. M., 1950, *Phil. Mag.*, **41,** 517.
Freund, L., 1935, *Ann. Phys., Lpz.*, **22,** 748.
Gray, L. H., 1944, *Proc. Camb. Phil. Soc.*, **40,** 72.
Hanna, G. C., 1950, *Phys. Rev.*, **80,** 530.
Jesse, W. P., Forstat, H., and Sadauskis, J., 1950, *Phys. Rev.*, **77,** 782.
Pigge, H., 1934, *Ann. Phys., Lpz.*, **20,** 233.
Valentine, J. M., 1952, *Proc. Roy. Soc.* A, **115,** 624.

XCVI. *Intermolecular Force and Coefficient of Self-diffusion*

By B. N. Srivastava and M. P. Madan
Department of Physics, University of Lucknow*

[Received May 5, 1952]

Abstract

In this paper the Chapman–Enskog theory of non-uniform gases, as applied to the phenomenon of self-diffusion, has been utilized to evaluate the intermolecular force constants. The collision integrals occurring in the Chapman–Enskog formula for self-diffusion, as evaluated by Hirschfelder, Bird and Spotz by assuming the 12 : 6 power form of the Lennard-Jones potential function, have been used. The temperature variation of self-diffusion has been utilized to obtain the constant ϵ of the Lennard–Jones function, which represents the maximum negative energy of interaction of two molecules. The intermolecular separation r_0 for zero interaction energy occurring in the same potential function has been calculated by actual substitution. The recent data on self-diffusion as reported by Winn, Winter and others have been used to obtain these constants and the values compared with those given by Hirschfelder *et al.* from viscosity and virial coefficient data.

§1. Introduction

In the kinetic theory of gases a quantity of great interest is the coefficient of self-diffusion, which is a measure of the rate at which a group of gas molecules diffuses into another group composed of identical molecules. Naturally it is not possible to follow the motion of individual molecules possessing no features distinguishing them from the other molecules of the gas, and hence no direct determination of the coefficient of self-diffusion could be made until recently. The only method available was an indirect one given by Lord Kelvin (1904) in which the coefficient of self-diffusion was evaluated by working with different triads of gases including the gas in question. Recently however, two important methods have been developed for measuring self-diffusion, in which, rigorously speaking, the inter-diffusion coefficient between two isotopes of the same substance is actually measured and this is taken to be equal to the self-diffusion coefficient of the gas. If the tracer isotope is a stable one, then the diffusion process is observed with a mass spectrometer ; while if it is a radioactive isotope, the usual methods of detecting radioactivity provide a means of measuring the diffusion. In this way quite a large amount of data on self-diffusion at different temperatures have been

* Communicated by the Authors.

reported by a number of workers in recent years. It is the purpose of this paper to calculate the intermolecular force constants by utilizing these data and comparing the results thus obtained with previous determinations by other methods which are however for naturally occurring isotopic mixtures.

§ 2. Formulae and Method of Calculation

The inter-diffusion of gases in general depends on the force fields of the diffusing molecules. Expressions for the coefficient of diffusion in terms of the interaction potential between the molecules have been derived by Chapman and Enskog and are as follows (Chapman and Cowling 1939) :—

The first approximation to the coefficient of diffusion is

$$[D_{12}]_1=3E/2nm_0, \quad . \quad . \quad . \quad . \quad . \quad . \quad . \quad . \quad (1)$$

and the second approximation is

$$[D_{12}]_2=[D_{12}]_1/(1-\Delta), \quad . \quad . \quad . \quad . \quad . \quad . \quad . \quad (2)$$

where

$$\Delta=5(C-1)^2\frac{P_1n_{12}+P_2n_{21}+P_{12}}{Q_1n_{12}+Q_2n_{21}+Q_{12}}$$

and

$$P_1=M_1{}^3E/(\mu_1)_1$$

$$P_{12}=3(M_1-M_2)^2+4M_1M_2A$$

$$Q_1=[M_1E/(\mu_1)_1](6M_2{}^2+5M_1{}^2-4M_1{}^2B+8M_1M_2A)$$

$$Q_{12}=3(M_1-M_2)^2(5-4B)+4M_1M_2A(11-4B)+2E^2M_1M_2/(\mu_1)_1(\mu_2)_1$$

with similar relations for P_2 and Q_2 ; and

$$m_0=m_1+m_2, \qquad M_1=m_1/m_0, \qquad M_2=m_2/m_0,$$

$$n_0=n_1+n_2, \qquad n_{10}=n_1/n_0, \qquad n_{20}=n_2/n_0,$$

$$n_{12}=n_1/n_2, \qquad n_{21}=n_2/n_1,$$

where the m's are the masses of the gas molecules and n's their number densities. $(\mu_1)_1$ and $(\mu_2)_1$ are the first approximations to the viscosities of the two components, given by $5kT/8\Omega_2{}^{(2)}$ in each case ; the quantities A, B, C and E are functions of the collision integrals given by

$$A=\Omega_2{}^{(2)}/5\Omega_1{}^{(1)} ; \qquad B=[5\Omega_2{}^{(1)}-\Omega_3{}^{(1)}]/5\Omega_1{}^{(1)},$$

$$C=2\Omega_2{}^{(1)}/5\Omega_1{}^{(1)}, \quad \text{and} \quad E=kT/8M_1M_2\Omega_1{}^{(1)},$$

and the various collision integrals $\Omega_n{}^{(l)}$ refer to the interaction of a molecule of component 1 with one of component 2. Δ is a small correction so that $[D_{12}]_2$ rarely differs from $[D_{12}]_1$ by more than 1%, which is within the limits of experimental error. We shall therefore take $[D_{12}]_1$ to be equal to the experimentally determined values of the diffusion coefficient. The first approximation $[D_{12}]_1$ depends only on encounters between molecules of opposite type and thus to a first approximation, encounters between like molecules do not affect diffusion.

The collision integrals $\Omega_n^{(l)}$ occurring in the above formulae depend upon the form of the intermolecular potential function. As already discussed by Buckingham (1938) and others, the interaction energy between two molecules for a separation r is best represented by the Lennard-Jones equation of the form

$$E(r)=4\epsilon[(r_0/r)^{12}-(r_0/r)^6], \quad . \quad . \quad . \quad . \quad . \quad . \quad . \quad (3)$$

where r_0 is the separation for which energy of interaction is zero and ϵ is the energy difference between the separated molecules and the molecules in the configuration for which they have the maximum negative energy. Hirschfelder, Bird and Spotz (1948) have carried out the numerical evaluation of the collision integrals $\Omega_n^{(l)}$ for this form of the interaction potential function and have tabulated the values of the functions $W^l(n\ ;\ x)$ which are related to the $\Omega_n^{(l)}$ of Chapman and Cowling by

$$\Omega_n^{(l)}=r_0^2(2\pi kTm_0/m_1m_2)^{1/2}W^l(n\ ;\ x),$$

where $x=\epsilon/kT$.

Hirschfelder *et al.* on the basis of the Chapman-Enskog theory give for the diffusion coefficient the expression

$$[D_{12}]_1=\frac{0{\cdot}00092916T^{3/2}[(M_1+M_2)/M_1M_2]^{1/2}}{p(r_{12})^2W^1(1\ ;\ kT/\epsilon_{12})}, \quad . \quad . \quad . \quad (4)$$

in which D_{12} is the coefficient of diffusion in $cm^2\ sec^{-1}$, p is the pressure in atmospheres and M_1, M_2 represent, here, the molecular weights, and $W^1(1\ ;\ kT/\epsilon_{12})$ is a slowly varying function of kT/ϵ_{12}. Equation (4) is readily deduced from eqn. (1). It is obvious from the above equation that $T^{3/2}/[D_{12}]_1$ will obey the same variation with temperature as $W_1{}^1$ *provided* r_{12} *is assumed to be constant.* It is therefore possible to evaluate ϵ_{12} (provided it is assumed to be constant) from the observed temperature variation of $T^{3\ 2}/[D_{12}]_{exp} \simeq T^{3/2}[D_{12}]_1$ and from this value of ϵ_{12}, the value of $r_{0(12)}$ the zero-energy intermolecular separation for molecules 1 and 2 can be found by actual substitution in eqn. (4).

This procedure is adopted below for oxygen, nitrogen, argon, neon, carbon dioxide and methane, for which the data for variation of self-diffusion coefficient with temperature are given by Winn (1947, 1948, and 1950), Winter (1951), Hutchinson (1949), Groth and Sussner (1944) and Harteck and Schmidt (1933). The data of Winn give D_{11} which is calculated from the relation (as shown by Hutchinson)

$$D_{11}=[2M_2/(M_1+M_2)]^{1/2}[D_{12}]_{exp},$$

where M_1 and M_2 are the molecular weights of the two isotopes. His data have therefore been reconverted to give $[D_{12}]_{exp}$ for the diffusion of one isotope into the other which is the quantity actually measured by him. In order to determine ϵ_{12}, the following procedure was adopted :

Hirschfelder's tables were utilized to give a plot of $W_1{}^1$ against kT/ϵ, from which a second graph was plotted for $[W_1{}^1]_2/[W_1{}^1]_1$ against various initial values of $[W_1{}^1]_1$ for a given ratio of $[kT/\epsilon]_2/[kT/\epsilon]_1$, the suffixes 1, 2

outside the square brackets refer to temperatures T_1 and T_2. Such graphs were plotted for the values 1·5, 1·8, 2·0, 2·5 and 3 of the ratio $[kT/\epsilon]_2/[kT/\epsilon]_1$ and are given in fig. 1. Then a graph of $T^{3/2}/[D_{12}]_{exp}$ was plotted against T (fig. 2) which served to check the accuracy of the experimental data and further gave us a number of additional points

Fig. 1

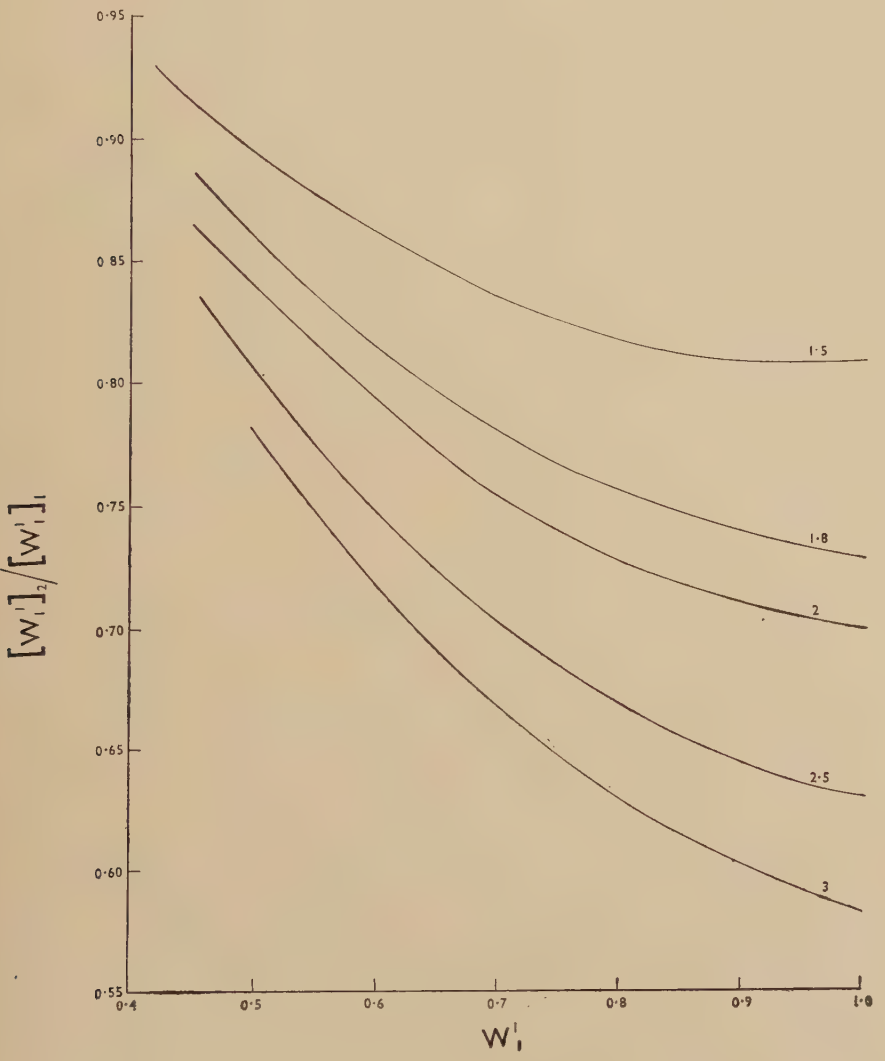

for calculation. From the $T^{3/2}/[D_{12}]_{exp}$ versus T graph, values for $[T^{3/2}/(D_{12})_{exp}]_2/[T^{3/2}/(D_{12})_{exp}]_1$ for the various ratios of kT/ϵ were calculated at a number of initial temperatures from the graph and for each calculated value of $[T^{3/2}/(D_{12})_{exp}]_2/[T^{3/2}/(D_{12})_{exp}]_1$ the corresponding value of $W_1{}^1$ was read from the appropriate ratio graph of $[W_1{}^1]_2/[W_1{}^1]_1$. From this

value of W_1^1 the corresponding initial value of kT_1/ϵ was read from W_1^1 versus kT/ϵ graph. Knowing the initial temperature which we took for $[D_{12}]_{exp}$ on $T^{3/2}/(D_{12})_{exp}$ graph the constant ϵ was obtained by simple substitution. In this way a number of values were obtained for ϵ_{12} and the arithmetic mean calculated.

Fig. 2

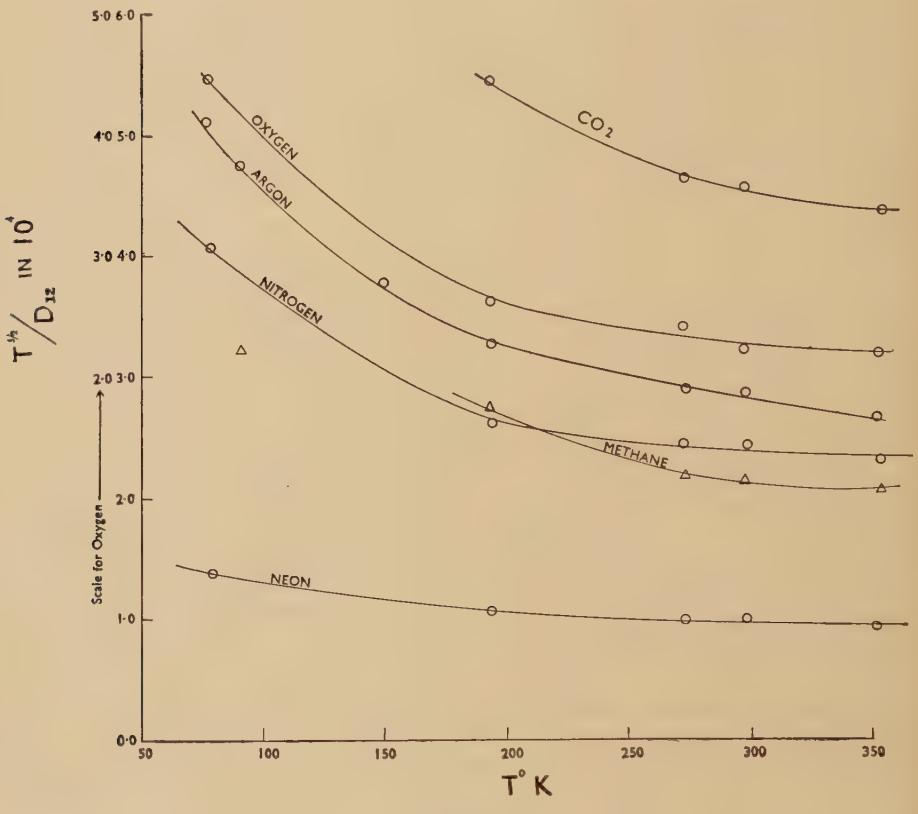

§ 3. Results

The observed data, mostly of Winn (1950), are plotted in fig. 2 for argon, neon, oxygen, nitrogen, carbon dioxide and methane. For argon the ratio $[T^{3/2}/(D_{12})_{exp}]_2/[T^{3/2}/(D_{12})_{exp}]_1$ calculated from $T_2/T_1=x_1/x_2=1{\cdot}5$ at initial temperatures 192° K and 204° K comes out to be 0·869 and 0·875 respectively; and for $x_1/x_2=2$ at initial temperature 90° K, it comes out to be 0·711; for $x_1/x_2=2{\cdot}5$ at initial temperatures 90° K and 105° K it comes out to be 0·646 and 0·667. Similarly for $x_1/x_2=3$ at temperatures 90° K and 105° K it comes out to be 0·611 and 0·633. These being read on the respective $[W_1^1]_2/[W_1^1]_1$ graphs yield for the ratio 1·5 the values for W_1^1 as 0·580 and 0·562; for the ratio 2 the value is 0·890; for the ratio 2·5 the values for W_1^1 are 0·882 and 0·80 and for the ratio 3 the values are 0·865 and 0·785. These by reference to the W_1^1 versus kT/ϵ graph

gave the values for ϵ_{12}/k as 117·1, 118·5, 130·4, 131·3, 128·6, 127·3 and 125·0 giving the mean value 125·5. Using these values of ϵ_{12} the corresponding $r_{0(12)}$ values as calculated from eqn. (4) came out to be 3·435,

Table 1

Argon			Neon		
Temp. Range °K	ϵ/k	r_0 in Å	Temp. Range °K	ϵ/k	r_0 in Å
90–180	130·4	3·331			
90–225	128·6	3·346	75–187·5	44·9	2·682
90–270	125·0	3·378	75–225	49·7	2·630
105–262·5	131·3	3·371	84–168	46·2	2·699
105–315	127·3	3·403	90–180	53·7	2·634
192–288	118·5	3·423	90–270	51·7	2·650
204–306	117·1	3·435			
Mean	125·5	3·384	Mean	49·2	2·659

Oxygen			Nitrogen		
Temp. Range °K	ϵ/k	r_0 in Å	Temp. Range °K	ϵ/k	r_0 in Å
114–342	129·5	3·271	75–187·5	101·4	3·436
135–337·5	110·6	3·342	75–225	100·0	3·455
150–270	130·4	3·198	90–225	112·6	3·395
150–300	118·1	3·287	90–270	103·5	3·510
165–297	117·9	3·198	120–300	102·6	3·519
165–330	108·6	3·263	150–300	94·3	3·551
Mean	119·2	3·260	Mean	102·4	3·478

Carbon dioxide			Methane		
Temp. Range °K	ϵ/k	r_0 in Å	Temp. Range °K	ϵ/k	r_0 in Å
180–360	145·2	4·135	196–352·8	176·6	3·593
195–351	147·7	4·124	220–330	157·2	3·617
210–315	156·7	4·063	224–336	138·2	3·678
225–337·5	146·1	4·122	228–342	144·5	3·703
Mean	148·9	4·111	Mean	154·1	3·648

3·423, 3·331, 3·371, 3·346, 3·403 and 3·378, giving the mean value as 3·384 in Å.U. A similar procedure was adopted for other gases also.

The ϵ_{12} and $r_{0(12)}$ values thus obtained are given in table 1 for the gases investigated, together with the temperature ranges for which they have been calculated. These results are compared in table 2 with those of Hirschfelder and others from data on viscosity and virial coefficients.

Table 2

Gases	From self-diff.		From Viscosity*		From virial coeff.*		From Viscosity†			
							Low temp.		High temp.	
	ϵ/k	r_0	ϵ/k	r_0	ϵ/k	r_0	ϵ/k	r_0	ϵ/k	r_0
Argon	125·5	3·384	124·0	3·418	119·5	3·41	112·0	3·483	126·2	3·414
Neon	49·2	2·659	35·7	2·80	35·7	2·74	41·0	2·769	—	—
Oxygen	119·2	3·260	113·2	3·433	117·5	3·58	112·7	3·435	134·9	3·325
Nitrogen	102·4	3·478	91·46	3·681	95·9	3·72	89·8	3·687	117·1	3·537
CO_2	148·9	4·111	190·0	3·996	185·0	4·57				
Methane	154·1	3·648	136·5	3·822	142·7	3·81				

* Hirschfelder *et al.* (1948). † Srivastava and Madan (1952).

§ 4. Discussion of Results

For an exact evaluation of ϵ the accuracy required in the measurement of D_{12} is too high to be realized experimentally. The experimental error in D_{12} is usually of the order $\pm 1\%$ which would produce an error of about $\pm 15\%$ in the value of ϵ. Thus the value of ϵ as determined from measurements of self-diffusion can be taken to be correct to $\pm 15\%$.

For neon, it will be seen from table 2 that the value of ϵ from self-diffusion is higher than that calculated from viscosity. It may be remarked that the neon molecule is known to be much harder and it is possible that this discrepancy might be due to that cause.

For nitrogen and carbon dioxide the observed deviations may be due to insufficient data at low temperatures.

It is seen from table 1 that in the small range of temperatures over which diffusion measurements have been made there is no systematic change in the values of ϵ_{12} and $r_{0(12)}$ as the temperature is progressively increased. This shows that an equation of the form (4), with the intermolecular potential as given by (3), is fully confirmed by the existing data and is a simultaneous verification of the Chapman–Enskog theory and the Lennard–Jones form of the intermolecular potential function.

It may be remarked that values of ϵ from viscosity and virial coefficients refer to the normal gases and may thus be taken to apply to the most abundant isotope (or in the case of neon to the normal mixture).

Theoretical considerations seem to show that it is unlikely that there will be any measurable difference between the coefficient of self-diffusion for the most abundant isotope, and the coefficient of inter-diffusion for that isotope and any other. It is therefore not possible to say whether the slight differences found here between the values calculated from self-diffusion data and from viscosity data are due to experimental errors or due to an actual difference between the two isotopes.

The foregoing calculations are based on the assumption that both ϵ and r_0 are constants. The consequences of their variation with temperature are being investigated and will be reported later.

We record our thanks to the Uttar Pradesh Government for the award of a research grant.

References

Buckingham, R. A., 1938, *Proc. Roy. Soc.* A, **168,** 264.
Chapman, S., and Cowling, T. G., 1939, *The Mathematical Theory of Non-uniform gases* (Cambridge : University Press).
Groth, W., and Sussner, E., 1944, *Z. phys. Chem.*, **193,** 296.
Harteck, P., and Schmidt, H. W., 1933, *Z. phys. Chem.* B, **21,** 447.
Hirschfelder, J. O., Bird, R., and Spotz, E. L., 1948, *J. Chem. Phys.*, **16,** 968.
Hutchinson, F., 1949, *J. Chem. Phys.*, **17,** 1081.
Kelvin, Lord, 1904, *Baltimore Lectures*, p. 295 (London : C. J. Clay & Sons).
Srivastava, B. N., and Madan, M. P., 1952, under publication.
Winn, E. B., 1947, *Phys. Rev.*, **72,** 77 ; 1948, *Ibid.*, **74,** 698 ; 1950, *Ibid.*, **80,** 1024.
Winter, E. R. S., 1951, *Trans. Faraday Soc.*, **47,** 342.

XCVII. *Plastic Deformation Features on Cleavage Surfaces of Metal Crystals*

By J. Holden
Royal Holloway College, University of London*

[Received May 6, revised June 15, 1952]

Abstract

Surface measurements are made upon kink bands, twin bands and bend planes produced in specimens cleaved from single crystals. The microscopic structure of kink bands is illustrated, while the method used to determine the twinning elements indicates relations in the shape of the twinned region. Polygonization structures produced by inhomogeneous deformation followed by annealing are illustrated interferometrically and related to growth features found in metal crystals. In the case of hexagonal close-packed crystals, deformed by glide, a type of deformation band structure of the active glide plane is illustrated.

§ 1. Introduction

The methods of interferometry (Tolansky 1946), can be applied to the measurement of the topography of deformation structures found upon metal surfaces in those cases where a high degree of perfection of the surface can be attained initially. In the case of the metals which possess good cleavage properties the surface revealed by cleaving at liquid air temperatures fulfills this requirement well; furthermore this surface is of particular interest in plastic deformation studies since the plane of good cleavage is also, in most cases, the prominent glide plane. A recent review of the deformation processes of zinc crystals (Jillson 1950), has drawn attention to the variety of markings found upon the cleavage surfaces of that particular metal. An introductory survey of the structure of markings found on the cleavage planes of Zn, Mg, Bi and Sb crystals is made in the present paper, the quantitative methods of interferometry being of particular use in classifying the markings observed on the cleavage surface after the crystals had been subjected to plastic deformation experiments.

§ 2. Growth Features

Single crystals of the cleavage metals were grown from relatively high purity material (Zn 99·997%, Mg, Bi and Sb 99·99%), by the usual travelling furnace method with the modification that the growing crystal was free from undue restraints from its container. When growing crystals of metals which twin readily, this is essential in order to avoid large

* Communicated by the Author.

regions of the resultant crystal having a twin orientation. The well known imperfection of metal single crystals grown from the melt, that the cleavage surface is frequently not perfectly plane but displays boundaries between areas of slightly differing inclination, is suited to interferometric illustration. Figure 1 (Plate LXV) shows interference fringes crossing such an ' optical mosaic ' boundary in the case of a Zn cleavage. The inclination between the two basal areas is 1° 2′, a typical value for crystals which display only one or two mosaic boundaries on their cleavage face. Survey of the entire cleavage shows that the boundaries although smoothly curved tend over most of their length to lie at right angles to a possible glide direction. The area illustrated in fig. 1 is typical in this respect, as can be seen from the position of the boundary with respect to the twin band and associated bend plane produced in the crystal mechanically. Furthermore, in specimens displaying a number of boundaries the consequent tilting of the various cleavage areas forms a cleavage which is either completely concave or completely convex.

The growth conditions which affect the presence of optical mosaic boundaries have been extensively discussed (Holden, A. N. 1950), but the feature is of interest to the plastic deformation experiments to be described, in that the latter can lead to the production of such boundaries within the crystal in a regular manner.

§ 3. Twin Bands and Bend Planes

The cleavage of plate-shaped specimens from a single crystal rod results in cleavage surfaces which display the traces of twinning movements at various stages of development and which owe their origin to the local cleavage impact. Many of the twinning movements do not progress very far into the crystal and display on the cleavage surface the typical lenticular trace. The accommodation of these limited twin regions within the original crystal is brought about by the sharp bending of the basal planes of the crystal about the position of termination of the twinning movement on the twinning plane K_1. Figure 3 shows diagrammatically the shape of such a twinned region as determined by successive sectioning of a specimen while fig. 2 (Plate LXV) illustrates interference fringes contouring a section of the twin trace on the cleavage plane in the region XY. It can be seen by following a fringe of given order through the section that the amount of bending at the bend plane is that which is necessary to accommodate the twinned region within the larger restraining matrix. Under less restrained conditions of twinning, when for example a plate specimen is subject to an external shear in an appropriate direction, bend planes are not seen since the twinned regions develop to such a degree as to pass completely through the specimen and occupy a considerable volume. Such twinned regions are illustrated in fig. 4 (Plate LXV), the surface being the (III) cleavage of Bi. It will be observed that the interference fringes give a precise measurement of the angles produced on the crystal surface by the

twinning movement and in the case of the crystallographic cleavage surfaces it is only necessary to measure the angle made by the twin band on the cleavage surface to determine the shear, s, involved in the twinning movement. For non-cleavage metals the method of Mathewson (1928) for determining the twinning plane K_1 can be extended to include the determination of the direction and amount of shear in twinning by the use of interferometric goniometry such as is illustrated in fig. 4 (Plate LXV) (Holden, J. 1951).

From fig. 2 (Plate LXV), using the notation of fig. 3 it is seen that $\theta T \simeq bB$ where θ and b are the angles produced on the cleavage surface by the twin band and bend plane respectively. T is related to T_n the

Fig. 3

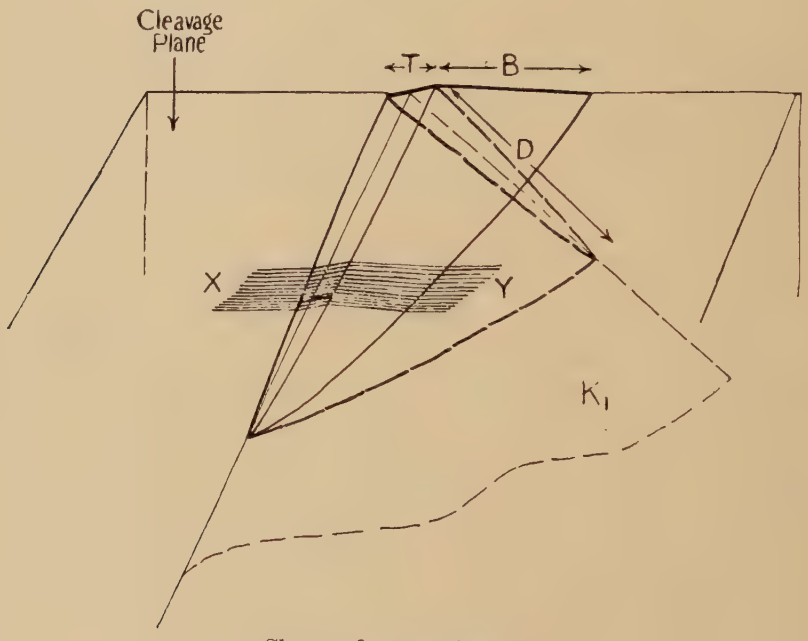

Shape of twinned region.

development of the twin in a direction n normal to the twin plane K_1 by the relation $T_n = T \sin \phi$ and B is related to the development of the twin in the direction of shear η_1 by the equation $B = D \cos \phi$; ϕ being the angle between the plane K_1 and the cleavage plane. The extent of the twin region in the direction normal to n and η_1 is seen as the trace of the twin in the cleavage plane, this being the direction of greatest development, the twinning movement spreading at a very early stage of its development to the limits of the crystal in this direction. It is thus seen that in the early stages of the twin development the ratio of the extent of the twin region in the directions η_1 and n is given by $(D/T_n) = \theta/(b \cos \phi \sin \phi)$. In the case of twinning in Zn, $\theta = 4° 5'$;

$\phi = 47° 2'$, while values of b can be directly measured for a range of restricted twinning movements such as are found during the cleavage of plate specimens. The ratio is found to be constant and characteristic of the particular metal crystal for twinning movements produced under similar conditions. In the case of the cleavage of Zn plates at liquid air temperatures values of $b = 44 \pm 2'$ are found giving $(D/T_n) = 11 \pm 0{\cdot}5$, while for Mg under similar conditions $(D/T_n) = 13 \pm 0{\cdot}5$. The sharply positioned bend plane would suggest that the development of a twinning movement within a crystal in the directions n and η_1 is dependent upon a limitation of the maximum angle of bending which the bend planes can attain in order to accommodate the twinned region. This is of interest in connection with the properties of individual boundaries as produced in the polygonization of hexagonal crystals. As will be described in a following section such polygon boundaries are subject to an upper limit of approximately 1° to the change of orientation which can take place at any one boundary. Figure 5 (Plate LXV) illustrates the termination of a twin region as indicated by its trace on the cleavage plane ; the narrow twin band is out of focus in order to achieve adequate contrast of the bend plane running alongside and terminating with the twin band. The close relation between the bend plane and the twin band traces can be observed when a local indent of the cleavage surface causes the collapse of part of the twin region or where twin regions react with each other. In these cases the position of the bend plane indicates that the proportions of the twinned region in the directions n and η_1 fall within the limits previously noted.

§ 4. Kink Bands

Cleavage of a Zn crystal rod by the gentle impact of a sharp edge depends upon orienting the cleavage blade parallel to the basal plane. Thus the crystal is in a position in which it may suffer compressive stress along the basal planes. This condition has been shown on a macroscopic scale to lead to the formation of kink bands (Orowan 1942). The typical bands formed on a microscopic scale during the cleavage of a Zn crystal at liquid air temperatures are shown in fig. 6 (Plate LXVI). The trace of these bands is at right angles to a glide direction and it is seen that the individual markings collect together into relatively broad bands. This is in contrast to the fine scale markings seen on the cleavage faces of crystals which only twin under the compressive stresses associated with cleavage. In the case of Bi, for example, fine markings on the same scale as kink bands are observed, however, they are more evenly spaced and also run parallel to the trace of twin planes. The characteristic topography of a collection of kink bands in Zn is illustrated in fig. 7 (Plate LXVI) in the case of a specimen in which by choice of appropriate cleavage direction only one set of bands have been produced. It is seen that the broad bands are places where individual kink movements of opposite arrangement have piled up. The symmetry of the piling is

marked in fig. 7 (Plate LXVI) but it is always found for all broad bands that the location of the band is about the meeting of individual kink bands of opposite arrangement. Figure 8 (Plate LXVI) illustrates a particularly simple case of the resultant position of individual kink bands; the local kink at the crystal surface is most precise and the structure performs under suitable illumination conditions as a diffraction grating of the appropriate number of 'slits' and spacing. The change of height of the crystal surface at an individual kink band can be measured interferometrically, but the measurement of the distance along the surface over which this height change takes place calls for careful phase microscopy. The dimensions of the individual kinks of fig. 8 (Plate LXVI) are found to be as follows: change of level of the surface at the kink; 900 ± 100 Å; width of the kink $3{\cdot}8 \pm 0{\cdot}4\,\mu$; distance between pairs of opposite kinks $45 \pm 5\,\mu$. The kink structure was produced on a cleavage plate approximately 1 mm in thickness at liquid air temperatures. The surface angle for the isolated kink bands is thus $1{\cdot}4 \pm 0{\cdot}3°$ and this order of magnitude is again found for the individual kinks within the broad piled up bands.

The cleavage surface of Zn crystals shows kinking movements freely when the crystals are suitably compressed (Jillson 1950), or indented. Individual kink movements can also be studied microscopically on Zn cleavages since the termination of a restricted twinning movement is usually associated with the generation of groups of individual kink bands. Precise measurements upon the dimensions of these kink bands in their early stages of development are at present being attempted.

§ 5. Inhomogeneous Deformation

When a plate cleavage specimen free from surface markings (in particular the tilt boundaries of growth) is bent to a radius of a few centimetres about an axis lying in the cleavage plane and at right angles to a glide direction, then annealed for, say, 12 hours at 100–150° c below the melting point of the metal, the originally curved cleavage surface becomes faceted, the boundaries of the facets running accurately at right angles to the appropriate glide direction. Figure 9 (Plate LXVII) illustrates the facets on a Zn crystal plate treated in this manner, the radius of bending being 3·2 cm and the annealing time 10 hours at 300° c. The interference fringes indicate that the facets are inclined to each other at angles in the range 34′ to 42′. Identical results are obtained if an entire single crystal rod is bent and annealed and then the cleavage specimens obtained. The cleavage thus faithfully follows the slight inclinations of the cleavage plane. By cleaving successive thin plates off the crystal rod the three dimensional picture of the facet system can be built up. In the case of the bending axis described the facet system changes only gradually over the length of the crystal rod, some facets prominent in one section becoming less prominent and being replaced by others as the sectioning moves over lengths of some centimetres.

Should the axis of bending while still being in the cleavage plane not coincide with a direction at right angles to a glide direction then the facets at any cleavage appear bounded by polygons, as illustrated by the micrograph of fig. 10 (Plate LXVII). As the bending of the specimens becomes more severe it is found that the number of facets increases, since there appears to be a limit to the angle possible between the facets produced by the annealing, which for the relatively pure Zn crystals is about 1°. This upper limit can be demonstrated in the case of the local curvatures produced by allowing a steel ball bearing to fall upon the cleavage plate. On the opposite face of the plate to that receiving the impact is raised a shallow dome ; by choice of suitable balls a wide range of local curvature can be produced and accurately measured interferometrically. When such a specimen is annealed on a hot stage microscope the first effect observed is the appearance of a number of concentric rings at the position of the dome ; if the annealing temperature is relatively high the rings soon become quite separate and can be counted. The rings mark areas of slightly changing tilt which can be directly measured at any particular ring or the number of rings can be counted and in conjunction with the known initial dome curvature an average value of the change of inclination at each bounding ring arrived at. For Zn, measurements made upon a wide range of local curvatures indicate that the change of inclination at a boundary does not exceed 1° 5′. This value refers to material of 99·997% purity and annealing temperatures up to 350° C. Continued annealing of a specimen causes the rings to develop into hexagons, the sides appearing in positions such that their traces are at right angles to directions of glide. At the same time the boundaries move away from the position of the dome thus eliminating it as a feature. Progress of the hexagon boundaries through the crystal continues over a period of hours the distance between neighbouring boundaries increasing, eventually it is seen that highly symmetrical patterns of polygons are formed away from the original dome position in the directions of glide on the crystal face. In these directions the curvature being relieved is greatest about one glide direction and smaller and equal for the other two directions. In this movement of tilt boundaries any twin bend planes which may be produced in the crystal by external means enter into the composite patterns. By their method of production and properties the boundaries described are polygon boundaries (Lacombe 1948, Cahn 1948). The temperature of annealing could be decreased and the time of annealing increased within wide limits to produce similar structures. The traces of kink bands were apparently unaffected by such annealing processes.

The manner in which the polygonization structures orient themselves suggests the origin of the optical mosaic phenomenon mentioned in connection with the growth of single crystals. It is observed in metal crystals grown under conditions favourable to the production of numerous

optical mosaic boundaries that cleavage of the crystals shows that the boundaries form on the cleavage surface a system of very irregular polygons. However, one system of sides tends to predominate and to lie in a direction at right angles to a glide direction. The limit to the maximum angle of inclination at a polygon boundary, as determined in the deformation experiments, also indicates an interpretation of optical mosaic structures in terms of polygonization, since in the case of good single crystals (crystals containing only one or two mosaic boundaries), the residual misorientation between the parts of the crystal after the growth process is generally close to the upper limit characteristic of polygonization (cf. fig. 1 (Plate LXV)).

§ 6. Glide Deformation

Cleavage of a single crystal rod of Zn or Mg can be carried out after the crystal has been subject to tensile stress and caused to glide. A specimen some 20 cm long being used in order to allow the cleavage to be made well away from the gripped ends. When the specimen is extended slowly at a moderately high temperature the cleavage face shows to the eye the appearance of widely spaced straight bands running completely across the face accurately at right angles to the active glide direction. Interference fringes contouring these bands show that each local band is due to the juxtaposition of equal and opposite local curvatures of the glide plane. Figure 11 (Plate LXV) shows the topography of one band in the case of a Zn crystal subject to 12% glide strain in a time of 30 minutes, the crystal being cleavaged at a random position well away from the gripped ends. The band illustrated was one of six evenly spaced on a cleavage face measuring approximately 18 mm in the active glide direction. The bands extended into the crystal and were normal to the glide direction as could be observed by cleaving the crystal rod into thin plates. This sectioning showed that the individual bands had their maximum curvatures at a given section and slowly faded away on each side being replaced by other bands coming to their maximum curvature. With increasing glide strain the number of bands was not found to greatly increase in the case of these hexagonal crystals, however, the curvature within the existing bands was found to build up in a regular manner.

Deformation at room temperature at similar rates to the higher temperature deformations resulted in band formation of the same type but the bands were, in general, not so completely discrete and symmetrical and did not completely cross the crystal face. Unlike the higher temperature bands, which for a given glide strain were few in number and almost identical in curvature, the more rapid room temperature extensions to the same glide strain gave rise to more numerous smaller bands (that is in terms of their superficial extension on the glide plane in

the direction of glide), of a more diverse range of curvature. The hardening of a hexagonal single crystal rod can be rapidly attained by bending and unbending, for simplicity about an axis in the cleavage plane at right angles to a glide direction. In this case the cleavage face is found to be traversed by a close packed system of bands at right angles to the glide direction. The corrugated nature of the glide plane under these conditions is illustrated in fig. 12 (Plate LXVI).

The large scale S-bands and the finer scale corrugations can be polygonized by annealing, since they consist essentially of local curvatures. Figure 13 (Plate LXVII) shows the detail of a polygonized S-band in a Zn crystal, the band having been made to be of particularly marked curvature (by subjecting the crystal to considerable glide strain), in order to show up in the micrograph. The maximum angle of tilt at a boundary formed by the polygonization of an S-band was found to be within the limit already stated for polygonization structures of simpler type.

§7. Summary

The consistent structures found upon the glide plane of metal crystals subject to a range of plastic deformation experiments, and revealed by cleavage, substantiate the method as a means of preparing a metal surface for precise measurement. The methods of interferometry permit illustration of the three dimensional structure of twinned regions, kink bands, polygon boundaries and glide deformation bands and also lead to measurements bearing upon theoretical concepts of crystal imperfections. Further measurements upon fine scale structures found upon the cleavage surfaces of the metals used in the present survey and upon other metals are in course of publication.

Acknowledgments

The writer would like to express his thanks to Professor S. Tolansky for his interest and for the privilege of working in his laboratory and to Dr. F. C. Frank for his encouragement. The work was carried out during the tenure of an I.C.I. Research Fellowship in the University of London.

References

Cahn, R. W., 1949–50, *J. Inst. Met.*, **76**, 121.
Holden, A. N., 1950, *Trans. Amer. Soc. Met.*, **42**, 319.
Holden, J., 1951, *Thesis.*
Jillson, D. C., 1950, *Journal of Metals*, **188**, 1009.
Lacombe, P., 1948, Bristol Conference, *Strength of Solids.*
Mathewson, C., 1928, *Proc. A.I.M.E.*, **1.**
Orowan, E., 1942, *Nature, Lond.*, **149**, 643.
Tolansky, S., 1946, *Phil. Mag.*, **37**, 453.

EXPLANATION OF PLATES.

Plate LXV.

Fig. 1

Optical mosaic boundary, Zn. (×120)

Fig. 2

Twin band and bend plane, Zn. (×100)

Fig. 4

Large twinned regions, Bi. (×40)

Fig. 5

Termination of twinned region, Mg. (×40)

Fig. 11

Topography of glide deformation band; the vertical represents the glide direction, Zn. (×30)

Plate LXVI.

Figs. 6, 7, 8

Kink bands, Zn. (×220)

Fig. 12

Deformation bands, Zn. (×30)

Plate LXVII.

Fig. 9

Polygonization boundaries; the horizontal represents the glide direction, Zn. (×50)

Fig. 10

Polygonization boundaries, Zn. (×30)

Fig. 13

Polygonization of glide deformation band, Zn. (×40)

XCVIII. *The Transverse Momentum Spectrum of the Decay Products of Charged V-particles*

By Carl M. York
The Physical Laboratories, University of Manchester*

[Received July 17, 1952]

Abstract

The momentum distributions in the centre of mass system for the charged secondary from the two reactions, $V^{\pm}\rightarrow\mu^{\pm}+\pi^{0}+\nu$ and $V^{\pm}\rightarrow\mu^{\pm}+\nu+\nu$, have been calculated. The second of the above processes has been used to calculate the transverse momentum spectrum of the charged secondaries. This has been compared with the measured spectrum from charged V-particles and found to be consistent with it. It is not possible to distinguish between the two decay schemes by a study of the momentum distributions, but alternative methods of distinguishing between them are discussed.

§ 1. Introduction

In a detailed study of charged V-particles, Armenteros *et al.* (1952) have given evidence that the transverse momentum distribution of the decay products did *not* fit a single two body decay scheme. It is the purpose of this paper to calculate the transverse momentum distribution assuming a three body decay scheme and to compare this distribution with the V-particle data. Two possible decay schemes have been suggested, viz.

$$V^{\pm}\rightarrow\mu^{\pm}+\pi^{0}+\nu, \quad . \quad . \quad . \quad . \quad . \quad . \quad . \quad (1)$$

$$V^{\pm}\rightarrow\mu^{\pm}+\nu+\nu. \quad . \quad . \quad . \quad . \quad . \quad . \quad . \quad (2)$$

These two modes of decay will be considered in the following calculations.

§ 2. Calculation of the Transverse Momentum Distribution

The charged V-particles are observed to decay in flight and the transverse momentum distribution of the charged secondaries can be readily obtained from the experimental data. Because this distribution is invariant under a Lorentz transformation, it will be calculated in the centre of mass system of the decaying $V^{\pm}$-particle and then compared with the distribution observed in the laboratory system.

* Communicated by Professor P. M. S. Blackett, F.R.S.

If a three body disintegration scheme is assumed, the transverse momentum distribution of the decay products of charged V-particles can be analysed in terms of two factors. The first is that in the centre of mass system for the decay, the charged secondary will be emitted in any direction with equal probability. This angular distribution will cause a transverse momentum distribution for any given momentum of the charged secondary particle in the centre of mass system. The second factor is that, in a three body scheme, the momentum of the secondary particle will not be a constant, but will vary depending upon the mode of decay.

As a result, the transverse momentum distribution must be expressed as the product of these two independent distributions. Because one does not know the momentum of the secondary in the centre of mass system from the experimental data, it is necessary to average the angular distribution over the momentum distribution in the centre of mass system to obtain a transverse momentum distribution which is directly comparable with the experimental data.

(*a*) *The Angular Distribution*

Armenteros *et al.* (1951) have shown that for a given value of the momentum, p, in the centre of mass system, the transverse momentum, p_T, is distributed according to the expression

$$\frac{p_T dp_T}{p\sqrt{(p^2-p_T{}^2)}}, \quad \ldots\ldots\ldots \quad (3)$$

as a result of the random orientation of the direction of the charged secondary. This then is the angular distribution of p_T, which must be averaged over the distribution of values taken by p.

(*b*) *The Momentum Distribution in the Centre of Mass System*

Michel (1950) has given a general treatment of the interaction of four Fermions. In a later paper (1952) he has calculated the energy distribution for the μ-meson in the decay scheme (2) above. We can obtain the differential momentum distribution from the generalized form of the energy distribution given in Michel's first paper. As a basic simplification to this expression, however, let us assume that the matrix element of the interaction is independent of the energies of the particles produced by the $V^{\pm}$-particle disintegration. If this approximation is made, it is no longer possible to distinguish between Fermions and Bosons, and the form of the energy distribution is determined by the density of states available to the decay products in phase space. This approximation seems justified in that the general form of the distribution is preserved, and the experimental data available for comparison is very meagre.

Let us call g the coupling constant of the reaction, M the rest mass of the decaying particle, μ the rest mass of the charged decay product, p the momentum of this charged secondary particle, and λ the rest mass of one of the neutral secondary particles. The other neutral decay product

is assumed to be a neutrino of zero rest mass. The energy distribution given by Michel (1950) can be used to obtain the momentum distribution,

$$F(p)\,dp = \frac{g^2M^2}{12\hbar(2\pi\hbar^2c^2)^3}\,\frac{(W-\sqrt{(p^2+\mu^2)})^2}{[M(W-\sqrt{(p^2+\mu^2)})+\frac{1}{2}\lambda^2]^3}$$
$$\times\{[3M(W-\sqrt{(p^2+\mu^2)})+p^2][2M(W-\sqrt{(p^2+\mu^2)})+3\lambda^2]+3\lambda^2\}$$
$$\times p^2\,dp. \quad . \quad . \quad . \quad . \quad (4)$$

$W=(M^2+\mu^2-\lambda^2)/2M$ is the maximum total energy received by the μ-meson in the centre of mass system of the disintegration.

Fig. 1

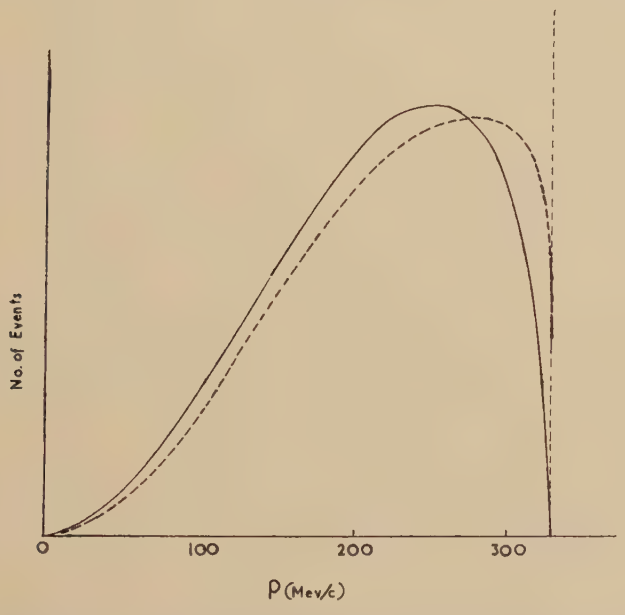

Momentum distribution of the charged secondary in the centre of mass system. (The solid line represents the case $V^{\pm}\rightarrow\mu^{\pm}+\pi^0+\nu$; the dashed line $V^{\pm}\rightarrow\mu^{\pm}+\nu+\nu$.)

This function is plotted as a solid line in fig. 1 for the reaction (1) given above. When μ is taken as the μ-meson rest mass and λ that of a π^0-meson, the upper momentum limit of 330 Mev/c corresponds to a $V^{\pm}$-particle rest mass of 1380 m_e. This upper momentum limit has been chosen to give a reasonable fit with the data.

For the decay scheme (2) we set λ equal to zero. Equation (4) then can be simplified to give

$$F(p)\,dp = \frac{g^2}{12\hbar(2\pi\hbar^2c^2)^3}[3(M^2+\mu^2)-6M\sqrt{(p^2+\mu^2)}+2p^2]p^2\,dp. \quad (5)$$

This function is plotted as a dotted line in fig. 1. As before the upper limit has been taken to be 330 Mev/c. This corresponds to a $V^{\pm}$-particle rest mass of 1330 m_e.

It is clear from fig. 1 that the momentum spectra for the two cases are very nearly the same except at the upper momentum limit. At the limit the dashed curve has a finite value and the solid curve goes to zero. Because the two curves have such similar shapes, one can be sure that when they are used to average the angular distribution, very similar results will be obtained. Hence only the distribution given in eqn. (5) will be used to calculate the desired transverse momentum distribution.

(*c*) *The Transverse Momentum Distribution*

The transverse momentum distribution is given by the expression

$$P(p_T)=\int_{p_T}^{p_{\max}} \frac{p_T}{p\sqrt{(p^2-{p_T}^2)}} F(p)\, dp. \quad . \quad . \quad . \quad . \quad (6)$$

Using eqn. (5) above for $F(p)$ and integrating we obtain the result

$$P(p_T)\, dp_T = K\left\{\sqrt{(p_{\max}^2-{p_T}^2)}\,[3(M^2+\mu^2)-3MW+\tfrac{2}{3}(p_{\max}^2+2{p_T}^2)]\right.$$
$$\left.-\frac{3M}{2}({p_T}^2+\mu^2)\ln\frac{W+\sqrt{(p_{\max}^2-{p_T}^2)}}{W-\sqrt{(p_{\max}^2-{p_T}^2)}}\right\} p_T\, dp_T, \quad . \quad . \quad . \quad (7)$$

where K is a constant, and $W=\sqrt{(p_{\max}^2+\mu^2)}$.

The expression $P(p_T)$ is plotted in fig. 2. The area under the curve is normalized to be the same as the area under the histogram of the combined experimental data given by Armenteros *et al.* (1952) and Barker *et al.* (1952).

§ 3. Conclusions

(*a*) The $V^{\pm}$-particle data of Armenteros *et al.* (1952) is consistent with a single three-particle decay scheme.

(*b*) The transverse momentum distribution of the charged secondaries is insensitive to the assumed decay scheme of the $V^{\pm}$-particle.

In view of the very small amount of data available and the difficulty of rapidly obtaining more, a somewhat different line of approach seems necessary to distinguish between the modes of decay. Michel (1952) has pointed out that if the decay scheme (2) above actually occurs, then one would expect the reaction

$$V^{\pm} \rightarrow e^{\pm}+\nu+\nu, \quad . \quad . \quad . \quad . \quad . \quad . \quad . \quad . \quad (8)$$

to compete with it and have a comparable lifetime. However, no electron secondary has been reported thus far in the literature. This does not rule out (2) as the true mode of decay, but is an argument against it. On the other hand, the π^0-meson in scheme (1) has never been observed and an exceptionally clear case will be required to identify unambiguously an

electronic cascade resulting from the π^0-decay associated with a charged V-particle. Such an event or a clear case of an electronic secondary as indicated in (8) would be more useful for deciding which is the true scheme of disintegration than a study of the momentum spectra.

The excellent agreement between eqn. (7) and the data of the Pic-du-Midi group, as shown in fig. 2, must be considered fortuitous. Because the histogram has been made up from only eighteen events, the possible statistical fluctuation of any point on the histogram is large. It should also be noted that if there is more than one type of charged V-particle, it would be possible to fit the observed transverse momentum distribution

Fig. 2

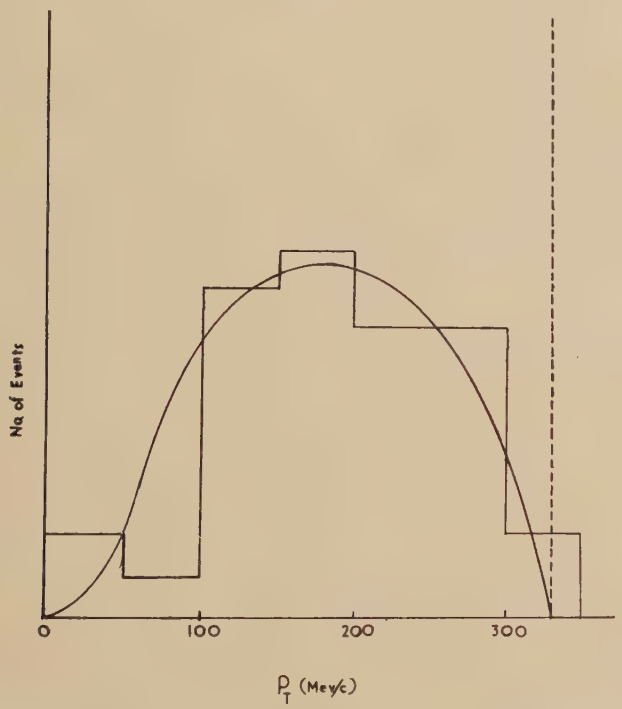

The transverse momentum distribution of the charged decay product of $V^{\pm}$-particles which decay in flight. (The solid curve represents the decay scheme $V^{\pm} \rightarrow \mu^{\pm} + \nu + \nu$ and the histogram gives the $V^{\pm}$-particle data of the Pic-du-Midi group.)

by a suitable mixture of several two body or two and three body decay schemes. That such a mixture might be necessary is indicated by the recent announcement of O'Ceallaigh *et al.* (1952) that a new charged meson which decays into two particles has been discovered. It may well be that the charged V-particles are a mixture of these new mesons and the κ-mesons found by O'Ceallaigh (1951).

Acknowledgments

The author is indebted to Dr. J. Podolanski for several enlightening discussions of this problem and for checking the integration of eqn. (6). The interest of the members of the Pic-du-Midi group has been very stimulating throughout the course of the work. The author would like to express his gratitude to Professor P. M. S. Blackett for extending the facilities of his laboratory during the author's stay in Manchester. Thanks are also due to the United States Educational Commission in the United Kingdom for financial support.

References

Armenteros, R., Barker, K. H., Butler, C. C., and Cachon, A., 1951, *Phil. Mag.*, **42,** 1113.

Armenteros, R., Barker, K. H., Butler, C. C., Cachon, A., and York, C. M., 1952, *Phil. Mag.*, **43,** 597.

Barker, K. H., Butler, C. C., Sowerby, M., and York, C. M., 1952. (Private communication.)

Michel, L., 1950, *Proc. Phys. Soc.* A, **63,** 514.

Michel, L., and Stora, L., 1952, *Comptes Rendus*, **234,** 1257.

O'Ceallaigh, C., 1951, *Phil. Mag.*, **42,** 1032.

O'Ceallaigh, C., and Menon, M. G. K., 1952, Report by C. F. Powell at the Copenhagen Conference, June, 1952.

XCIX. CORRESPONDENCE

The Influence of Lattice Vibration Spectrum on Electronic Thermal Conductivity

By F. H. J. Cornish
Clarendon Laboratory, Oxford
and
D. K. C. MacDonald
National Research Council, Ottawa, Canada *

[Received June 5, 1952]

It is generally well known that the present theoretical analysis of electron transport phenomena in metals rests upon an integral equation (the Boltzmann equation) for the electron distribution function. To solve this equation various assumptions and approximations, sometimes relatively crude, have to be made which we will not enumerate here in detail. As regards the thermal vibration of the lattice, however, the metal is assumed isotropic (when we may speak of longitudinal and transverse modes of oscillation) and in general the lattice wave velocity is treated as a constant. These two approximations indeed constitute the Debye model for the spectrum.

Based on these assumptions previous treatments, e.g. Wilson (1937), Sondheimer (1950), have always predicted a minimum in the thermal conductivity of a pure monovalent metal at about $T=0{\cdot}2\Theta$. The experiments of Berman and MacDonald (1951) on very pure sodium showed no trace of such a minimum. Seeking the cause of this discrepancy we are examining carefully the assumptions used in the theory.

As a first step, still taking the metal to be isotropic the transport equation has been solved without taking the lattice wave velocity to be constant (cf. Cornish and MacDonald 1951). For the thermal conductivity our calculations show that a minimum is still predicted. Hence the constant wave velocity assumption is not in itself the cause of this discrepancy between theory and experiment.

We hope to publish in greater detail later.

References

Berman, R., and MacDonald, D. K. C., 1951, *Proc. Roy. Soc.* A, **209,** 368.
Cornish, F. H. J., and MacDonald, D. K. C., 1951, *Phil. Mag.*, **42,** 1406.
Sondheimer, E. H., 1950, *Proc. Roy. Soc.* A, **203,** 75.
Wilson, A. H., 1937, *Proc. Camb. Phil. Soc.*, **33,** 371.

* Communicated by the Authors.

The Mean Energy of Three-Track Nuclear Disintegrations Produced by Cosmic-ray Particles

By D. A. Tidman and P. E. Hodgson
Imperial College of Science and Technology, London*

[Received July 5, 1952]

In 1949, Brown, Camerini, Fowler, Heitler, King and Powell measured the total energy of the particles emitted from disintegrations caused by cosmic rays as a function of star size for stars of from 4 to 18 tracks. They fitted their results with the empirical formula $E=4N^2+37N$, where E is the total energy emitted in low- or medium-energy particles, which, if charged, make black or grey tracks (i.e. those with ionization greater than 1·5 times the minimum ionization of singly-charged particles), and N is the number of such charged particles. However, these investigators missed a considerable number of the small stars (Barford and Davis 1952). The stars missed are likely to be those of higher energy, which would considerably affect the above relation for small values of N. It therefore seemed worthwhile to repeat the measurements of the mean energy for small stars.

Three-track stars in the G5 emulsion exposed under no absorber and examined with high scanning efficiency by Barford and Davis were measured and their mean energy determined in the following way.

The tracks of all particles of energy greater than 35 Mev which make an angle of less than 34° with the plane of the emulsion were grain counted, and the energies of the particles determined. Assuming that they were emitted isotropically the total number of such particles was calculated. As it was not possible to grain count tracks of particles between 25 and 35 Mev, their number was determined by fitting the energy spectrum of emitted protons determined by Camerini *et al.* (1950) to the observed distribution of particles with energies greater than 35 Mev, and extrapolating back to the region between 35 and 25 Mev. The mean energy and number of evaporation particles less than 25 Mev was obtained from previous work using C2 emulsion (Harding, Lattimore and Perkins 1949, Hodgson 1952). The number of neutrons produced in these disintegrations was taken as 1·2 times the number of protons. The binding energies of the emitted particles were added to their kinetic energies and a correction made for deuteron and triton emission (Fowler 1950).

As a result of this analysis the mean energy of the three-track stars was found to be 196 ± 18 Mev. This may be compared with the value of 147 Mev obtained for three-track stars by extrapolating the formula of Brown *et al.* The difference between these two values may indicate that they tended to miss the more energetic disintegrations.

* Communicated by Sir George P. Thomson, F.R.S.

References

Barford, N. C., and Davis, G., 1952, *Proc. Roy. Soc.* (in the press).
Brown, R., Camerini, U., Fowler, P. H., Heitler, H., King, D. T., and Powell, C. F., 1949, *Phil. Mag.*, **40**, 862.
Camerini, U., Fowler, P. H., Lock, W. O., and Muirhead, H., 1950, *Phil. Mag.*, **41**, 169.
Harding, J. B., Lattimore, S., and Perkins, D. H., 1949, *Proc. Roy. Soc.* A, **196**, 325.
Hodgson, P. E., 1952, *Phil. Mag.* (in the press).

A Note on the Measurement of Lifetime of Unstable Particles

By J. G. Wilson
The Department of Physics, University of Leeds
and
C. C. Butler
The Physical Laboratories, University of Manchester*

[Received July 23, 1952]

Up to the present, only very approximate estimates of the lifetimes of the rare unstable particles, identified in recent years in cosmic ray phenomena, have been made. Several novel features are encountered when the problem of making a lifetime determination is examined. If the lifetime is longer than about 10^{-10} sec. there will be the possibility that *charged* unstable particles will come to rest in matter, and direct timing methods may be possible, provided that sufficient examples of decay can be observed and that the events under examination are not obscured by other phenomena. No comparable mechanism, however, is known which will bring *uncharged* particles to rest, and for these there seems little prospect of the application of direct timing methods. Up to now, it has not proved practicable to use conventional timing methods for any of the new particles, and the only data available which include a direct time element are cloud chamber photographs in which the act of decay is seen. The photographs also enable many of the different decay phenomena to be distinguished, and for most of the particles it is from these photographs that measurements of lifetime must now be made.

One kind of determination makes use of either measurements or estimates of the total flux of the particles under consideration, and the useful preliminary values of lifetime have in fact been reached in this way. We think that this approach is capable of only limited development, because it is so difficult to identify those particles which do not decay, and that more definite information must be based explicitly on the data contained in actual records of identifiable decay processes.

* Communicated by the Authors.

An examination of typical data—for example that of Armenteros *et al.* (1952) and of Astbury *et al.* (1952)—shows that single groups of workers collect suitable data slowly, and so it is important that it shall be possible to combine data from many groups. In this note we suggest the way in which observations should be reported in order that they may be combined with others in a straightforward manner.

Each photograph in which the decay of a particle is recorded is of the following type: at some point the unstable particle entered the useful volume of the cloud chamber (i.e. the part of the chamber which is sufficiently illuminated and which is within the depth of focus of the recording camera), and at a second point, if it had not decayed, it would have left this volume. The distance which it would have traversed between these two points, x_0, may be described as the ' potential path length '. In fact, in each photograph decay took place after a ' path length ', x, which is shorter than x_0. The data required from each event consists of the lengths x, x_0, together with additional information which will allow these lengths to be transformed to time intervals t, t_0. Uncertainties of measurement are particularly serious for the transformation factor and for this reason we propose that the acceptable form of reporting observations should give separately the path lengths x, x_0 and the observed features upon which the transformation factor may be based.

It must be noted that the distances x, x_0 cannot be measured to the extreme limits of the useful part of the chamber, for some short distance is required within which the act of decay may be recognized. These distances must therefore be measured inside fiducial surfaces located at some predetermined distance within the useful limits of the chamber, and reported measurements should give clear indication what reduction, if any, of this kind has already been made. For charged particles ($V^{\pm}$, τ), the direction of motion of the primary particle is well defined, but for uncharged particles ($V^0{}_{1,\,2}$) this is not so, and it then becomes necessary to state the information upon which the trajectory of the particle has been determined. This may be based, for example, upon the identification of the source from which the particle has come, or upon the momenta and geometry of the secondary particles, together with the assumption of a particular decay scheme.

The transformation from the measured distances x, x_0 to the proper time intervals t, t_0 may occasionally be made directly when the ionization of a (charged) primary allows an estimate of the velocity of the particle to be made (see Astbury *et al.* 1952), but more often it will be derived from the measured momentum of the primary and an assumed value of its mass, or estimated from measurements made entirely upon the secondary particles. The reliability of the transformation factor will certainly vary widely from one example to another, and it is particularly important that the observational basis of each value should be reported adequately.

From a set of values of the traversal times t, t_0 the most probable lifetime can be deduced following the procedure discussed by Peierls (1935)

and Hole (1947). A statistical treatment has been given by Bartlett (1936). It is readily shown that if the average value of x/x_0 is close to one half, then the lifetime, τ, is probably longer than the average value of t_0, and a very large amount of data will be required before a reasonably accurate value of τ can be deduced. It will be shown in later publications that this is the situation which obtains for $V^{\pm}$-particles, for some at least of the apparatus now in use. For these particles, larger values of t_0 are accordingly desirable, and may be obtained either by using a larger chamber or by modifications of selection which increase the number of slow particles recorded.

References

Armenteros, R., Barker, K. H., Butler, C. C., Cachon, A., and York, C. M., 1952, *Phil. Mag.*, **43**, 597.

Astbury, J. P., Chippindale, P., Millar, D. D., Newth, J. A., Page, D. I., Rytz, A., and Sahiar, A. B. (private communication).

Bartlett, M. S., 1936, *Proc. Roy. Soc.* A, **154**, 124.

Hole, N., 1947, *Arkiv für Matematik, Astronomi och Fysik*, band **3B**, No. 12.

Peierls, R., 1935, *Proc. Roy. Soc.* A, **149**, 467.

Hyperfine Structure in Neodymium Ethyl Sulphate

By B. Bleaney, H. E. D. Scovil and R. S. Trenam

Clarendon Laboratory, Oxford *

[Received July 9, 1952]

Hyperfine structure in the paramagnetic resonance spectrum of neodymium ethyl sulphate was first observed by Bleaney and Scovil (1950), who analyzed the spectrum in terms of the usual Hamiltonian (with $S=\frac{1}{2}$, $I=7/2$ for the two odd isotopes 143 and 145).

$$\mathscr{H}=\beta g_{\parallel}H_zS_z+\beta g_{\perp}(H_xS_x+H_yS_y)+AS_zI_z+B(S_xI_x+S_yI_y)+P\{I_z^2-\tfrac{1}{3}I(I+1)\}.$$

Further measurements of the strong field spectrum at 3 cm wavelength, using proton resonance to measure the magnetic field, have yielded the following values for the parameters (A, B in units of 10^{-4} cm^{-1}):

$g_{\parallel}=3{\cdot}535\pm0{\cdot}001$ $\quad$ $g_{\perp}=2{\cdot}073\pm0{\cdot}002$

Isotope 143	Isotope 145	Ratio
$\lvert A\rvert=380{\cdot}3\pm0{\cdot}1$	$A=236{\cdot}4\pm0{\cdot}1$	$1{\cdot}6083\pm0{\cdot}0012$
$\lvert B\rvert=198{\cdot}9\pm0{\cdot}5$	$B=123{\cdot}7\pm0{\cdot}5$	

The values of B are less accurate, partly because not all the hyperfine structure is fully resolved, and partly because the theory has not been

* Communicated by the Authors.

carried far enough. The energy levels, with the magnetic field perpendicular to the axis, have been evaluated by fourth order perturbation theory. A small discrepancy between theory and experiment remains in the spacing of the hyperfine structure, which might be due either to higher order effects or to a nuclear quadrupole term with $|P|$ of the order of $2 \cdot 10^{-4}$ cm^{-1}. The latter possibility has been eliminated by making observations at 3 cm wavelength of weak transitions corresponding to changes $\Delta m = \pm 1$ in the nuclear magnetic quantum number, which should be split into doublets by the nuclear quadrupole interaction (Bleaney 1951). No such splitting could be detected, giving an upper limit for P for either isotope of 1 10^{-4} cm^{-1}.

To obtain further information about P the hyperfine transitions have been plotted into zero magnetic field using wavelengths of from 7 to 20 cm. At zero field, eight strong transitions are allowed for each isotope, three of which involve only the two parameters $(A-2P)^2$ and B^2. By taking these transitions in pairs, three values of each of these parameters are obtained which are just consistent within the experimental error. They are (in units of 10^{-4} cm^{-1})

$\lvert A-2P\rvert$		$\lvert B\rvert$	
143	145	143	145
$383 \cdot 0 \pm 1 \cdot 0$	$233 \cdot 7 \pm 1 \cdot 0$	$197 \cdot 6 \pm 1 \cdot 0$	$125 \cdot 5 \pm 1 \cdot 0$
$381 \cdot 3 \pm 1 \cdot 3$	$235 \cdot 2 \pm 1 \cdot 5$	$198 \cdot 4 \pm 0 \cdot 4$	$124 \cdot 6 \pm 0 \cdot 5$
$382 \cdot 5 \pm 0 \cdot 6$	$234 \cdot 0 \pm 0 \cdot 6$	$198 \cdot 5 \pm 0 \cdot 4$	$124 \cdot 7 \pm 0 \cdot 5$

By combining the weighted average of these values with measurements of transitions involving only A^2 and B^2, the following values for all the constants were obtained.

143	145	Ratio (143 : 145)
$\lvert A\rvert = 381 \cdot 3 \pm 0 \cdot 3$	$\lvert A\rvert = 235 \cdot 5 \pm 0 \cdot 2$	$1 \cdot 619 \pm 0 \cdot 003$
$\lvert B\rvert = 198 \cdot 5 \pm 0 \cdot 3$	$\lvert B\rvert = 124 \cdot 9 \pm 0 \cdot 5$	$1 \cdot 590 \pm 0 \cdot 007$
$\lvert P\rvert = \ 0 \cdot 7 \pm 0 \cdot 3$	$\lvert P\rvert = \ 0 \cdot 8 \pm 0 \cdot 3$	

It will be seen that the zero field measurements are inconsistent in that the ratios of A and B differ from each other and from the strong field value. The sign of P, relative to A, is opposite for the two isotopes, but little significance can be attached to this, or to the actual magnitude of P, until the reason for the discrepancies has been established. At present no satisfactory explanation has been found, but it is planned to repeat the zero field measurements with a crystal grown from heavy water. The reduced line width obtained thereby should increase the accuracy sufficiently to provide a good test of the spin Hamiltonian used to represent the results.

These small inconsistencies do not affect the size of the nuclear magnetic moments, in which the main uncertainty lies in the value of $\overline{1/r^3}$. Taking $\overline{1/r^3} = 34 \cdot 10^{24}$ cm^{-3}, Elliott and Stevens (1950) give $\mu_{143} = 1 \cdot 4$, $\mu_{145} = 0 \cdot 85$ nuclear magnetons. It seems probable that the actual values of P are not greater than $1 \cdot 10^{-4}$ cm^{-1}, corresponding to an upper limit

for the nuclear quadrupole moments of $1{\cdot}2\ 10^{-24}$ cm^2. The signs of the nuclear magnetic moments are not determined by the measurements, but from the optical spectrum of the separated isotopes, Murakawa and Ross (1951) give $\mu_{143}=-1{\cdot}0\pm0{\cdot}2$, $\mu_{145}=-0{\cdot}62\pm0{\cdot}09$ nuclear magnetons. The discrepancy between these values and ours may be due partly to the fact that, in the optical case, all contributions to the hyperfine structure except those from the 6s electrons are ignored, and partly to uncertainty in the value of $\overline{1/r^3}$.

References

Bleaney, B., 1951, *Phil. Mag.*, **42**, 441.
Bleaney, B., and Scovil, H. E. D., 1950, *Proc. Phys. Soc.* A, **63**, 1369.
Elliott, R. J., and Stevens, K. H. W., 1951, *Proc. Phys. Soc.* A, **64**, 205.
Murakawa, K., and Ross, J. S., 1951, *Phys. Rev.*, **82**, 967.

On the Production of κ-mesons

By U. Haber-Schaim and G. Yekutieli
The Weizmann Institute of Science, Rehovoth, Israel*

[Received June 22, 1952]

Recent experiments of the Bristol group (Daniel *et al.* 1951) have indicated that heavy mesons (κ-mesons or kappons, for short) are found in appreciable numbers. In some stars produced by very energetic primaries (>50 Bev) a ratio between the number of kappons and pions $n_\kappa/n_\pi=0{\cdot}6$ was claimed. Such a large ratio suggests that the kappons like the pions are strongly coupled to the nucleons.

One may try to account for the production of the kappons by either of the following assumptions :

(*a*) The kappon is a Yukawa type particle which interacts with the nucleon through a ' kapponic charge ' quite independently of the existence of the ' pionic charge '. This would lead us to believe for example, that the force between two nucleons at rest is derivable from two Yukawa potentials with ranges $\hbar/m_\kappa c$ and $\hbar/m_\pi c$.

(*b*) The production of both kinds of mesons is the result of *one* field. In this case neither of the mesons is a Yukawa particle in the full sense of the word.

We shall not investigate these assumptions here but rather limit ourselves to their manifestation in the case of very strong coupling when Fermi's statistical theory is applicable (Fermi 1950, 1951).

In this extreme case assumption (*a*) will lead us to the conclusion that the kappons are produced in a volume of the order of

$$\Omega_\kappa=\frac{4\pi}{3}\left(\frac{\hbar}{m_\kappa c}\right)^3$$

---

* Communicated by the Authors.

whereas the volume available for pion production will be

$$\Omega_\pi = \frac{4\pi}{3}\left(\frac{\hbar}{m_\pi c}\right)^3.$$

Hence even at the highest energies $(n_K/n_\pi) \leqslant [(m_\pi/m_K)^3]$ except for possible spin factors. On the other hand, assumption (*b*) will lead to $\Omega_K = \Omega_\pi$. In this case the high energy limit of n_K/n_π will be determined by spin factors only.

The number of kappons n_K, and pions n_π, produced in nucleon–nucleon collisions is calculated in the following way. Both kappons and pions are taken to be bosons with spin zero which can be either charged or neutral. Only the pions are treated as extreme relativistic particles in c.m. system whereas for the kappons the exact relation between energy and momentum is used and the integrals in momentum space are computed numerically. The results of the calculation are summarized in table 1, where W' is the energy in the laboratory system. The following values for the masses are used: $m_K = 0{\cdot}69$ and $m_\pi = 0{\cdot}15$ in nucleon mass units.

Table 1. n_K and n_π as Functions of Energy of Incident Nucleon

W' in Mc^2	Assumption (*a*)			Assumption (*b*)		
	n_K	n_π	n_K/n_π	n_K	n_π	n_K/n_π
20	0·011	2·60	0·0042	0·63	1·78	0·35
50	0·019	3·63	0·0052	1·17	2·34	0·50
100	0·027	4·55	0·0060	1·64	2·85	0·57
200	0·038	5·53	0·0069	2·25	3·43	0·66
300	0·046	6·20	0·0074	2·64	3·85	0·69
500	0·057	7·18	0·0080	3·17	4·38	0·72
700	0·065	7·80	0·0084	3·56	4·75	0·75
1000	0·075	8·50	0·0088	4·05	5·10	0·79

Table 1 clearly favours assumption (*b*).

Additional evidence concerning the two assumptions can be drawn by comparing the interaction mean free paths of kappons, l_K, and pions, l_π, in photographic emulsions (compare Daniel *et al.*, p. 22). Under assumption (*a*) one obtains a ratio $(l_K/l_\pi) = 5{\cdot}4$ whereas $(l_K/l_\pi) = 1$ under assumption (*b*).

References

Daniel, R. R., Davies, J. H., Mulvery, J. H., and Perkins, D. H., 1951, *Bristol Conference of V Particles and Heavy Mesons.*

Fermi, E., 1950, *Prog. Theo. Phys.*, **5**, 570; 1951, *Phys. Rev.*, **81**, 683.

Paramagnetic Resonance in Praseodymium Ethylsulphate

By B. Bleaney and H. E. D. Scovil
Clarendon Laboratory, Oxford*

[Received July 21, 1952]

The paramagnetic resonance spectrum of praseodymium ethylsulphate in a crystal diluted with lanthanum has been observed at 20° K, using radiation of wave numbers 0·332, 0·687 and 0·789 cm^{-1}. A single electronic transition is observed, with a hyperfine structure of six equally-spaced components. This confirms the known nuclear spin (5/2) of the only stable isotope, 141.

The ground state of the free Pr^{+++} ion is $4f^2$, $^3H_4$, which, under the action of a crystalline electric field of C_{3h} symmetry, splits into a singlet and four doublets. The theory of Elliott and Stevens (unpublished) shows that a doublet, whose states may be written as

$$\cos\theta\,|J_z=\pm 4\rangle+\sin\theta\,|J_z=\mp 2\rangle$$

(the upper sign refers to one state, the lower to the other), should lie at the bottom. This is not a Kramers' doublet, and, since the states contain no values of J_z differing by unity, the normal type of resonance transition is not allowed. If there is any dissymmetry in the crystalline field which admixes the two states, however, transitions are allowed with the r.f. magnetic field parallel to the crystalline axis. We have tentatively tried to allow for such an effect by adding a term in S_x to the usual spin Hamiltonian. It would then be written

$$\mathcal{H}=g_{\parallel}\beta H_z S_z+AS_zI_z+\Delta S_x, \quad \ldots\ldots\ (1)$$

with an effective spin $S=\frac{1}{2}$. The absence of matrix elements in the magnetic field between the two states of the doublet is indicated by the absence of the usual terms $g_{\perp}\beta(H_xS_x+H_yS_y)$ and $B(S_xI_x+S_yI_y)$. This Hamiltonian gives energy levels

$$W=\pm\tfrac{1}{2}\sqrt{(\Delta^2+\{g_{\parallel}\beta H_z+Am\}^2)}, \quad \ldots\ldots\ (2)$$

where m is the nuclear magnetic quantum number, and transitions are allowed only between states of the same m. (We have omitted the nuclear electric quadrupole term, as this is likely to be negligible compared with the other terms.)

Observations at three wave-lengths show six lines, equally spaced in magnetic field, as would be expected from the form of eqn. (2), when m is given the values 5/2, 3/2, ... −5/2, W is kept constant, and H is varied. The field corresponding to the centre of the spectrum is not quite proportional to the frequency of observation. This indicates that Δ is very small (approximately 0·04 cm^{-1}) and gives $g_{\parallel}=1{\cdot}69\pm0{\cdot}01$, $A=0{\cdot}083\pm0{\cdot}001$ cm^{-1}. When the axis of the crystal is rotated away

* Communicated by the Authors.

from the magnetic field, the spectrum moves rapidly into higher fields and out of the range of our magnet, indicating that $g_\perp$ is very small ($<0{\cdot}3$). Susceptibility measurements of van den Handel (1941) indicate also that $g_\perp=0$, but give a slightly smaller value (1·56) for $g_\parallel$.

This discrepancy may be due to one of two causes :

(*a*) The resonance lines are several hundred gauss broad and asymmetrical in shape, the intensity rising slowly on the low field side and falling steeply on the high field side. We have assumed that the point of maximum intensity gives the position of the unbroadened line. The asymmetrical shape would, qualitatively, be expected from the form of eqn. (2), but only if Δ were comparable with the frequency of observation.

(*b*) Our assumed Hamiltonian (1) may be wrong. The admixture of the two states and consequent splitting of the electronic doublet is presumably associated with the Jahn–Teller effect, which lifts the degeneracy by allowing a distortion of the crystal field which lowers the total energy of the system. It is doubtful whether the addition of a simple term such as ΔS_x fully represents this complex process, which is little understood (cf. Bleaney and Bowers 1952).

References

Bleaney, B., and Bowers, K. D., 1952, *Proc. Phys. Soc.* A, **65**, 667.
van den Handel, J., 1941, *Physica*, **8**, 513.

The Dispersion Formulae and the Polarization Fields

By Sir K. S. Krishnan, F.R.S., and S. K. Roy
The National Physical Laboratory of India, New Delhi*

[Received June 18, 1952]

In the usual derivation of the Drude formula for the dielectric constant of a dense medium as a function of the frequency of the incident waves, since one does not invoke the presence of a polarization field, and since further it is known that the Lorentz dispersion formula reduces to the Drude formula in the special case when the polarization field is made to vanish, any verification of the Drude dispersion formula is sometimes taken to imply the absence of a polarization field. This conclusion is not justified, and it is the main purpose of this note to emphasize that the Drude formula for the dielectric constant as a function of the frequency of the incident waves (as distinguished from the formula for the dielectric constant as a function of the density) is perfectly consistent with the occurrence of a polarization field having the Lorentz value, or any other value. This will be the case even when the polarization field factors

* Communicated by the Authors.

p_{ij} defining the polarization field acting on any oscillator of type i due to all the oscillators of type j in the medium differ from the Lorentz value $4\pi/3$, and differ from one another. In other words, irrespective of the actual polarization field that occurs in the medium, i.e. irrespective of the actual values of p_{ij} that define this field, the observational data for the dispersion of the dielectric constant can always be represented by the Drude formula

$$\epsilon_\omega - 1 = \sum_i \frac{A_i}{\omega_i^2 - \omega^2}, \quad \ldots \ldots \quad (1)$$

the characteristic frequencies ω_i that appear in the formula being the resonance frequencies of the medium.

The same observational data can also be fitted alternatively into a formula of the type

$$\epsilon_\omega - 1 = 4\pi\chi = 4\pi \sum_i \chi_i, \quad \ldots \ldots \quad (2)$$

where

$$\chi_i = \frac{B_i}{\Omega_i^2 - \omega^2}(1 + \sum_j p_{ij}\chi_j), \quad \ldots \ldots \quad (3)$$

in which j can take all values $i, j, k, \ldots$. When all the p_{ij}'s have the same value, equal to p say, $\sum_j p_{ij}\chi_j = p\chi$, and eqn. (2) reduces to the form

$$\frac{\epsilon_\omega - 1}{\epsilon_\omega + \alpha} = \sum_i \frac{C_i}{\Omega_i^2 - \omega^2}, \quad \ldots \ldots \quad (4)$$

where

$$\alpha = \frac{4\pi}{p} - 1, \quad \ldots \ldots \quad (5)$$

and

$$C_i = pB_i. \quad \ldots \ldots \quad (6)$$

When p has the Lorentz value $4\pi/3$, it will be seen that α reduces to 2 and eqn. (4) to the simple Lorentz formula. For convenience we shall describe the type of dispersion formula defined by (2) and (3) as a generalized Lorentz formula, as distinguished from the simple Lorentz formula corresponding to $\alpha = 2$ in eqn. (4).

Thus any observational data on the dispersion of the dielectric constant of a dense medium can be fitted into a Drude formula, or alternatively into a generalized Lorentz formula involving any given set of polarization factors p_{ij}. This fitting into the alternative formulae can be done irrespective of what the *actual* polarization field in the medium may be, and even if there is no polarization field at all.

The equivalence of the Drude and the simple Lorentz formulae for the dispersion of the dielectric constant of a dense medium was first demonstrated by Livens (1912) for the case when the medium has a single resonance frequency, and by Herzfeld and Wolf (1925) for the case when the medium may have more than one resonance frequency. The equivalence extends, as we have just seen, also to the generalized Lorentz

formula corresponding to any specified set of polarization factors p_{ij} defining the interactions between the dipole moments of the different oscillators.

This equivalence arises from the following circumstance. The effect of any polarization field that may be present in a dense medium on its dielectric constant may be taken into account in two alternative ways, which are equivalent. The effective field that polarizes the medium may be taken to include, in addition to what is usually defined as ' the field in the medium ', the polarization field also, in which case the dispersion formula will be of the Lorentz type and the characteristic frequencies that appear in the formula will be the frequencies Ω_i of the individual oscillators, regarded as unaffected by the presence of the polarization field, i.e. unaffected by their mutual interactions. Alternatively one may also regard the polarization field as effective in changing the frequencies Ω_i to the corresponding resonance frequencies ω_i of the medium, and its effect on the dielectric constant as exercised indirectly through these frequencies. The result is the Drude dispersion formula. (The important part played by the polarization field in determining the infra-red resonance frequency of the alkali halide crystal, in which the polarization field involved is readily calculated, is discussed by us in a recent paper (Krishnan and Roy 1951).)

Conversely, starting with the Drude formula, and the known resonance frequencies ω_i that appear in the formula, and taking them to correspond to zero polarization field, one may postulate any desired polarization field and reduce the Drude formula to one of the Lorentz type. The frequencies Ω_i that appear in the latter formula will be different from the corresponding resonance frequencies ω_i by amounts that will be determined by the polarization field postulated.

Hence dispersion data as such can not give us any information regarding the nature of the polarization field that exists in the medium, though they enable us to obtain the resonance frequencies, directly if the data are expressed in the Drude form, since the characteristic frequencies ω_i that appear in this formula are just these frequencies, or after a simple calculation from the corresponding Ω_i if the data are expressed in the Lorentz form.

The position, however, is very different with expressions for the dielectric constant as a function of the density, where the equivalence of the Drude and the Lorentz types does not hold.

References

Herzfeld, K. F., and Wolf, K. L., 1925, *Ann. d. Physik*, **78**, 35.
Krishnan, K. S., and Roy, S. K., 1951, *Proc. Roy. Soc.* A, **207**, 447
Livens, G. H., 1912, *Phil. Mag.*, **24**, 268.

The X-ray Spectrum from a 70 MeV Synchrotron

By I. B. McDiarmid
Synchrotron Laboratory, Queen's University, Kingston, Ontario, Canada*

[Received July 11, 1952]

The spectrum of the x-rays produced in the forward direction by 70 MeV electrons striking a conventionally thick target is being measured. The scattering method has been used to determine the energies of 637 electron pairs produced by the x-rays in G5 emulsions and from this the spectrum has been deduced. The number of photons found below 25 MeV is considerably less than that predicted by the Bethe–Heitler–Schiff (1951) theory corrected for target thickness.

The target in the synchrotron here is a tungsten rod about $\frac{1}{4}$ in. in diameter. Presumably the x-rays are produced by what one might call glancing blows of the electrons on the target, and hence the effective thickness is not known accurately. However, measurements by Holloway and Janzen of the angular width of the beam indicate a target thickness of the order of 0·05 to 0·1 cm (Schiff 1946). The effect on the spectrum of a thick target has been calculated and a result, similar to that given by Eyges (1951), obtained. The main effect of the calculation is a relative lowering of the high energy end. The best agreement with theory, above 25 MeV, is obtained if we assume a 0·1 cm thick target. The smooth curve of fig. 1 is Schiff's integrated photon distribution corrected for this target thickness.

The G5 emulsions were placed in the centre of the beam 3 m from the target and given approximately 10 milli-r of radiation. After processing the plates were searched systematically for electron pairs and from the measured mean angle of scattering the energies calculated. The method used to measure the scattering and the evaluation of the constants in Williams' (1940) scattering theory for G5 emulsions have been described previously (McDiarmid 1951).

The pairs used for the spectrum determination were selected in the following way. The scattering was measured on all pairs in which both electrons travelled at least 300 μ in the emulsion. Those pairs were discarded for which the probable error in the energy determination of either electron (obtained from the measured 'noise level' and the length of track in the emulsion) would have been greater than 15%. This selection process discriminates slightly against the lower energy pairs and this was corrected for as follows. For a given energy and the measured 'noise level' the length of track required to give a probable error in energy less than 15% was calculated. From the distribution function of Rossi and Greisen (1941) and the known emulsion thickness

---

* Communicated by Professor J. A. Gray, F.R.S.

the fraction of electrons that escape before going this distance was calculated and from this the corrections to be applied to the number of pairs in the various intervals obtained. The total corrected number of pairs was approximately equal to the total number found in the emulsion indicating that the corrections applied were of the right order.

Fig. 1

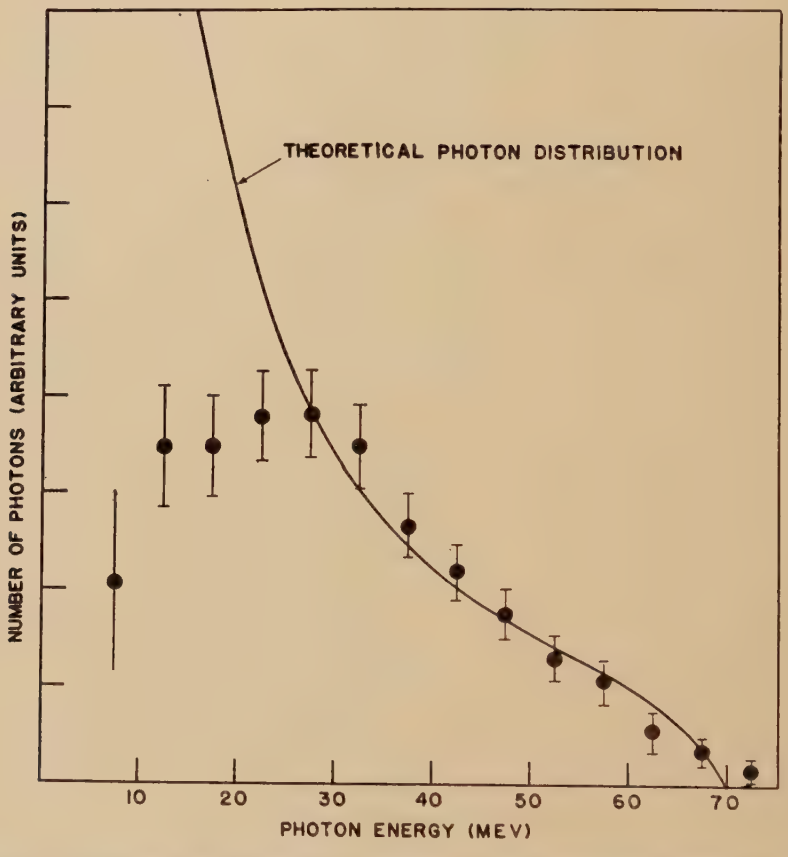

Number of photons as a function of energy. The theoretical curve is Schiff's integrated distribution corrected for a 0·1 cm thick target.

The corrected number of pairs in the different energy intervals was divided by the corresponding cross section for pair production, giving numbers proportional to the number of photons in the beam at these energies. The measured photon distribution obtained in this way is compared with the theoretical distribution in fig. 1. Evidently, there is a large discrepancy between the measurements and theory below 25 MeV.

The photon spectrum we have found is very nearly independent of energy in the region 15 to 25 MeV and this is in agreement with 'relative yields', as defined by Perlman and Friedlander (1948), of (γ—n) reactions

measured in this laboratory by Edwards and MacMillan (1952). The definition of yield leads to the approximate expression

$$\frac{Y_1}{Y_2} = \frac{N_1 I_1}{N_2 I_2} \quad \ldots\ldots\ldots\ldots \quad (1)$$

for the ratio of two yields, where Y is the yield measured here, N is the number of photons per Mev around the average energy producing the reaction, and I is the integrated cross section. From the yields measured in ^{12}C, ^{65}Cu, ^{63}Cu, and ^{109}Ag the ratios N_1/N_2 for several pairs of energies have been calculated from eqn. (1). The average energies producing the reactions and the integrated cross sections were taken from the work of Katz and Cameron (1951), and Diven and Almy (1950). In table 1

Table 1. Ratios of the Number of Photons Around Different Pairs of Energies.

	No. at 18 Mev / No. at 24 Mev	No. at 17 Mev / No. at 24 Mev	No. at 15 Mev / No. at 24 Mev	No. at 15 Mev / No. at 18 Mev
From yield measurements	0·97	1·0	1·0	1·0
From pair measurements	~1	~1	~1	~1
From Schiff's theory	1·42	1·53	1·75	1·26

these ratios are compared with the corresponding ratios given by the pair measurements and by Schiff's theory. It can be seen that the yield and pair measurements predict about the same ratios while the theory predicts much higher ratios.

A complete report of this work is being submitted to the Canadian Journal of Physics.

I wish to thank Professor J. A. Gray for suggesting this problem and for many helpful discussions. I am also indebted to the National Research Council of Canada for financial assistance.

References

Diven, B. C., and Almy, G. M., 1950, *Phys. Rev.*, **80,** 407.
Edwards, L. S., and MacMillan, F. A., 1952, to be published in *Phys. Rev.*, **87**.
Eyges, L., 1951, *Phys. Rev.*, **81,** 981.
Katz, L., and Cameron, A. G. W., 1951, *Can. J. Phys.*, **29,** 518.
McDiarmid, I. B., 1951, *Phys. Rev.*, **84,** 851.
Perlman, M. L., and Friedlander, G., 1948, *Phys. Rev.*, **74,** 444.
Rossi, B., and Greisen, K., 1941, *Rev. Mod. Phys.*, **13,** 241.
Schiff, L. I., 1946, *Phys. Rev.*, **70,** 87 ; 1951, *Ibid.*, **83,** 252.
Williams, E. J., 1940, *Phys. Rev.*, **58,** 292.

Interpretation of the de Haas–van Alphen Effect

By L. Onsager*
The Royal Society Mond Laboratory, University of Cambridge†

[Received July 14, 1952]

At low temperatures many metals exhibit an oscillatory variation of their magnetic susceptibilities with the field intensity. This effect was first discovered by de Haas and van Alphen in a study of bismuth. Recent investigations have shown that it is quite common ; the remaining negative findings might well be due to the limitations of experimental technique.

The effect is generally attributed to the helical motion of the free electrons, which ought to be quantized as far as the components of momentum perpendicular to the magnetic field are concerned ; the component parallel to the field remains a constant of motion capable of all values. The theory applicable to free electrons was elaborated by Blackman (1938), Shoenberg and Landau (1940), who recognized the effect of the periodic field in the crystal by the introduction of modified, generally anisotropic, effective electron masses. According to these theories oscillations of long period, which are studied with relative ease, can occur when two of the principal masses are small. The zone theory permits this in rather special locations in the reciprocal lattice, most commonly perhaps where Bragg reflections of equal strength intersect (Robinson 1950), but hardly over extended domains in momentum space ; wherever a small effective mass is found, its constancy is in doubt.

Under the circumstances, a more general approach to the problem is of interest. We retain the wave-packet picture, which is more or less implicit in previous theories. Let the energy in the absence of external electric and magnetic fields be a function $W(\mathbf{p})$ of the momentum $\mathbf{p}$; then the group velocity $\mathbf{v}$ is given by the relation $\delta W = \mathbf{v} \cdot \delta \mathbf{p}$, and an external force $\mathbf{X}$ will cause an acceleration given by $\dot{\mathbf{p}} = \mathbf{X}$.

Admittedly, the effect of a magnetic field cannot be described quite rigorously in these terms. We replace $\mathbf{p}$ by the 'kinetic momentum' $\mathbf{\Pi}$, which contains the vector potential $\mathbf{A}$:

$$\mathbf{\Pi} = \mathbf{p} + (e/c)\mathbf{A}$$

but the statement $W = W(\mathbf{\Pi})$ is somewhat ambiguous because the components of $\mathbf{\Pi}$ do not commute. It would appear that a comprehensive analysis of the difficulties which arise thus has not yet been achieved. In kinetic theories (Shockley 1950) it is customary to ignore such complications, and it does seem reasonable to hope that neither previous

* Communicated by the Author.
† Now at Sterling Chemistry Laboratory, Yale University, New Haven, Conn.

theories of diamagnetism nor the present generalization will be invalidated by the errors involved in the ' wave-packet ' approximation, or at least that the error in the computed susceptibility will not vary rapidly with the field intensity.

According to our picture, then, a magnetic field causes the vector $\mathbf{\Pi}$ to move along the line of intersection between a plane $(\mathbf{\Pi} \cdot \mathbf{H})$=constant and a surface $W(\mathbf{\Pi})$=constant in momentum space (Shockley 1950). The helical path of the electron, projected upon a plane perpendicular to the field, becomes an exactly similar curve in ordinary space, turned through a right angle and of dimensions changed in the ratio c/eH. The periodic component of the motion, which involves the components of $\mathbf{p}$ and $\mathbf{r}$ perpendicular to $\mathbf{H}$, is quantized. We apply the Bohr–Sommerfeld rule in the form

$$\oint \mathbf{p} \cdot d\mathbf{r} = (n+\Theta)h.$$

Then the cross section of the helical orbit is determined by the condition that the enclosed magnetic flux equal $(n+\Theta)$ ' force lines ', whereby we recognize a fundamental unit

$$1 \text{ force line} = hc/e = 4\pi g = 4{\cdot}135 \times 10^{-7} \text{ maxwell}$$

equal to the flux from one of Dirac's hypothetical magnetic poles. The energy levels are degenerate because the location of the helical axis is arbitrary ; the multiplicity of each level equals the number $H\Omega/4\pi g$ of force lines traversing the cross section Ω of the specimen. The area enclosed by an ' orbit ' in Π-space is proportional to the field intensity,

$$(n+\Theta)(he/c)H \text{ ; (momentum units)}$$

or

$$(n+\Theta)(e/hc)H \text{ ; (wave-number units).}$$

The known explanation of the de Haas–van Alphen effect depends on this, that with increasing field intensity, the electrons are redistributed among a decreasing number of levels. The capacity (degeneracy) of each level increases in proportion with the field intensity : the spacing of the levels becomes correspondingly more open. The top levels become depleted in succession, and the magnetic susceptibility will vary in phase with the state of depletion of the highest level which retains an appreciable number of electrons. In the cases which have been accessible to study by known techniques, we have reason to believe that the top energy level ζ of the electrons was kept sensibly constant by reservoirs of electrons which would not produce appreciable oscillations at the prevailing field intensities. Under those conditions, when the intensity of the field is increased, the nth quantum state will be (more than half) depleted as soon as its energy exceeds ζ. The field necessary to accomplish this depends simply on the *area in momentum space* enclosed by the curve $W(\mathbf{p})=$ on some plane $(\mathbf{p} \cdot \mathbf{H})$=constant. If the area in question does not depend on the component of momentum parallel to $\mathbf{H}$, that is, if the surface $W(\mathbf{p})=\zeta$ is a cylinder, then the depletion will take

place simultaneously along the entire length of the cylinder and cause rather large oscillations. This improbable contingency does not seem to be realized in any case which has been studied. If the Fermi surface $W(\mathbf{p})=\zeta$ is convex, then depletion will start slowly at the ends and proceed at an accelerated pace towards the middle. The rapid last stage of depletion will correspond to the maximum area of intersection, and in line with the known theoretical results for ellipsoidal surfaces, we shall observe oscillations whose period depend on this maximum area. Alternatively, the Fermi surface may resemble a hyperboloid of one sheet, in which case we shall expect oscillations which correspond to the *minimum* area of intersection. It is even conceivable that the Fermi surface may take the shape of an endless tube of variable cross section spanning the entire length of a cell in wave-number space. In that case we have to expect superposed oscillations of two different periods, which will give us measures of the smallest and the greatest cross section, respectively. According to preliminary results obtained in this laboratory, such a situation may prevail in graphite.

To summarize: the oscillatory diamagnetism reflects specific geometrical features of the Fermi surface; the nth maximum (counted from $1/H=0$) occurs for a field intensity H_n given by the relation

$$n+\Theta=(hc/e)A/H_n,$$

where A is any extremal area of intersection between the Fermi surface and the family of planes $(\mathbf{H}\,.\,\mathbf{p})=$constant.

The phase Θ contains a known correction which depends on the signs of the principal curvatures of the Fermi surface. Otherwise, the present considerations add nothing much to the existing theory as regards the phases and the amplitudes of the oscillations. Indeed, the generalized theory hardly foresees results which could not be interpreted in terms of ellipsoidal Fermi surfaces except this, that one negative principal mass is permissible and indicates a hyperboloid.

In order to explain the observed amplitudes and phases in full detail, the theory has to invoke effects which are not fully understood. This situation remains unchanged.

References

Blackman, M., 1938, *Proc. Roy. Soc.* A, **166,** 1.
Robinson, J. E., 1950, *Diss.*, Yale.
Shockley, W., 1950, *Phys. Rev.*, **79,** 191.
Shoenberg, D., 1940, *Proc. Roy. Soc.* A, **175,** 49.

C. *Notices of New Books and Periodicals received*

The Principles of the Control and Stability of Aircraft. By Prof. W. J. Duncan, D.Sc., F.R.S. [Pp. XVI+384.] (Camb. Aeronautical Series ; C. U. P. 1952.) Price 40*s.* net.

The pace of aeronautical progress is such that there is little time for the consolidation of knowledge, and still less for the writing of text-books. The appearance of a first volume in a Cambridge Aeronautical Series is therefore very welcome. The volume under review is an excellent book, and fills a serious gap in the literature : no major work exclusively devoted to stability and control of aircraft has appeared for forty years. It contains chapters on the mechanics of flight, on the equations of motion and their solution, on longitudinal-symmetric and lateral-antisymmetric motion, on flap controls and on aerodynamic derivatives. A chapter is devoted to each of the important subjects of static stability and manoeuvrability, distortion, and compressibility effects. Two chapters, on spinning and on landing flaps, by Professor A. D. Young, are also included. The reviewer found the book extremely informative and very readable, if a little academic in parts ; it is excellently set out and printed, and is remarkably free from errors. A. R. C.

Electronic and Ionic Impact Phenomena. By H. S. W. Massey and E. H. S. Burhop. [Pp. 669.] (Oxford University Press.) Price 70*s.* net.

Owing to the severe limitations of space in this Journal, an adequate review of a closely written volume of 669 pages is clearly not possible. Nor can the reviewer pretend to have read it all at this stage. But it is a work that can be most strongly recommended, and one in which the authors have undoubtedly succeeded in their aim to give a balanced view of the subject from both the theoretical and experimental standpoints. It is indeed full of information ; yet in those portions which the reviewer has tested, because of a special interest in them, the data are critically selected and presented. Collisions of electrons and ions with atoms, molecules, surfaces and ions of opposite sign, as well as their passage through gases, all have chapters devoted to them, and the volume will serve as a valuable source of reference in many fields of work.

A. M. T.

The Auger Effect. By E. H. S. Burhop. [Pp. 188.] (Cambridge Monographs on Physics.) Price 27*s.* 6*d.*

In his introductory chapter the author describes and illustrates the cloud-chamber events which were interpreted by Auger as radiationless re-arrangements of the electrons of an excited atom. There too are discussed certain other radiationless transitions, the most important of which are internal conversion of γ-rays and internal production of electron pairs. Under ' Theory of the Auger Effect ' are listed the formulae necessary for the calculation of the transition rates for the different phenomena. The equivalence of the two treatments of the Auger Effect—as an internal absorption of radiation and as a direct interaction between electrons—would be more easily seen if the same normalization of the wave-functions had been used in the two cases. An exhaustive summary of the experimental methods used in studying the effect is given. The various roles which the radiative transition is required to play in the interpretation of X-ray spectra are examined in detail. Useful collections of curves and tables of calculated internal conversion coefficients are included in the chapters on internal conversion. The influence of the Auger effect on meson capture and its relation to atomic and molecular spectra are treated more briefly. G. E. L-W.

The Alchemists, Founders of Modern Chemistry. By F. Sherwood Taylor. [Pp. 246.] (William Heinemann.) Price 12*s.* 6*d.*

The results of Dr. Taylor's 20 years of study of the history of alchemy are distilled into this fascinating book. Although, as the author says, alchemy has been described as the pursuit of error, its study is useful in giving an insight into the history of the evolution of advanced techniques, and into the characters of serious experimenters whose most lasting contribution to science was the demonstration that their modes of thought could lead to useful results only by accident.

Dr. Taylor describes this book as a sort of interim report on his findings—for the study of the history of alchemy is involved, confusing and controversial. Not only is it difficult for us nowadays to appreciate the underlying theoretical ideas which made their efforts to transmute elements seem plausible, but the alchemists deliberately concealed their most important instructions and results in a tangle of obscure symbolical language. Dr. Taylor makes the point that the transmutations that the alchemists dreamed of are possible nowadays in the atomic pile, and that this has indeed had precisely the effect that the alchemists feared—the placing of gigantic power in the hands of those who may misuse it.

The book is illustrated with many quotations from original sources, often accompanied by the translation into modern terminology. There are also valuable chapters on the transition from alchemy to chemistry—a change which was accomplished less easily than is often represented—and on the relation between alchemy and science. E. M.

Schwerkraft und Weltall. By P. Jordan. In *Die Wissenschaft*, Vol. 107, 1952. (Braunschweig : Vieweg und Sohn.) [Pp. 207.]

The first part of this book gives an introduction to Riemannian geometry and general theory of relativity. A welcome feature is the emphasis on physical interpretation. The second part covers the field indicated by the sub-title 'Grundlagen der theoretischen Kosmologie'. It is based mainly on the author's own ideas about treating the gravitational 'constant' as a field function in the 5-dimensional formulation of the Maxwell–Einstein theory. A. S.

Mathematics, Queen and Servant of Science. By E. T. Bell. (G. Bell & Sons Ltd., London 1952.) [Pp. 437.] Price 21*s.*

This book originated from two earlier popular books of the author's 'The Queen of Science', and 'The Handmaiden of Science'. It presents very readable accounts of culminating points in past and present mathematics, with a special emphasis on mathematical logic, theory of numbers, algebra, the concept of invariance, and applications to mathematical physics. A. S.

[*The Editors do not hold themselves responsible for the views expressed by their correspondents.*]

Phil. Mag. Ser. 7, Vol. 43, Pl. LXI.

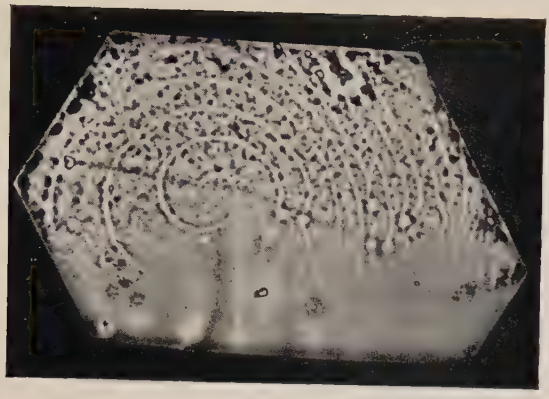

Fig. 1

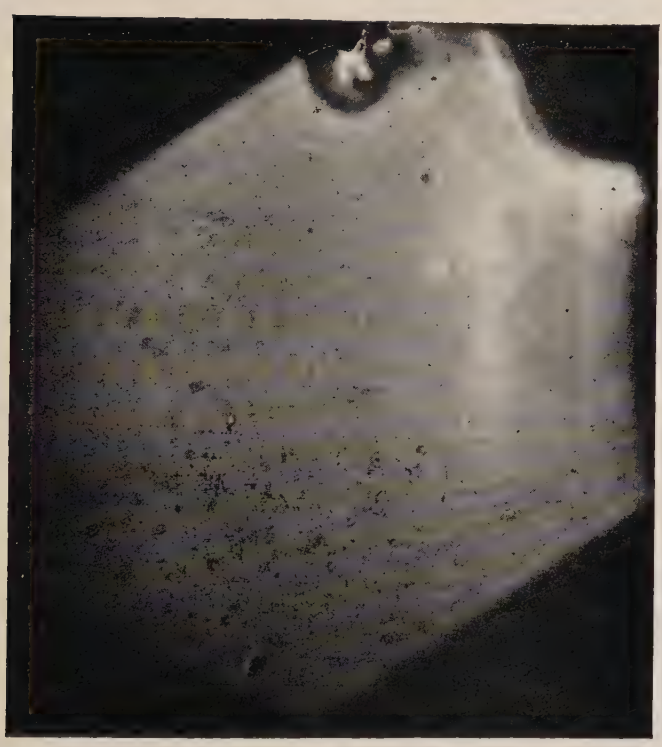

Fig. 2

Fig. 3

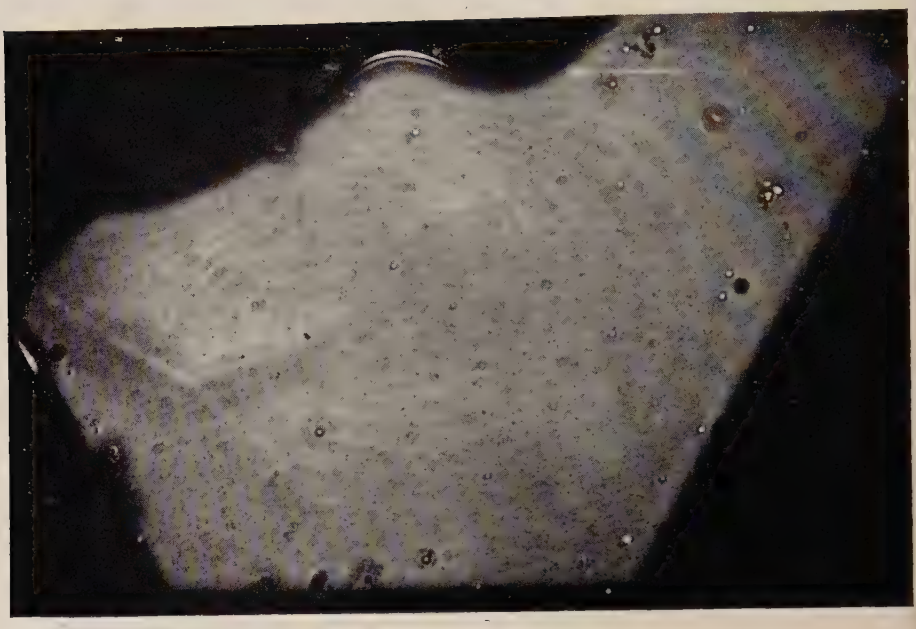

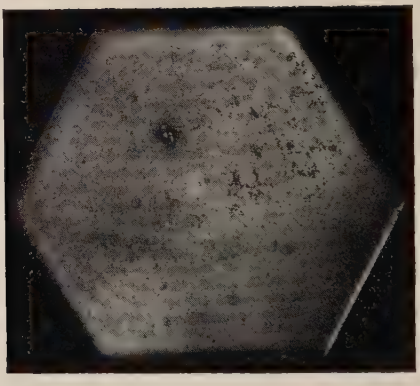

Fig. 5

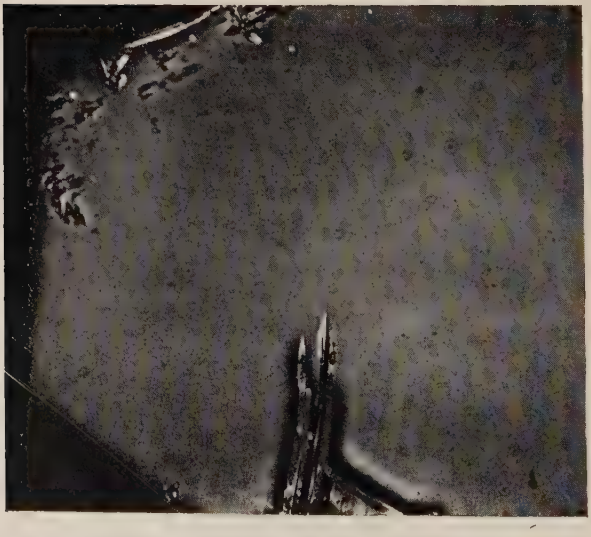

Fig. 6

Phil. Mag. Ser. 7, Vol. 43, Pl. LXIII.

Fig. 7

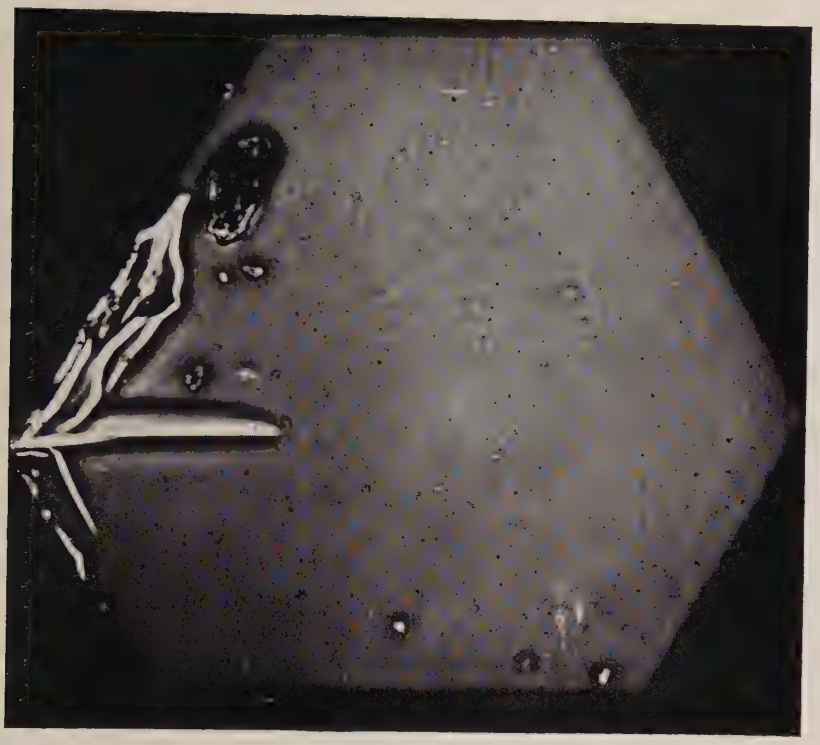

Fig. 9

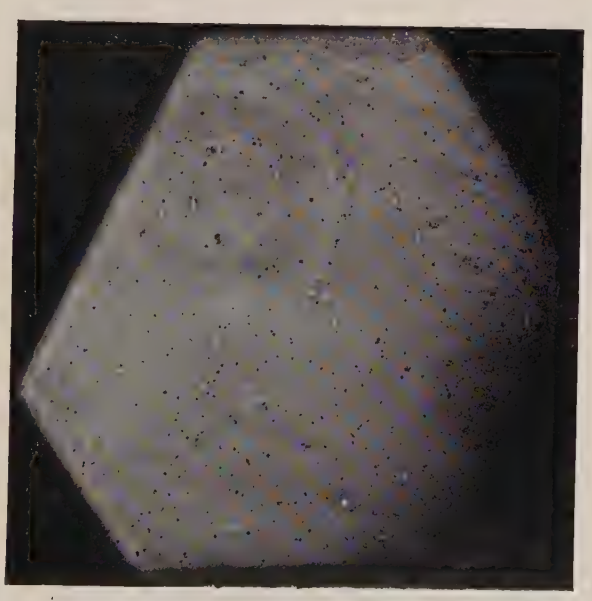

Fig. 8

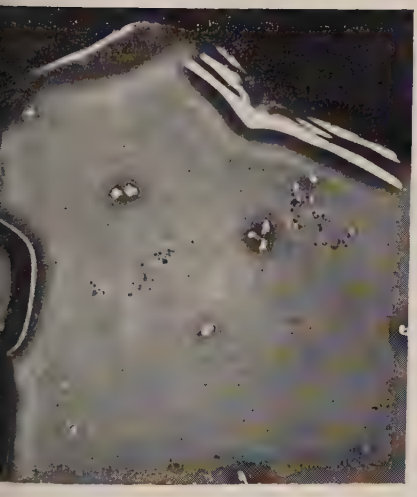

Fig. 10

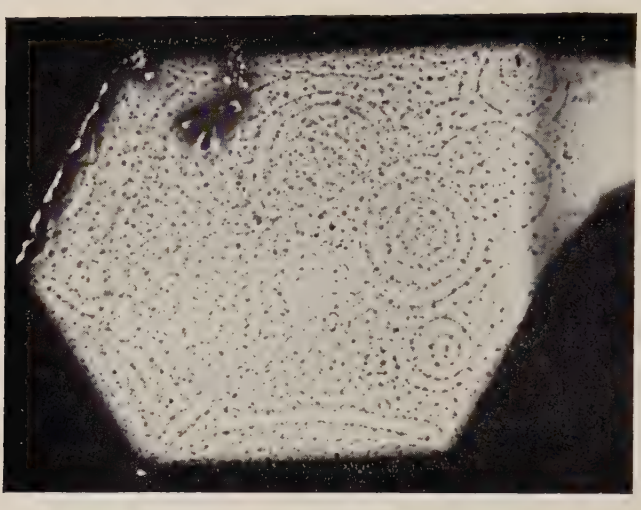

Fig. 11

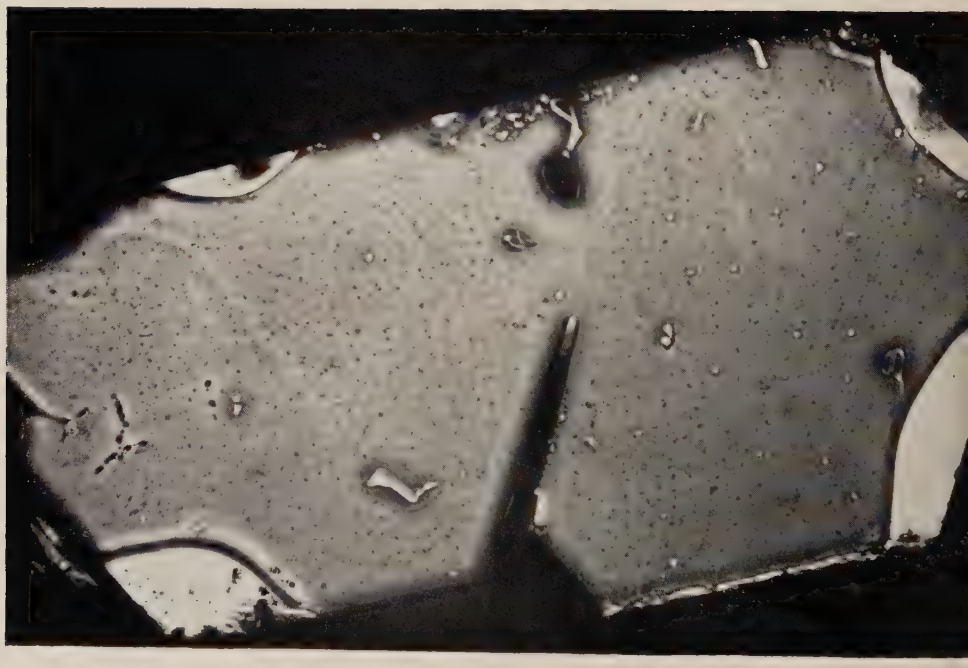

Fig. 12

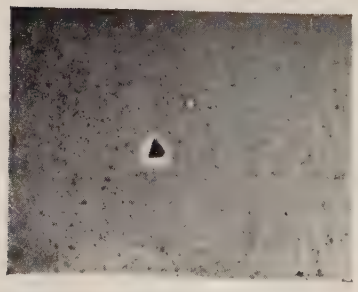

Fig. 13

Fig. 1

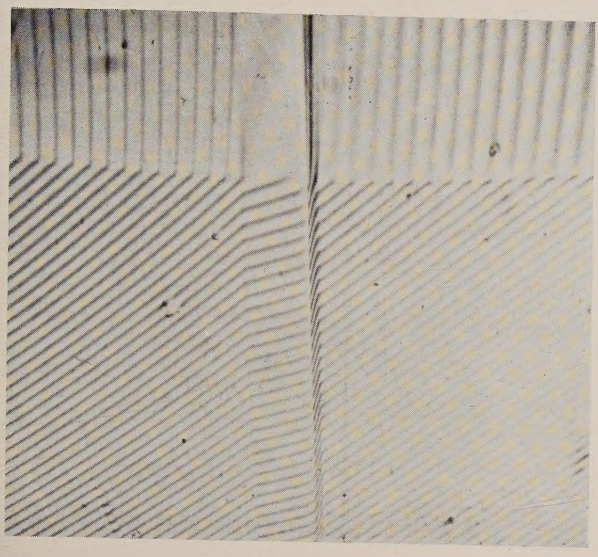

Fig. 4

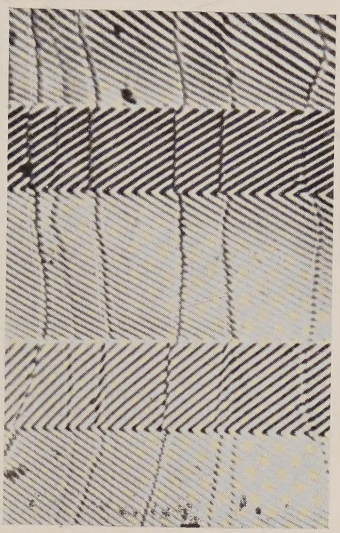

Fig. 11

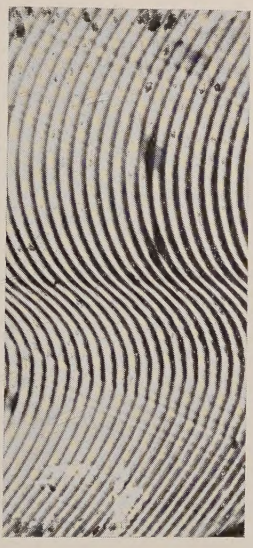

Fig. 2

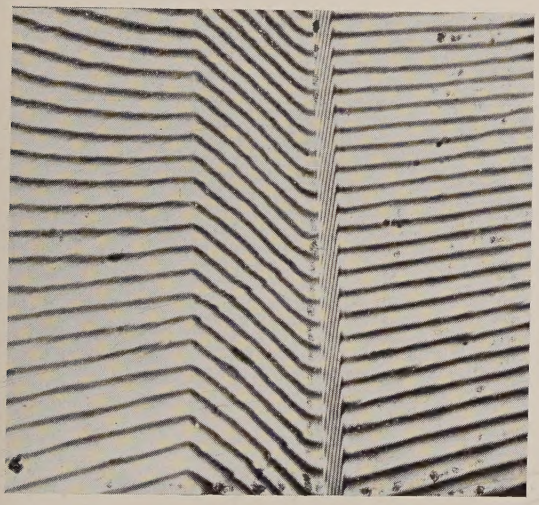

Fig. 5

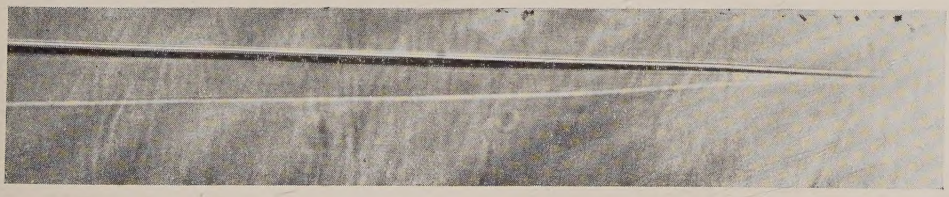

Fig. 6

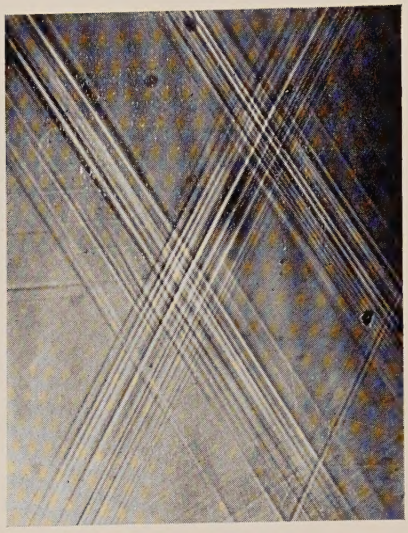

Fig. 12

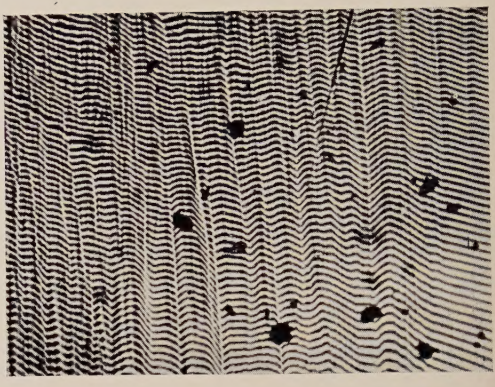

Fig. 7

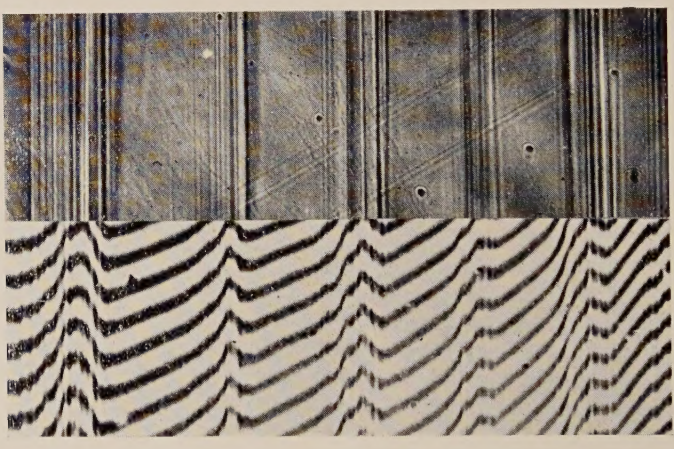

Fig. 8

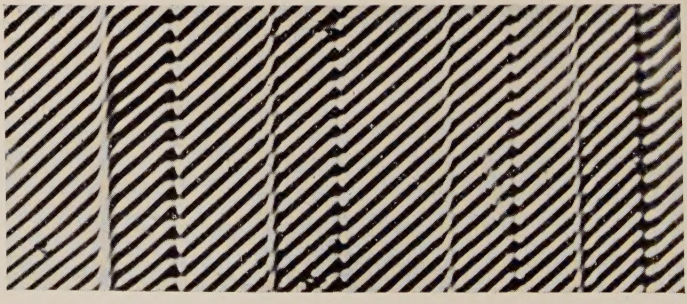

Phil. Mag. Ser. 7, Vol. 43, Pl. LXVII.

Fig. 9

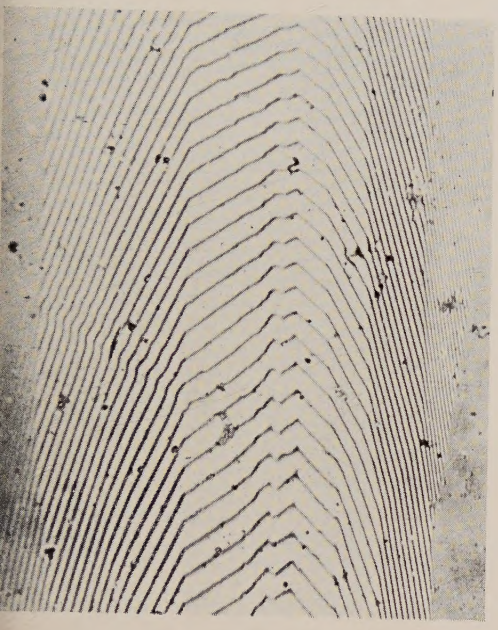

Fig. 10

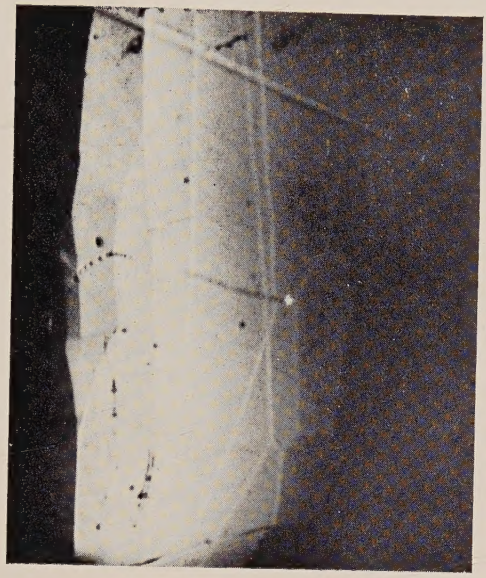

Fig. 13